Universität Potsdam

Institut für Erd- und Umweltwissenschaften

ON THE ASSESSMENT OF SURFACE URBAN HEAT ISLAND: SIZE, URBAN FORM, AND SEASONALITY

BIN ZHOU

2017

Kumulative Dissertation
zur Erlangung des akademischen Grades
doctor rerum naturalium
(Dr. rer. nat)
in der Wissenschaftsdisziplin
Physische Geographie

eingereicht an der
Mathematisch-Naturwissenschaftlichen Fakultät
der Universität Potsdam

Tag der Einreichung: 21. Juni 2017
Tag der Disputation: 20. November 2017

Bin Zhou: *On the assessment of surface urban heat island: size, urban form, and seasonality*

GUTACHTER:
Prof. Dr. Jürgen P. Kropp
Institut für Erd- und Umweltwissenschaften, Universität Potsdam
Potsdam-Institut für Klimafolgenforschung (PIK)

Prof. Dr. Annegret Thieken
Institut für Erd- und Umweltwissenschaften, Universität Potsdam

Prof. Dr. Christoph Schneider
Geographisches Institut, Humboldt-Universität zu Berlin

Published online at the
Institutional Repository of the University of Potsdam:
URN urn:nbn:de:kobv:517-opus4-404383
http://nbn-resolving.de/urn:nbn:de:kobv:517-opus4-404383

ABSTRACT

To what extent cities can be made sustainable under the observed megatrends of urbanization and climate change remains a matter of unresolved scientific debate. Our inability in answering this question lies partly in the deficient knowledge regarding pivotal human-environment interactions. Regarded as the most well documented anthropogenic climate modification, the urban heat island (UHI) effect – the warmth of urban areas relative to the rural hinterland – has raised great public health concerns globally. Worse still, heat waves are being observed and are projected to increase in both frequency and intensity, which further impairs the general well-being of urban dwellers.

Albeit with a substantial increase in the number of publications on UHI in the recent decades, the diverse urban-rural definitions applied in previous studies have remarkably hampered the general comparability of results achieved. In addition, few studies have attempted to synergize the land use data and thermal remote sensing to systematically assess UHI and its contributing factors. As a consequence, it remains a challenge to achieve a complete picture of the UHI effect.

Given these research gaps, this work presents a general framework to systematically quantify the UHI effect based on an automated algorithm, whereby cities are defined as clusters of maximum spatial continuity on the basis of land use data, with their rural hinterland being defined analogously. By combining land use data with spatially explicit surface skin temperatures from satellites, the surface UHI intensity can be calculated in a consistent and robust manner. This facilitates monitoring, benchmarking, and categorizing UHI intensities for cities across scales. In light of this innovation, the relationship between city size and UHI intensity has been investigated, as well as the contributions of urban form indicators to the UHI intensity.

Apart from a novelty in methodology, the achievements of this work are three-fold. Firstly, a log-linear relationship between surface UHI intensity and city size has been confirmed among the 5,000 European cities and settlements. The relationship can be extended to a log-logistic one, when taking a wider range of small-sized cities into account.

Secondly, this work reveals a complex interplay between UHI intensity and urban form. City size is found to have the strongest influence on the UHI intensity, followed by the fractality and the anisometry. However, their relative contributions to the UHI intensity depict a pronounced

regional heterogeneity, indicating the importance of considering spatial patterns of UHI while implementing UHI adaptation measures.

Lastly, this work presents a novel seasonality of the UHI intensity for individual clusters in the form of hysteresis-like curves, which implies a phase shift between the time series of UHI intensity and background temperatures. Combining satellite observation and urban boundary layer simulation, the seasonal variations of UHI are assessed from both screen and skin levels. Taking London as an example, this work attributes the discrepancies between the seasonality observed at different levels mainly to the peculiarities of surface skin temperatures associated with the incoming solar radiation. In addition, the efforts in classifying cities according to their UHI characteristics highlight the important role of regional climates in determining the UHI.

In summary, this work delivers manifold contributions to the understanding of the UHI phenomenon, which have complemented and advanced a number of previous studies. It serves as one of the first studies conducted to systematically and statistically scrutinize the UHI. The outcomes of this work are of particular relevance for the overall spatial planning and regulation at meso- and macro levels in order to harness the benefits of rapid urbanization, while proactively minimizing its ensuing thermal stress.

ZUSAMMENFASSUNG

Inwiefern Städte unter den beobachteten Megatrends der Urbanisierung und des Klimawandels nachhaltig gestaltet werden können, bleibt in der wissenschaftlichen Diskussion umstritten. Dies ist zum Teil auf unzureichende Kenntnisse der ausschlaggebenden Mensch-Umwelt-Interaktionen zurückzuführen. Als die am vollständigsten dokumentierte anthropogene Klimamodifikation hat der Urbane Hitzeinsel (UHI) Effekt – eine Temperaturerhöhung von Stadtgebieten im Vergleich zu umliegenden ländlichen Räumen – weltweit große Sorgen hinsichtlich der Gesundheit der Bevölkerung hervorgerufen. Dazu kommt noch ein immer häufigeres und intensiveres Auftreten von Hitzewellen, wodurch das allgemeine Wohlbefinden der Stadtbewohner weiter beeinträchtigt wird.

Trotz eines deutlichen Anstiegs der Zahl der UHI-bezogenen Veröffentlichungen in den letzten Jahrzehnten haben die unterschiedlichen Definitionen von städtischen und ländlichen Gebieten in bisherigen Studien die allgemeine Vergleichbarkeit der Resultate stark erschwert und beschränkt. Darüber hinaus haben nur wenige Studien den UHI-Effekt und seine Einflussfaktoren anhand einer Kombination der Landnutzungsdaten und der thermischen Fernerkundung systematisch untersucht. Daher bleibt die Herausforderung, ein vollständiges Bild des UHI-Effektes zu erhalten, weiterhin bestehen.

Angesichts der Forschungslücken, stellt diese Arbeit einen allgemeinen Rahmen zur Quantifizierung von UHI-Intensitäten mittels eines automatisierten Algorithmus vor, wobei Städte als Agglomerationen maximal räumlicher Kontinuität basierend auf Landnutzungsdaten identifiziert, sowie deren ländliche Umfelder analog definiert werden. Durch Verknüpfung der Landnutzungsdaten mit Landoberflächentemperaturen von Satelliten kann die UHI-Intensität robust und konsistent berechnet werden. Dies erleichtert die Überwachung, das Benchmarking, und die Kategorisierung von UHI-Intensitäten für Städte auf verschiedenen Ebenen. Anhand dieser Innovation wurde nicht nur der Zusammenhang zwischen Stadtgröße und UHI-Intensität untersucht, sondern auch die Auswirkungen der Stadtform auf die UHI-Intensität quantifiziert.

Neben dieser methodischen Innovation sind die Ergebnisse dieser Arbeit im Folgenden zusammengefasst. Erstens wurde eine log-lineare Beziehung zwischen UHI-Intensität und Stadtgröße unter Berücksichtigung der 5,000 europäischen Städte und Siedlungen bestätigt. Werden kleinere Städte auch berücksichtigt, ergibt sich eine log-logistische Beziehung.

Zweitens besteht ein komplexes Zusammenspiel zwischen den Indikatoren der Stadtform und der UHI-Intensität: die Stadtgröße stellt den stärksten Einfluss auf die UHI-Intensität dar, gefolgt von der fraktalen Dimension und der Anisometrie. Allerdings zeigen ihre relativen Beiträge zur UHI-Intensität eine signifikante regionale Heterogenität, welche die Bedeutung räumlicher Muster während der Umsetzung von UHI-Anpassungsmaßnahmen hervorhebt.

Des Weiteren ergibt sich eine neue Saisonalität der UHI-Intensität für individuelle Städte in Form von Hysteresekurven, die eine Phasenverschiebung zwischen den Zeitreihen der UHI-Intensität und der Hintergrundtemperatur andeutet. Diese Saisonalität wurde anhand von Luft- und Landoberflächentemperaturen untersucht, indem die Satellitenbeobachtung und die Modellierung der urbanen Grenzschicht kombiniert wurden. Am Beispiel von London ist die Diskrepanz der Saisonalitäten zwischen den beiden Temperaturen vor allem auf die mit der einfallenden Sonnenstrahlung verbundene Besonderheit der Landoberflächentemperatur zurückzuführen. Darüber hinaus spielt das regionale Klima eine wichtige Rolle bei der Entwicklung der UHI.

Zusammenfassend leistet diese Arbeit vielfältige Beiträge zum tieferen Verständnis des UHI-Phänomens. Erweitert und vorangebracht wurden die Schlussfolgerungen von mehreren vorherigen Studien. Diese Arbeit ist eine der ersten Studien dieser Art, die eine systematische und statistische Untersuchung des UHI-Effektes ermöglicht. Die Ergebnisse sind von besonderer Bedeutung für die allgemeine räumliche Planung und Regulierung auf Meso- und Makroebenen, damit sich Vorteile der rapiden Urbanisierung nutzbar machen und zeitgleich die daraus resultierende Hitzebelastung proaktiv vermindern lassen.

ACKNOWLEDGMENTS

This work would not have been possible without the advice and support of many individuals and organizations.

First of all, I would like to thank my supervisor Prof. Dr. Jürgen Kropp for the opportunity of writing my doctoral thesis in his group and for his continued support and scientific guidance. I am in particular grateful to the freedom he gave me to pursue challenging research ideas: some failed while others constituted the cornerstone of this work.

I thank Prof. Dr. Annegret Thieken and Prof. Dr. Christoph Schneider for reviewing my dissertation; Prof. Dr. Axel Bronstert for chairing my doctoral defense, and Prof. Dr. Anders Levermann and Dr. Maik Heistermann for agreeing to be members of the examination committee.

I am immensely indebted to Dr. Diego Rybski for his day-to-day supervision, valuable discussions, and constructive criticism. His deep insights and expertise in complexity science have extensively broadened my scope of research, which will undoubtedly nourish my future career in academia.

I would like to thank Prof. Dr. Yifang Ban for hosting my research stay at KTH and the colleagues there at the Geoinformatics division for their generous help. Sincere thanks go to Dr. Koen De Ridder, Dr. Dirk Lauwaet, Dr. Hans Hooyberghs from VITO for their input concerning the work in Chapter 4.

Special thanks also go to all the past and present staff, colleagues at the Climate Change and Development Group of PIK for their general support and smooth collaboration, as well as for all the scientific and private enrichment to our daily lives.

I am grateful to Diego, Prajal, Boris, and Jürgen for their invaluable feedback on the earlier versions of the dissertation; to David, Shaoyang, and Weishi for proofreading the manuscript. They are of course absolved of responsibility for its remaining limitations and blind spots.

I want to thank Climate-KIC, EIT, for award of a PhD scholarship as well as for the wide-ranging training opportunities provided in academia and beyond.

Last but not least, I would like to thank my family and friends for their constant support and love throughout my life.

Bin Zhou
December 5, 2017

CONTENTS

LIST OF FIGURES

LIST OF TABLES

ACRONYMS

AIC Akaike Information Criterion

ASTER Advanced Spaceborne Thermal Emission and Reflection Radiometer

AVHRR Advanced Very High Resolution Radiometer

CCA City Clustering Algorithm

CFD Computational Fluid Dynamics

ECMWF European Centre for Medium-range Weather Forecasting

ETM+ Enhance Thematic Mapper

GHG Greenhouse Gas

GSW Generalized Split Window

LCZ Local Climate Zones

LST Land Surface Temperature

MODIS Moderate Resolution Imaging Spectroradiometer

NDVI Normalized Difference Vegetation Index

RTE Radiative Transfer Equation

SEVIRI Spinning Enhanced Visible and Infrared Imager

SLSTR Sea and Land Surface Temperature Radiometer

TIR Thermal Infrared

TIRS Thermal Infrared Sensor

TOA Top of Atmosphere

UBL Urban Boundary Layer

UCL Urban Canopy Layer

UHI Urban Heat Island

VIIRS Visible and Infrared Imagery Radiometer Suite

1

INTRODUCTION

1.1 MOTIVATION

To date, more than half of the world's population lives in cities. The percentage of urban residents is expected to soar further, reaching 66 % by 2050, which equals approximately another 2.5 billion people (United Nations, 2015). Cities are on one hand hubs of great efficiency, innovation, and knowledge sharing due to higher concentration of human capital and better life quality than rural areas (Shapiro, 2006; Bettencourt and West, 2010); on the other hand, the accelerated urbanization has brought about a multitude of social and environmental problems, such as traffic congestion, air pollution, and heat stress (OECD, 2014). Some problems may even transcend city borders, resulting in far-reaching consequences.

Worthy of particular mention is human-induced climate change caused primarily by anthropogenic Greenhouse Gas (GHG) emissions. Although cities are estimated to cover merely 0.45 % to 3 % of the global land (Gamba and Herold, 2009; Liu et al., 2014), they account for approximately 70 % of total anthropogenic GHG emissions (UN-Habitat, 2011). The changing climate is likely to have triggered an unprecedented sequence of extreme weather events in the last decades (IPCC, 2014). In particular, heat waves such as the ones swept across Europe in summer 2003, Russia in 2010, and the USA in 2011 are expected to occur with a higher frequency and duration in the future (Fischer and Schär, 2010; Coumou and Rahmstorf, 2012). The increased heat waves, together with the poor emergency management and ill-prepared health services have led to excess morbidity and mortality predominantly in the elderly population (Fouillet et al., 2006; Oudin Åström et al., 2011; Zhang et al., 2015).

Cities bear the brunt of intensifying heat waves, as people and assets are increasingly concentrated in cities. Worse still, the lack of surface moisture and greatly diminished advective cooling typically present during heat waves further exacerbate the Urban Heat Island (UHI) effect – an

elevated temperature of urban areas relative to their rural surroundings (Oke, 1973). This makes cities more vulnerable and decreases the livelihoods and well-being of urban dwellers (Oke, 1987; Li and Bou-Zeid, 2013). Moreover, the UHI is shown to increase energy consumption for air-conditioning in cities, which in turn results in extra release of waste heat and air pollutants into the atmosphere during energy production (Akbari et al., 2001). All this together causes an additional mean temperature increase of up to 2 °C in cities (Ohashi et al., 2007; Salamanca et al., 2011; de Munck et al., 2013); an ensuing degradation of air quality associated with urban smog formation (Akbari et al., 2001; Akbari, 2005); and substantial CO_2 emissions, which might impede human efforts towards a sustainable low-carbon society. In the worst emission scenario, when the UHI is taken into account, the total economic costs of climate change for cities are estimated to reach 10.9 % of GDP by 2100 (Estrada et al., 2017). This is 2.6 times larger than without considering the UHI.

Therefore, in view of climate change mitigation and adaptation, it is of increasing importance to better understand the principle of urban climate. Incorporating the knowledge acquired into urban planning and design practices is urgently needed in order to shape our cities more climate-resilient, liveable, and sustainable (Mills, 2014).

1.2 STATUS QUO OF EMPIRICAL UHI STUDIES

The study of the Urban Heat Island (UHI) can be dated back to Luke Howard's *The climate of London* in which he first recognized the effect of urban areas on local climate through his meteorological observations (Howard, 1833; Mills, 2014). Considered as the most well documented example of anthropogenic climate modification (Arnfield, 2003), the UHI has been gaining gradually more importance in the last decades. The study of the UHI addresses two of the most serious environmental challenges today – urbanization (population growth) and climate change – and their reciprocal impacts (Kalnay and Cai, 2003; Parker, 2010; Stewart and Oke, 2012).

1.2.1 *Formation and attribution of the UHI*

As summarized by Oke (1987), the formation of the UHI phenomenon can be ascribed to (in descending order of importance):

(i) the anthropogenic modification of natural landscapes (reduced albedo, less vegetation, increased roughness and thermal admittance)

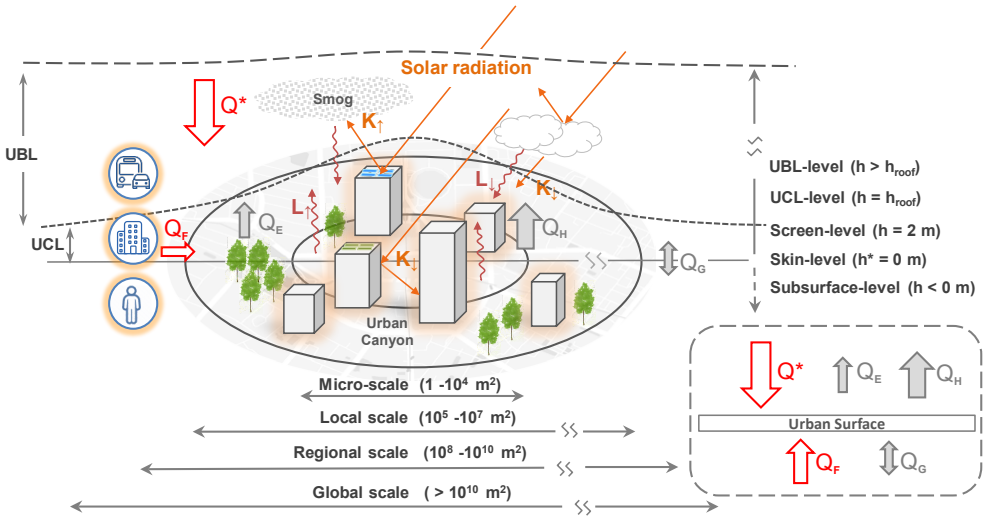

Figure 1.1: Schematic of the surface energy balance and the boundary layers over urban areas– Urban Boundary Layer (UBL) and Urban Canopy Layer (UCL), as well as spatial scales (horizontal) and levels (vertical) of urban meteorology and climatology. The notations are clarified in detail below Eq. (1.1). (adapted from Oke, 1988; Kato and Yamaguchi, 2005).

and the consequent changes in the surface energy budget (Oke, 1982; Oke, 1988; Georgescu et al., 2009);

(ii) anthropogenic heat (Sailor and Lu, 2004; Sailor, 2011) released from
- vehicles and industrial sites through fossil fuel combustion,
- heating, ventilation and air-conditioning for buildings,
- and human metabolism;

(iii) increased incoming long-wave radiation caused, e.g., by air pollution (Rouse et al., 1973; Oke et al., 1991; Nunez et al., 2000).

These modifications result in a series of atmospheric and thermophysical changes in the urban boundary layer, favoring heat storage and trapping in cities. As a consequence, the air temperature-based UHI intensity usually reaches its maximum on clear, calm nights and could be as much as 12 °C (Oke, 1987).

Similarly, the formation of the UHI can also be described from an energy budget perspective. The energy balance of urban surface without significant advection, as illustrated in Fig. 1.1, can be expressed as:

$$Q^* + Q_F = Q_H + Q_E + Q_G \tag{1.1}$$
$$Q^* = K^* + L^* = K_\downarrow - K_\uparrow + L_\downarrow - L_\uparrow$$

where

Q^* net all-wave radiation (asterisk indicates net radiation, similarly hereinafter),

Q_F anthropogenic heat flux,

Q_H sensible heat flux,

Q_E latent heat flux,

Q_G conduction to or from soil,

K short-wave radiation (arrows indicate incoming $\downarrow$ or outgoing $\uparrow$, similarly hereinafter),

L long-wave radiation.

From the point of view of incoming energy, urban built-up areas, usually sealed with concrete or asphalt, have lower albedo than the natural land cover, which remarkably decreases the outgoing short-wave radiation ($K_{\uparrow}-$). Moreover, dense building blocks and relatively narrow roads between them form the urban street canyon structure characterized by a small sky-view factor. This results simultaneously in an increase of short-wave absorption (K^*+) and net long-wave radiation (L^*+) due to radiation trapping (Arnfield and Grimmond, 1998; Kusaka and Kimura, 2004; Ryu and Baik, 2012). The excess heat absorbed and trapped is even harder to dissipate from cities, since the increased aerodynamic roughness of urban areas dramatically reduces the wind speed, and so does the advective cooling (Coceal and Belcher, 2005).

Furthermore, air pollution plays a minor but non-negligible role in amplifying the UHI. A high concentration of suspended particulate matter coincident with air pollution could slightly increase the long-wave radiation reaching the surface ($L_{\downarrow}+$) by re-emitting the absorbed short-wave radiations downward (Estournel et al., 1983; Oke et al., 1991; Nunez et al., 2000). Therefore, it is reasonable to expect that measures aiming to reduce ambient air pollution will bring about a range of co-benefits, among others, attenuated UHI intensity and decreased mortality (Stedman, 2004).

With regard to the heat fluxes, cities are characterized by a high fraction of impervious surfaces (less vegetation and less moisture availability) and an abundance of construction materials with high thermal admittance (ability to store and release heat). These properties alter the partitioning of surface energy fluxes in favor of the sensible heat (Q_H+) rather than the latent heat (Q_E-), i.e. the incoming radiation is transformed into heat instead of a flux of moisture into the atmosphere.

In the last decades, the aforementioned causative factors of the UHI have been confirmed and further broadened through a variety of studies around the world (see, e.g., Arnfield, 2003; Voogt and Oke, 2003 for a review). Urbanization and climate change proceed at an unprecedented speed. There is an increasing concern about the impact of the enhanced radiative forcing on the UHI, which is induced by the soaring GHG concentration in the atmosphere. McCarthy et al. (2010) used an urban land surface scheme coupled to a global climate model to quantify the impact of climate change on the UHI. They suggested that climate change could potentially increase the UHI by 30 % in regions coincident with rapid population growth. Under this new challenge, an update on our knowledge about the UHI is due in the future, taking climate change into account.

1.2.2 *Scales and levels of the UHI*

With respect to the methodology, studies addressing the urban climate can be mainly categorized into:

(i) *modeling approaches* of varying complexity which aim at simulating the surface energy balance in Eq. (1.1) by appropriately parametrizing urban land surfaces and dominant physical processes over cities (see, e.g., Kanda, 2007; Grimmond et al., 2010, 2011; Best and Grimmond, 2015 for review);

(ii) *empirical approaches*, conventionally based on observational near-surface (2 m) air temperature or surface skin temperature data, attempting to calculate the UHI intensity of cities and to assess the contribution of various site-specific descriptive quantities (e.g., population density, imperviousness, greenness, climatological factors) to the UHI intensity (Arnfield, 2003; Imhoff et al., 2010; Weng et al., 2011).

In both approaches, two terms have to be distinguished: *scale* and *level*. The former refers to the horizontal resolution of investigations, whereas the latter refers to the vertical dimension.

Depending on the purpose of application and computational capacities, the modeling approaches can be performed at multiple scales ranging from micro-scale (1 - 10^4 m^2), through local/neighborhood scale (10^5 - 10^7 m^2) and regional/meso-scale (10^8 - 10^{10} m^2), to global scale ($> 10^{10}$ m^2), as shown in Fig. 1.1.

In an urban microclimate model (e.g. ENVI-met model), urban elements such as building blocks, streets, and trees are adequately resolved.

The interactions between urban elements and the surrounding atmosphere are solved using Computational Fluid Dynamics (CFD) models (Bruse and Fleer, 1998). Due to the computationally demanding nature of microclimate models, their application has long been restricted to assessing the impact of small-scale urban design scenarios and estimating the human thermal comfort in an area covering not more than a couple of streets (Chow et al., 2011; Taleghani et al., 2015).

In comparison, models of moderate resolution (at local and regional scales) are more efficient in terms of computation, making them extremely advantageous for regional or global-scale modeling. As a trade-off, each urban grid cell is represented as a set of urban canopy parameters such as aspect ratio (ratio of wall height to street width), vegetation fraction, sky view factor, etc. Best and Grimmond (2015) summarized the results obtained from the first urban land surface model comparison project (see Grimmond et al., 2010, 2011) and concluded that the simple models may perform as well as the complex ones. They suggested the selection of models should "*. . . balance the requirement for complexity within models against what is actually required for a model to be fit for purpose*".

Therefore, the *scale* does matter when studying the urban climate, not least when implementing adaptive and mitigating strategies against the UHI, because such solutions exhibit significant scale-dependent efficacy (Georgescu et al., 2015). In empirical studies, the scale is determined by the density of measurement networks or the spatial resolution of sensors.

Depending on the sensed medium and the height at which the measurement is taken, the UHI can be defined at different levels (see Fig. 1.1):

(i) Urban Boundary Layer (UBL) level (air temperature),

(ii) Urban Canopy Layer (UCL) level (air temperature),

(iii) Screen level (air temperature),

(iv) Skin level (surface skin temperature),

(v) Subsurface level (soil/groundwater temperature).

Air temperatures could be measured in the Urban Canopy Layer (UCL) and the Urban Boundary Layer (UBL). The former lies between the ground and mean rooftops, whereas the latter is above the UCL up to the height where the influence of UCL can still be detected (Roth et al., 1989). More often, air temperatures are measured at 2 m height (screen level) by weather stations located in urban/rural areas or mobile transect. These measurements possess a long-term record, but a lack of spatial details.

Moreover, weather stations are unevenly distributed and located mostly in the Northern Hemisphere and with a relatively large number in developed countries. This raises concerns about the representativeness of the results obtained.

On the contrary, surface skin temperatures sensed by air-borne or space-borne platforms are superior in delivering a spatially explicit representation of the UHI, but relatively inferior in tracking the UHI with high temporal frequency. However, for remote and inaccessible regions where ground-based measurements can hardly be undertaken, satellite-based sensors can still provide observations in a near-real-time manner.

Since Rao (1972) first investigated the UHI based on satellite observations, sensor technologies have been evolving constantly, thereby increasing both the quality and quantity of surface skin temperature data. The literature addressing the UHI by means of thermal remote sensing has been growing in the last decades (see, e.g., Voogt and Oke, 2003; Tomlinson et al., 2011 for a review). These studies, by virtue of their broad geographical coverage and variety of adopted sensors, have notably complemented and reinforced the overall understanding of the UHI.

The UHI can nevertheless be investigated by measuring subsurface temperatures (usually ground water temperatures) beneath the urban/rural surfaces with the aim of establishing a relation between the surface landscape and the underlying shallow aquifers (see, e.g., Ferguson and Woodbury, 2007; Zhu et al., 2010; Menberg et al., 2013).

UHI studies conducted at different levels are distinguished from each other in terms of measurement techniques, mediums sensed, and more importantly, in terms of predominant underlying physical processes. It is therefore crucial to precisely document the methodology applied in studies for better searchability and comparability (Arnfield, 2003). In this thesis, it is the surface UHI effect and its contributing factors that are primarily addressed. The following section will take a detailed look at the fundamentals of the thermal remote sensing of the UHI and the underlying operational sensors.

1.2.3 *Thermal remote sensing of the UHI*

Under cloud-free conditions surface skin temperature can be estimated by sensors with Thermal Infrared (TIR) spectral bands (8-13 μm) onboard – either geostationary or polar orbiting – satellites. At first the brightness temperature is inversed from Top of Atmosphere (TOA) radiances captured by the sensors according to the Planck's law. Based on the brightness temperature, the surface skin temperature can be obtained as long as the following three effects are corrected or compensated for: i) atmo-

spheric attenuation, ii) angular effects, and iii) surface emissivity effects (Dash et al., 2002; Li et al., 2013).

Given a priori knowledge of land surface emissivities which can be estimated using classification-based models (e.g., Snyder et al., 1998), three groups of methods are available to compensate for the aforementioned effects, thus are able to retrieve surface skin temperature: i) single-channel methods, ii) multi-channel methods, and iii) multi-angle methods. Among others, Radiative Transfer Equation (RTE) and Generalized Split Window (GSW) are the two most frequently used algorithms pertaining to the methods i) and ii), respectively.

RTE corrects the at-sensor radiance measured by a single TIR window channel to surface radiance (Li et al., 2013). This approach is typically used for sensors with only one TIR band, such as the ones onboard Landsat series. Without relying on an a priori knowledge or estimates of atmospheric profiles, the GSW approach retrieves the temperature based on the differentiated absorption in adjacent TIR bands. It is less sensitive to the uncertainties of atmospheric conditions and the instrument noises (Wan and Dozier, 1996). Therefore, this approach is widely used for sensors with several TIR bands, such as MODIS and AVHRR. More technical details in regards to the advantages and disadvantages of these retrieval approaches are reviewed and summarized in Dash et al. (2002), Weng (2009), and Li et al. (2013).

This radiometric temperature obtained is also known as Land Surface Temperature (LST), a term preferably used in the remote sensing community. It denotes the surface radiometric temperature confined to the instantaneous field-of-view of the sensor (Prata et al., 1995). The more tilted a sensor is, the more vertical surfaces (e.g., walls, façade) are sensed. This view-angle-dependent characteristic is termed thermal anisotropy of LST which has been widely observed and investigated in various cities (Lagouarde et al., 2004; Lagouarde et al., 2012; Hu et al., 2014, 2016).

Physically, the radiometric temperature differs from thermodynamic or aerodynamic temperatures (air temperature) sensed by, e.g., a thermometer for a medium in thermal equilibrium (Li et al., 2013). These two temperatures are only equivalent for homogeneous and isothermal surfaces, which is seldom the case for surfaces in reality, in particular for the complex urban environment. Furthermore, regarding the current spatial resolution of TIR bands, a satellite pixel, ranging from 30 m to ~4 km (see Tab. 1.1), is an ensemble of several surface types with different temperatures and emissivities. With regard to urban areas, it is urban canyon structures and construction materials, alongside other artificial

Sensor	Satellite	Spatial resolution	Orbital frequency	Image acquisiton time (local time)	Data available since
SLSTR	Sentinel-3	~1 km	Twice daily	~1000 & ~2200	2016
VIIRS	Suomi NPP	~750 m	16 days	~0130 & ~1330	2012
TIRS	Landsat 8	30 m	16 days	~1000	2013
ETM+	Landsat 7	30 m	16 days	~1000	1999
MODIS	Aqua	~1 km	Twice daily	~1330 & ~0130	2002
MODIS	Terra	~1 km	Twice daily	~1030 & ~2230	2000
ASTER	Terra	90 m	Twice daily	Request only	1999
AVHRR	NOAA-platforms	~1.1 km	Twice daily	~0930	2006
AVHRR	MetOp-A	~1 km	29 days	~0930 & ~2130	2006
AVHRR	MetOp-B	~1 km	29 days	~0845 & ~2045	2012
SEVIRI	Meteosat-8	~3 km	Geostationary	Every 15 min	2005
GOES Imager	GOES 8-15	~4 km	Geostationary	Every 30 min	1994

Table 1.1: Selected operational sensors capable of retrieving LST from TIR bands, adapated from Tomlinson et al. (2011).

landscapes (e.g., parks, lakes) that account primarily for the anisotropy (Voogt, 2008; Hu et al., 2016).

To minimize the anisotropy that inheres in LST measurements, there are in practice two strategies available (Hu et al., 2016):

(i) restricting the sensor view angles within a narrow range. As for MODIS LST data, Hu et al. (2014) suggested a zenith view angle threshold of 35°. This measure ensures a quasi bird's eye or "quasi-nadir" view of land surface while maintaining sufficient amount of data for further analyses.

(ii) temporally compositing LST over a longer period. Holderness et al. (2013) assessed the temporally averaged LST data at daily, monthly, and seasonal level and suggested that the monthly mean value of LST is the optimal balance between the level of sensitivity and aggregation, enabling the distinction of heat wave years from normal ones.

Table 1.1 lists the available operational sensors and their basic information. Geostationary satellites can capture diurnal cycles of surface skin temperatures with very high temporal resolution (up to 15 min) and moderate spatial resolution (e.g., for SEVIRI, 3 km at nadir but increasing to ~6 km when the viewing zenith angle gets larger). However, due to orbital constraints, the data cover only a constant region of the Earth. In contrast, sensors onboard polar orbiting satellites can provide LST data with consistent periodicity, high spatial resolution, and global coverage (Hu et al., 2016). Among them, MODIS is well suited for systematically monitoring and comparably assessing the UHI for a multitude of cities (see, e.g., Peng et al., 2012; Clinton and Gong, 2013; Zhou et al., 2013), particularly due to its short revisit periods and a relatively high accuracy of better than 1 K in most cases (Wan, 2008).

1.3 TOWARDS SYSTEMATIC SURFACE UHI ASSESSMENT: CHALLENGES AND RESEARCH GAPS

The availability of remotely sensed surface skin temperature with global coverage, as described in detail in Sec. 1.2.3, has given rise to a substantial number of empirical surface UHI studies conducted in cities of varying sizes and climatic conditions worldwide (Voogt and Oke, 2003; Weng, 2009). Simple schemes based on the dichotomous definition of urban-rural areas are widely used as an approach to quantifying the UHI intensity and conducting inter-comparisons between different cities. However, a recent review by Stewart (2011) revealed generally

poor scientific practice in the observational UHI literature. The majority of studies failed to communicate the site exposure and land cover characters, which compromised the scientific soundness of these studies. Besides, another ambiguity stems from diverse urban/rural definitions existing in the literature, also hampering the comparability of UHI studies. Therefore, how to quantify the UHI effect from a systematic and comprehensive perspective across countries constitutes one of the earliest motivations of this thesis.

1.3.1 *A consistent cross-scale definition of UHI intensity*

Different delineations of urban/rural areas and metrics used to quantify the UHI intensity lead to incomparable results. Schwarz et al. (2011) compared the indicators for quantifying surface UHI based on MODIS LST data for 263 European cities with special respect to the consistency in their temporal variations. They found general weak correlations among the UHI indicators, although they were all supposed to quantify the magnitude of UHI. This inconsistency caused by a non-unified urban definition applies both to case studies focusing on one or several cities and to ensemble (or cross-sectional) studies considering a large number of cities spread across countries. In the latter case, administrative boundaries of cities are usually demarcated according to the economic connections rather than the spatial continuity of built-up areas, making "city" a notion subject to country-specific peculiarities (Rozenfeld et al., 2008).

Results based on inconsistent UHI metrics could be misleading or even erroneous, which underlines the importance of a unified city definition and UHI metric. The fact that urban areas expand, shrink, and morph continuously requires an agile nature of the conceived method. It has to be adjusted to the dynamic urban land use at a reasonable pace. These challenges together give rise to the first research question (RQ1).

Research Question 1

How can one systematically quantify the intensity of UHI across scales despite the complexity and diversity of urban systems?

1.3.2 *The size effect of UHI*

As one of the most intuitive and fundamental parameters of a city, the city size (either measured by population or surface area) and its relationship with the UHI have remained a topic of interest in previous UHI

studies. Among the earliest ones are those by Fukui (1957), Chandler (1967), and Oke (1973). In general, the city size is observed to positively correlate with the UHI intensity, i.e. the larger a city is, the more intensive is its UHI. More precisely, a linear relationship between the UHI intensity and the logarithm of city size has been found in Europe (Oke, 1973), North America (Oke, 1973; Imhoff et al., 2010), and Japan (Sakabikara and Matsui, 2005). Moreover, the UHI intensity is also found to scale sublinearly with the population density of cities (Steeneveld et al., 2011). As our review proceeded, it seemed that no consensus could be achieved due in large part to the following two facts:

i) Cities considered in the studies are selected arbitrarily or confined to the data availability, which questions the representativeness of data. The regression based on such data is very likely to be biased with a large degree of uncertainty.

ii) Some studies are conducted several decades ago, and many changes have occurred since their publication, such as the accelerating urbanization, and the rapid development of sensor techniques. In particular, the latter aspect has remarkably altered the landscape of research, enabling us to revisit the size effect of UHI with an unprecedented depth and breadth.

Given these shortcomings of previous studies, the relationship between city size and UHI intensity needs some overdue updating in the era of Earth Observation, which comprises the focus of the second research question (RQ2).

Research Question 2

How does the city size determine the surface UHI intensity in the era of Earth Observation?

1.3.3 *The urban form and heat*

Each city presents its unique footprint on the Earth surface that can be characterized by a series of urban form (or landscape) indicators (McGarigal and Marks, 1994; Schwarz, 2010). The urban form exerts such a fundamental and profound impact on the functionality of a city that the aspects affected could hardly be enumerated completely: for instance, energy use in both transportation and residential sectors (Frank et al., 2006; Ewing and Rong, 2008), air quality (Stone, 2008), GHG emissions (Grazi et al., 2008), and vulnerability to extreme heat events (Stone et al., 2010), as well as public health (U.S. Environmental Protection Agency, EPA,

2001). Thus, a better understanding of urban form is of great relevance for the ongoing debate of sustainability and helps urban planners conceptualize solutions at distinct levels to achieve desirable urban forms (Jabareen, 2006).

On the other hand, cities are increasingly argued as fractal in form, i.e. presenting a statistical self-similarity or scale-invariance (Batty and Longley, 1987b; Batty and Longley, 1994). Viewing cities from a perspective of fractal geometry opens up new possibilities to analyse cities, which attempts to gain general insights into spatial organization of cities and its implications for urban planning. To this end, the third research question (RQ3) aims to bridge long-established analyses of urban climate with the burgeoning new science of cities (Batty, 2008).

Research Question 3

How does the urban form determine the surface UHI intensity?

1.3.4 *The seasonality of UHI*

The UHI intensity measured using air temperatures at screen level is well known to differ from that based on surface skin temperatures at the skin level (Norman and Becker, 1995; Prihodko and Goward, 1997; Jin and Dickinson, 2010). Prigent et al. (2003) compared the surface skin temperature with in situ measured air temperatures and suggested two different dominant regimes accounting for the discrepancy between the two temperatures: solar insolation during daytime and longwave radiation balance at night. A high share of vegetation, high soil moisture, and cloudy conditions are observed to converge the two temperatures (Prigent et al., 2003; Mostovoy et al., 2006; Gallo et al., 2011).

Since the surface skin temperature-based UHI exhibits a pronounced seasonality that can be quantified by hysteresis (Zhou et al., 2013), it is still unknown whether similar patterns exist in the air temperature-based UHI. Although a large body of literature has documented the seasonal variation of UHI, they are based either on the air temperature (Jauregui, 1997; Wilby, 2003; Kim and Baik, 2005) or on the surface skin temperature (Tran et al., 2006; Pongrácz et al., 2010), and rarely on both (Cui and Foy, 2012). Given this research gap, the fourth research question (RQ4) is devoted to addressing the seasonality of the UHI intensity by means of both observations and urban climate modelling.

Research Question 4

How does the UHI intensity vary seasonally at both screen and skin levels?

1.3.5 *The typology of cities according to the UHI characteristics*

The necessity of a scheme for the classification of cities originates from the fact that a one-size-fits-all type of adaptive and mitigating strategies against the UHI is generally not available (UN-Habitat, 2011; Georgescu et al., 2015). An adequate classification of cities according to their UHI characteristics (e.g., seasonality, magnitude) may give hints about whether or to which extent measures alleviating the UHI suggested by various case studies can be further transferred and implemented in other cities. This is gaining importance in the context of global warming, because strategies adapted to local conditions are of great demand for a myriad of cities which have suffered or are projected to unceasingly suffer from heat stress (Gago et al., 2013). It is also because approaches (e.g., micro-scale climate models, meso-scale urban canopy models) employed in case studies leading to the concrete adaptation measures (e.g., green roofs, cool pavement) are becoming increasingly sophisticated and computationally intensive (Schubert and Grossman-Clarke, 2013; Sun et al., 2016; Li et al., 2014). It is not realistic to conduct studies with such a high level of detail for each city, due in part to the limited computational capacity. On the other hand, the efficacy of adaptation measures seems to be strongly dependent on the city addressed in the case study, which calls for scrutiny of the commonality between cities.

Assuredly, some measures could nevertheless be adopted with an equally good adaptive performance in a wide range of cities. However, it is reasonable and logically sound to postulate that cities sharing similar UHI characteristics may more likely better benefit from a certain type of adaptation measures than those exhibiting completely different UHI features. The objective of the fifth research question (RQ5) is to develop a sound scheme to identify the typology of cities, making full use of UHI intensity data over years generated from the analyses conducted to answer the RQ1. RQ5 can therefore be expressed as

Research Question 5

What is a plausible scheme to classify cities according to their UHI characteristics, and what is their geographical pattern?

1.4 STRUCTURE OF THE THESIS

This thesis is organized as follows (a visual outline can be seen in Fig. 1.2). Chapter 2 addresses extensively almost all of the aforementioned research questions except RQ3, providing a general framework for the subsequent chapters. However, owing to its concise and heuristic nature,

Chapter 2 is unable to give in-depth insights into RQ2 and RQ4 which remain to be explicitly tackled in Chapters 3 and 4, respectively.

Chapter 3 mainly focuses on the impact of urban form on the UHI from a fractal perspective. The contributions of city size and two urban form indicators (fractality and anisometry) to the surface UHI are quantified, taking regional heterogeneities into account. Moreover, a simple model is used to elaborate the linkages between the heat transfer, city size, and fractality.

Chapter 4 is dedicated to analyzing the seasonality of the UHI intensity at the screen and skin levels, taking the Greater London area as an example. To this end, satellite observations and urban climate modeling are combined, contributing to understanding the relationship between air temperature and surface skin temperature.

Finally, Chapter 5 discusses and summarizes the findings of the individual chapters with regard to their implications for sustainable urban planning and climate change adaptation.

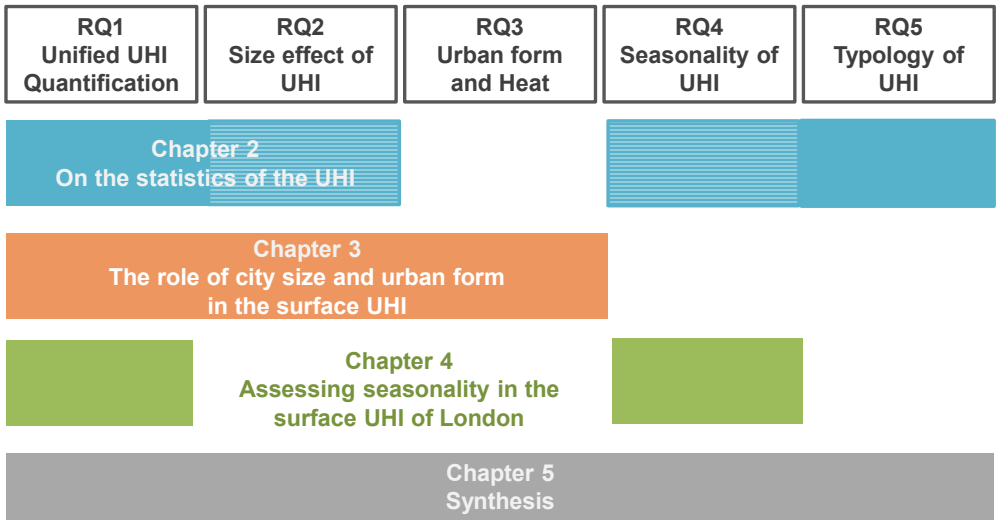

Figure 1.2: The outline of the thesis and the relation of chapters to the discussion of the research questions.

The four appendices give supplementary information about

- Details of the methodology utilized to quantify the UHI (Appendix A);
- Derivation of the relation between heat transfer, urban area, and fractal dimension (Appendix B);
- Influences of City Clustering Algorithm (CCA) parameters on the surface UHI intensity (Appendix C).

- Analysis of surface skin temperature decay under two boundary definitions (Appendix D);

Furthermore, it is worth mentioning that due to the cumulative nature of this thesis, a certain degree of recurrence is unavoidable.

2

URBAN HEAT ISLAND STATISTICS FOR EUROPE [1]

ABSTRACT

We perform a systematic study of all cities in Europe to assess the Urban Heat Island (UHI) intensity by means of remotely sensed land surface temperature data. Defining cities as spatial clusters of urban land cover, we investigate the relationships of the UHI intensity, with the cluster size and the temperature of the surroundings. Our results show that in Europe, the UHI intensity in summer has a strong correlation with the cluster size, which can be well fitted by an empirical sigmoid model. Furthermore, we find a novel seasonality of the UHI intensity for individual clusters in the form of hysteresis-like curves. We characterize the shape and identify apparent regional patterns.

KEYWORDS: Urban Heat Island, Statistics, Europe, Typology, Hysteresis, Seasonality

1 This chapter is based on the published paper Zhou, B., D. Rybski, and J. P. Kropp (2013). "On the statistics of urban heat island intensity". In: *Geophys. Res. Lett.* 40.20, pp. 5486–5491. DOI: 10.1002/2013GL057320

2.1 INTRODUCTION

The Urban Heat Island (UHI) is a phenomenon, where urban areas experience elevated temperatures relative to the surrounding hinterland (Oke, 1987). Most studies addressing the UHI effect can roughly be categorized into approaches of (i) numerical modeling the physical processes and (ii) empirical analysis, whereas the latter is either based on (a) air temperature records from weather stations or (b) Land Surface Temperature (LST) from remote sensing.

In the last decades, causative factors of the UHI effect given by Oke (1982) have been confirmed and further broadened through a variety of studies around the world. Compared to non-built surroundings, built-up areas of cities differ considerably in albedo, thermal capacity, roughness, etc. which can significantly modify the surface energy budget (Arnfield, 2003). A number of studies suggest that the intensity of UHI could be increased by anthropogenic heating (including contributions from vehicles, building sector, and human metabolism) (Sailor and Lu, 2004) as well as CO_2 and pollutants emissions (Taha, 1997; McCarthy et al., 2010).

In terms of methodology, physically-based numerical models simulate urban energy balance fluxes through the parameterization of urban surface processes (for an overview we refer to Masson, 2005; Grimmond et al., 2010). Empirical approaches, based on either air temperature or LST, attempt to reveal the linkage between the UHI intensity and various descriptive indicators of cities, spanning from biophysical properties (e.g. vegetation, imperviousness) to socio-economic indices (e.g. population density) (Weng et al., 2011; Holderness et al., 2013).

For a long time, UHI studies suffered from inconsistency and instability with regard to the urban-rural definition, hindering the intercomparison between results. Schwarz et al. (2011) compared indicators for quantifying the surface UHI with different urban-rural definitions and reported weak correlations among the indicators.

In any case, only individual, few, or up to hundreds of cities have been studied. We overcome this limitation in the number of considered cities by automatically quantifying the effect for all cities in Europe. Therefore, we apply a three step approach. First, we identify cities in the form of spatial clusters of urban land cover. Second, for each cluster we determine a boundary around the urban cluster of approximately equal area to the cluster area. Third, we calculate LST means of both, cluster and boundary, and define the UHI intensity as the difference between both mean temperatures. Applying this procedure for the entirety of Europe (constrained by the CORINE data, see Sec. 2.2), we are able to quan-

tify the UHI intensity for ~130,000 clusters in total from which there are almost 2,000 larger than 13 km².

We analyze two types of correlations. First, we investigate the UHI intensity of all clusters as a function of the cluster size. We find a characteristic increase with cluster area which we describe by a sigmoid curve. The UHI intensity is seasonally dependent and the saturation is maximal in summer (mean up to 3 °C) and considerably smaller in winter. Second, we study the UHI intensity of individual clusters as a function of the boundary temperature. Two findings are striking. On the one hand, not all cluster exhibit increasing UHI intensities with increasing boundary temperatures. For several, the opposite is found, i.e. decreasing cluster temperature with increasing boundary temperature (inverse UHI effect). On the other hand, we find seasonal differences. For the same boundary temperature, different UHI intensities are measured in spring and fall – a pronounced seasonality is found for many clusters, reflecting a characteristic signature and regional heterogeneity due to climate conditions.

2.2 DATA

Our work makes use of two major datasets, (i) land cover information and (ii) Land Surface Temperature (LST).

We base the identification of the urban clusters on the *CORINE land cover* data of the year 2006 at 250 m spatial resolution, covering 38 European Environmental Agency member states and cooperating countries except Greece, with a total area of 5.8×10^6 km² (Büttner et al., 2007). The 44 distinguished land use classes are subordinated into 5 main groups: (a) artificial surface, (b) agricultural areas, (c) forest and semi-natural areas, (d) wetlands, and (e) water bodies. Subsequently, the land cover data is reclassified into urban and non-urban ones as described in (Simon et al., 2010), i.e. binary data.

The LST data sets include the MYD11A2 Version 5 data from the Moderate Resolution Imaging Spectroradiometer (MODIS) on the NASA Aqua platform, providing 8-day-mean LST with a spatial resolution of ~1000 m, at around 13:30 and 01:30 local time, respectively. We assessed in this paper the LST daytime data from 2006 to 2011. The validation of LST Version 5 data with in-situ measurements indicated that the accuracy of LST data is better than 1 °C in most cases (Wan, 2008).

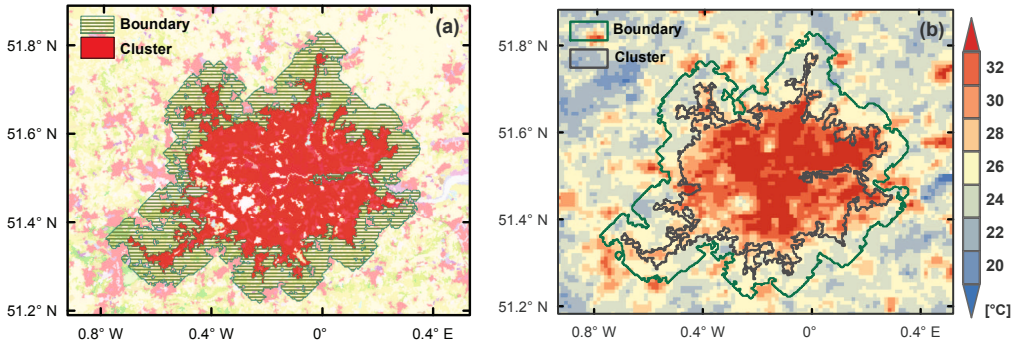

Figure 2.1: Example of a city cluster and a temperature pattern. (a) Urban cluster identified by CCA (red) and boundary (green hashed) for the Greater London Area with $l = 500\,m$. The urban area of other clusters (pink) are excluded from the identified boundary area. (b) LST for the same area as in (a) captured by the MODIS Aqua at ~13:30 local time from 02 June 2006 to 09 June 2006. The urban cluster and the urban heat distribution are in agreement.

2.3 METHOD

We define the UHI intensity of a city cluster (labeled with index i), as the difference between the temperature in the cluster and that of the surroundings, i.e. $\Delta T^{(i)} = T_C^{(i)} - T_B^{(i)}$, where $T_C^{(i)}$ and $T_B^{(i)}$ are mean temperatures of the cluster and the boundary, resp. This definition involves three steps:

1. Since administrative city boundaries differ from the actual extent, we define cities as clusters of urban land cover. Accordingly, to identify the European cities, we apply the City Clustering Algorithm (CCA) as proposed by Rozenfeld et al. (2008) to land cover rather than to population data, since fine-grained population census data are mostly unavailable. CCA involves a clustering parameter l determining up to which distance urban cells are connected with each other, i.e. urban cells within that distance are assigned to the same cluster. We specify $l = 500\,m$, i.e. double the resolution of the CORINE data. We denote the cluster size as $S_C^{(i)}$. The highly populated region of Belgium, the so-called Flemish Diamond (Brussels-Antwerp-Ghent-Leuven, see Appendix A, Fig. A.5) becomes the largest urban cluster under this initialization. Paris, the second largest urban agglomeration, is followed by London and Milan.

2. Analogously, we designate the surroundings of a cluster as the approximate equal-sized boundary area devoid of urban cells of other

clusters and sea waters. The boundary is built by consequently forming layers of cell size width around the city cluster (see Appendix A.1 for details). Consistently, we denote the boundary size as $S_B^{(i)}$. A similar UHI intensity calculation has been conducted by Peng et al. (2012), suggesting minor influence of the boundary size, i.e. 50 %, 100 %, and 150 % of the cluster size.

3. Since LST data are based on clear-sky conditions, we define a coverage threshold, i.e. the UHI intensity is regarded as valid only if the LST values are available for at least 50 % of the cluster and boundary cells. Moreover, quality control data are supplied with each MODIS pixel, classified into 4 levels (i.e. $\leqslant 1\,^\circ C$, $\leqslant 2\,^\circ C$, $\leqslant 3\,^\circ C$, $> 3\,^\circ C$) which we denote as ϵ. While calculating mean temperatures of clusters and boundaries, we use ϵ for weighting. First, the pixels with an mean LST error $\epsilon > 3\,^\circ C$ are filtered out. Then, the weights are assigned inversely proportional to ϵ^2, i.e. $W = 1/\epsilon^2$. The cluster temperature $T_C^{(i)}$ is therefore a W-weighted arithmetic mean of grid cell temperatures. Analogously, $T_B^{(i)}$ denotes the boundary temperature, considered as a measure for the *background temperature*. Finally, we calculate $\Delta T^{(i)} = T_C^{(i)} - T_B^{(i)}$.

Figure 2.1 (a) shows an example of a cluster identified by CCA and its boundary for the Greater London Area. As can be seen in Fig. 2.1 (b), the urban heat pattern mostly matches with the identified cluster, i.e. the city cluster exhibits elevated temperatures. The analogous Figure for mean summer temperatures can be found in Appendix A.2, Fig. A.2.

2.4 ANALYSIS

We systematically analyze the UHI intensities, ΔT, for all city clusters identified from the CORINE data by two means, (i) correlations with the cluster size and (ii) correlations with the boundary temperature. In the first case, the ΔT of all clusters are related to the corresponding cluster sizes at *one* observation (ΔT vs. S_C for a fixed date) and in the second case, the ΔT of one cluster are related to the corresponding boundary temperatures at *all* available observations (ΔT vs. T_B for a fixed cluster).

2.4.1 *UHI intensity and city size*

It is commonly believed that the UHI effect correlates with cluster size (Oke, 1973), but the characteristics of this correlation are poorly understood. Thus, we investigate how the UHI intensity depends on cluster

size by plotting ΔT as a function of the cluster size for all clusters and two observations in Fig. 2.2 (a) and (b). Various features can be observed. For large clusters the typical intensity reaches maximum values of ~2 °C in July [Fig. 2.2 (a)] and ~1 °C in February [Fig. 2.2 (b)]. There is considerable spreading of ~±2 °C, possibly reflecting local conditions.

In order to characterize the correlations, we perform a binning procedure. Choosing the number of bins and the number of clusters in the first bin (largest clusters), the number of clusters in subsequent lower bins increases exponentially. After identifying the bin limits, the cluster sizes and UHI intensities are averaged in each bin. This binning is motivated by the power-law size distribution of cities (e.g. Rozenfeld et al., 2011). The binned values in Fig. 2.2 (a) and (b) suggest a sigmoid relation on a logarithmic scale of cluster size. We employ the empirical function

$$\Delta T = \frac{a}{1 + (S_C/b)^{-c}} \,, \tag{2.1}$$

where a is the maximum value at which the fitting curve saturates and b, c determine the inflection and steepness of the curve, respectively.

Non-linear least square optimization is used for fitting Eq. (2.1) to the binned values. We find very good agreement between the fitted curves and the empirical values. However, individual city clusters can exhibit UHI intensities considerably above or below the fitting curve. Thus, the fit only characterizes typical behavior.

All parameters are studied time-dependently. In Fig. 2.2 (c) the parameter a, i.e. the saturation value, is plotted versus time for all available observations. The seasonal variability is reflected in the typical saturation UHI intensity with maximum values of up to 3 °C in summer (Jun-Aug) and down to 0.5 °C in winter (Dec-Feb). The other parameters exhibit seasonal variability as well. In Appendix A.3 we compare exemplarily LST with 2 m air temperature and find correlations between the temperature records but no correlations between the UHI intensities.

Despite good fitting performance, we need to mention that the analysis does not provide insights into whether there is actual saturation or not, since such a conclusion is restricted by the small number of large cities (as also seen in the power-law city size distribution). Nevertheless, it is apparent that the increase of UHI intensity with cluster size decelerates among larger city clusters.

2.4.2 *UHI intensity and surrounding temperature*

Since in the previous analysis much information has been averaged out by considering the ensemble of all clusters, next we study individual

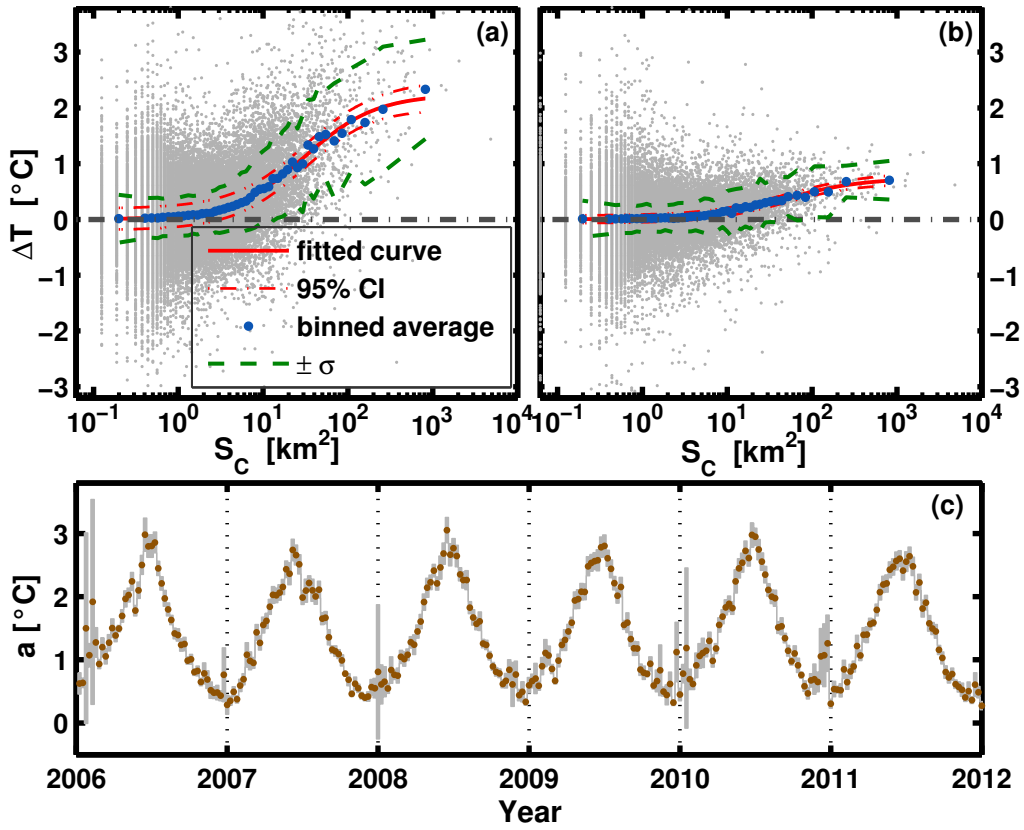

Figure 2.2: Urban Heat Island intensity as a function of cluster size and seasonal variability. Typical dependence for **(a)** summer days (04 July 2007 to 11 July 2007) and **(b)** winter days (02 February 2008 to 02 February 2008) at ~13:30 local time. Blue dots denote the mean of each bin with the data of individual clusters (grey dots) underlaid. The summer fitting curve exhibits a larger slope and asymptote. 95 % confidence intervals of the fitting based on binned data are shown by dashed-dotted lines. The standard deviations σ around the fits are shown by green dashed curves. **(c)** Time series of the parameter α which the fitting curve saturates at [see Eq. (2.1)]. The grey bars indicate the 95 % confidence intervals, suggesting a naturally larger uncertainty in parameter estimation in winter.

clusters. We select a cluster and plot the corresponding UHI intensity values of all observations versus the associated boundary temperature, in order to study ΔT given a certain temperature in the surroundings.

Figure 2.3 displays four examples. Since the raw values of ΔT versus T_B exhibit poor correlations in many cases, we calculate monthly means which are indicated by filled triangles and letters in Fig. 2.3. As can be seen, there are significant seasonal variations. In Paris [Fig. 2.3 (a)], the UHI intensity differs between $\Delta T \approx 3.3\,^{\circ}C$ in May and $\Delta T \approx 1\,^{\circ}C$ in September for the same boundary temperature of $T_B \approx 22\,^{\circ}C$. A numerical simulation performed by Georgescu et al. (2012) reported a maximum UHI intensity during summer for the Arizona Sun Corridor. The UHI was found to be less pronounced during spring and fall, and the least in winter.

In order to better characterize the UHI patterns, we perform a Fourier approximation of both, the time series of boundary temperatures, T_B, and UHI intensities, ΔT,

$$F(t) = \sum_{n=1}^{\nu} (g_n \cos \frac{2\pi n t}{P} + h_n \sin \frac{2\pi n t}{P}) + g_0 \,, \tag{2.2}$$

where $F(t)$ represents either, T_B or ΔT, $P = 46$ the number of observations for each year, t the times $\{t; t = 1, 2, ...276\}$, g, h the Fourier coefficients, and specifically g_0 is referred to as the mean of $F(t)$.

The order of the analysis, ν, is determined through the Akaike Information Criterion (AIC) (Akaike, 1973), which makes trade-offs between the number of regression parameters and fitting errors. Due to small sample size, we apply an adjusted version by Sugiura (1978). We find that for the majority of clusters, the boundary temperature and the UHI intensity can be well described with the second order Fourier Series ($\nu = 2$) involving five parameters each.

Examples of fitted Fourier curves are given by solid lines in Fig. 2.3. While in Fig. 2.3 (a) and (b) a positive relation can be observed (high UHI intensity coincides with high boundary temperature), in Fig. 2.3 (c) and (d) the opposite is found (but with smaller amplitude). This inverse UHI effect is also known as the *Oasis Effect* (Oke, 1987; Brazel et al., 2000; Georgescu et al., 2011), being attributed to the arid climate and the interplay with vegetation.

Beyond the positive or negative trend of UHI intensity vs. boundary temperature, the hysteresis-like shape of the fitted curve for Paris [Fig. 2.3 (a)] is evident and basically absent in the case of Milan [Fig. 2.3 (b)]. As a consequence, in the former, very different UHI intensities can occur given the same boundary temperature, i.e. higher UHI intensities in spring compared to fall. The directionality is always clockwise, in this

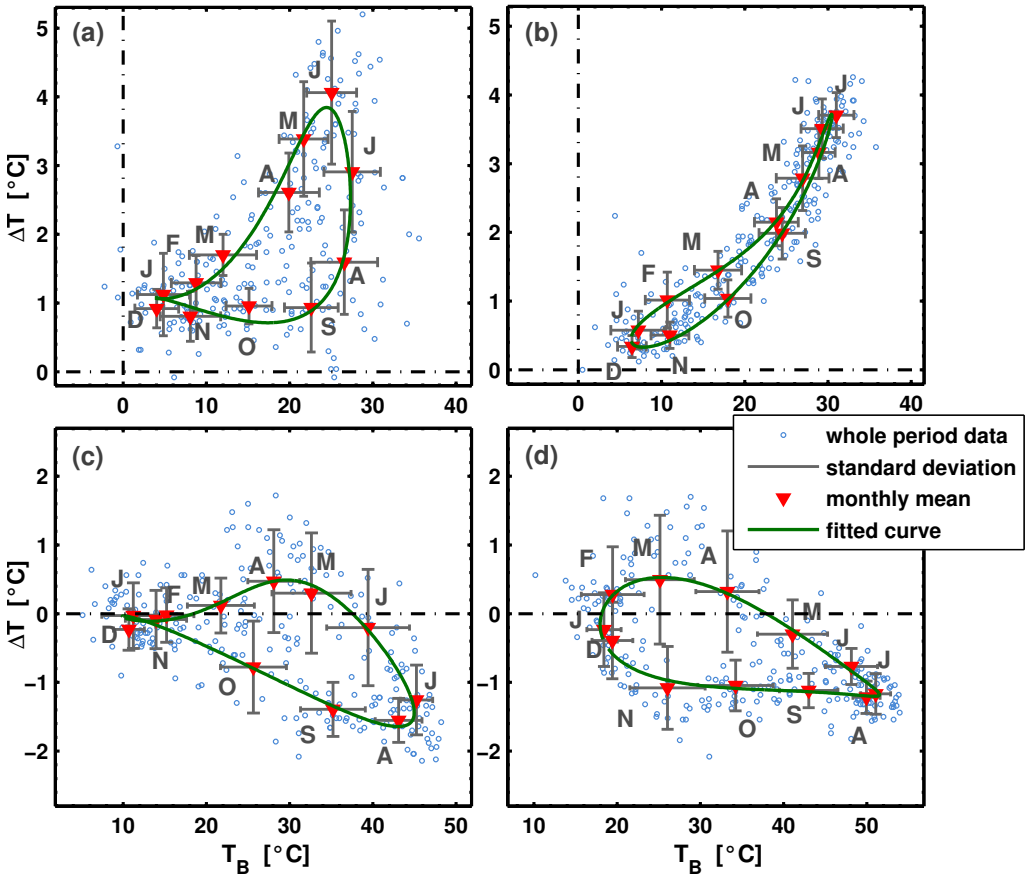

Figure 2.3: UHI characteristics of individual city clusters. The UHI intensity ΔT is plotted versus the boundary temperature T_B. The values are drawn as small circles, while monthly means are given as red triangles together with the standard deviations (grey error bars). The fitted curves according to Eq. (2.2) are plotted as green solid lines. **(a)** Paris, **(b)** Milan, **(c)** Madrid, and **(d)** Nicosia. The majority of city clusters exhibit a positive correlation between ΔT and T_B and clockwise hysteresis-like curves.

case with low UHI intensity in winter, higher values in spring, highest in summer, and vanishing intensity in fall. Depending on the location, similar behavior is found for many European city clusters.

The described seasonality in the shape of a hysteresis-like curve represents a phase shift between the UHI intensity and the boundary temperature. We hypothesize that this phenomenon could be due to a differing seasonality in the city and the surroundings, e.g. the temperature in the city follows the astronomical seasons driven by solar radiation and the temperature in the surroundings follows the meteorological seasons corresponding to the regional climate. However, our attempts to trace this claim down to differing vegetation properties of cities with more or less

pronounced seasonality were unsuccessful. Another explanation could be phenology, i.e. the different climate in the city and the surroundings could lead to differing onsets of phenological phases so that, e.g. the greening occurs sooner or later.

Last we want to verify how the UHI patterns are spatially distributed. Therefore, we classify the city clusters according to their hysteresis-like features. We perform the K-means clustering algorithm (Jain and Dubes, 1988) on the first harmonics g_0, g_1 and h_1 (6 parameters, counting ΔT and T_B separately) of the largest 2000 clusters. Each parameter is normalized before running the K-means clustering, i.e. $X^* = (X - \mu)/\sigma$, where μ is the mean of each parameter and σ is its standard deviation. To obtain an appropriate number of clusters (K), we use the mean silhouette $\bar{s}$ to evaluate the clustering performance as described by Rousseeuw (1987). We run the K-means clustering 200 times with predefined values of K to assess the non-deterministic nature of the algorithm. As can be seen in Fig. 2.4 (a), for $K = 7$, $\bar{s}$ is relatively large and exhibits the smallest variability, indicating a high clustering stability. City clusters are grouped into the same clusters when they are given the same cluster indices in most of the cases (more than 140 times out of 200 runs).

As can be seen in Fig. 2.4 (b–d), the various groups are situated in distinct geographical regions. Group 1 is mostly located in the North-West of Europe, i.e. British Isles and parts of the Atlantic Coasts. Cities of Group 2 are exclusively found in Scandinavia and the Eastern Baltic Coast. While Group 3 consists of Eastern European cities, Group 4 is found in Central Europe. Many large cities are assigned to Group 6, which also covers Central Europe. Group 5 and 7 are both situated in the Mediterranean regions but split into coastal and hinterland cities. Each group represents a specific type of UHI seasonality. Groups 1, 3, 4, and 6 are located in the temperate climate zone, which includes the majority of cities. For Group 2, the gentle rises of the curve [see Fig. 2.4 (i)] at both ends could be due to additional household heating in winter and prolonged daylight hours with an increase in absorbed radiation in summer, resp. Groups 4 and 6 exhibit similar hysteresis-like curves but with different magnitude [Fig. 2.4 (e) and (f)], which is in line with their common geography and the large fraction of big cities in Group 6. Similarly, Groups 5 and 7 differ in their proximity to the coasts but the seasonality is related [Fig. 2.4 (j) and (k)]. At water courses, part of the surface energy is converted into latent heat, resulting in lower mean temperatures. Although the grouping is based on the Fourier parameters only, the regional patterns emerge, suggesting that the UHI seasonality is not random, but stems from local climate conditions. Our results are consistent with earlier findings by Imhoff et al. (2010) who suggested

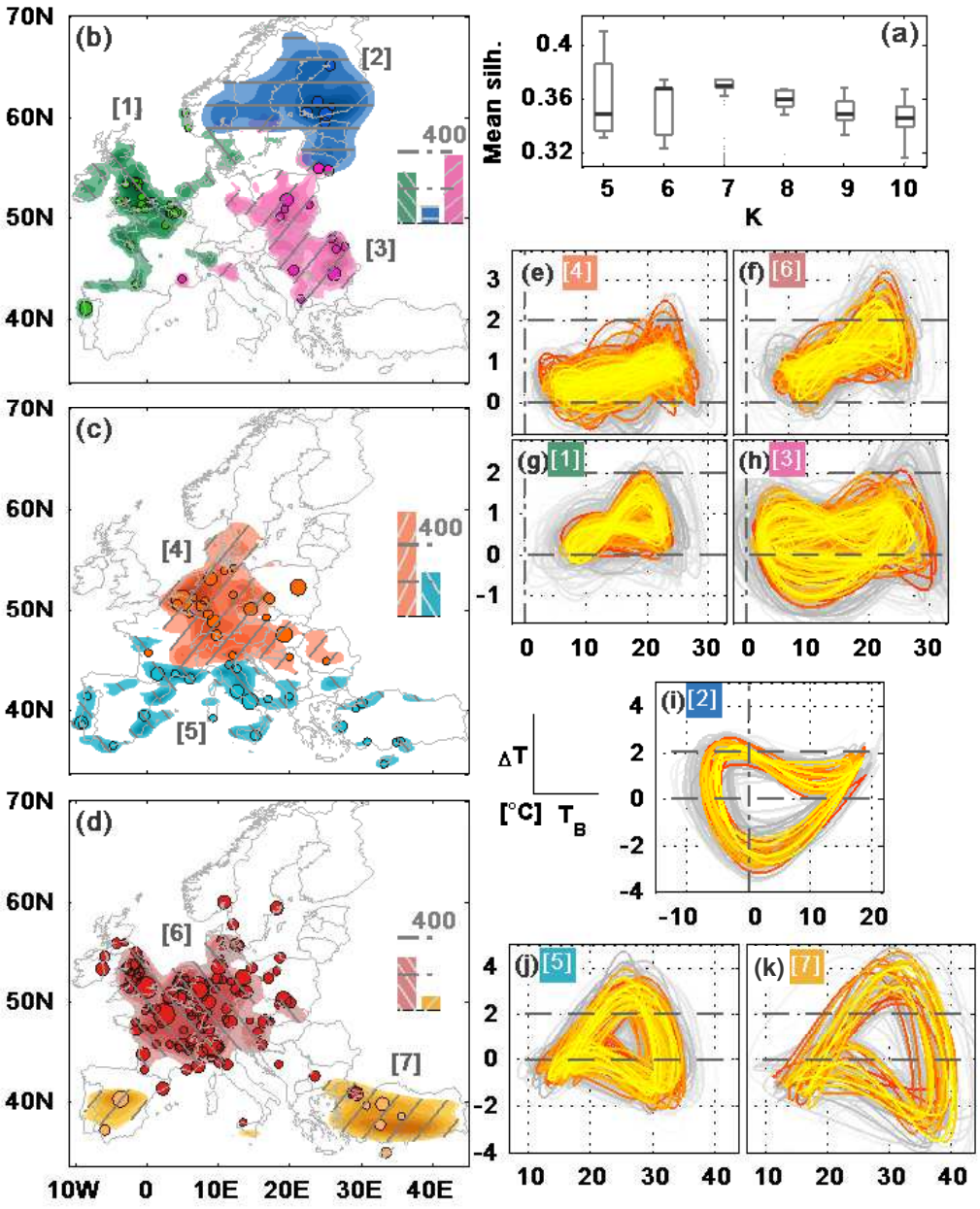

Figure 2.4: Regional patterns of UHI seasonality. **(a)** Boxplots of mean silhouette for varying cluster number K (200 runs for each K-value). For $K = 7$, the mean silhouette reaches a local maximum with the lowest variability. **(b)-(d)** Spatial distribution of the 7 groups identified using K-means clustering on the first Fourier coefficients. The largest 200 cities are marked with dots, where the size is proportional to the logarithm of the urban area. The panels include insets displaying the frequency of each group. In general, Group 1, 3, 4 and 6 are located in the temperate climate zone, whereas Group 2 is in the high latitudes. Group 5 and 7 are in the Mediterranean climate zone but differentiated into coastal and inland variants. There is an apparent concentration of large cities in Group 6. **(e)-(k)** Hysteresis-like curves of the respective clusters [as in Fig. 2.3]. The clusters whose data-to-centroid distances are below the 25th percentile, are drawn with colors varying from yellow (closest) to red. The remaining are set to background (grey).

a clear effect of the ecological setting (biomes) on diurnal and seasonal UHI intensities in the continental USA.

2.5 SUMMARY

While most studies investigating the UHI intensity are restricted to individual case studies or a limited number of cities, we introduce a statistical approach for the systematic assessment of the UHI effect of all cities and towns in Europe. This analysis is possible because it is entirely based on remote sensing data (land cover and land surface temperature) and the systematic treatment by means of the city clustering algorithm.

We study how the UHI intensity depends on the city cluster size. The empirical values suggest a sigmoid shape and the employed fitting function reaches an asymptotic constant value for large city clusters. In light of ongoing urbanization in many parts of the world, the actual shape of the relation between UHI intensity and city size is of particular interest. Further analyses are necessary to clarify if there is saturation for large city sizes or not. Individual city clusters exhibit intensities considerably above or below the typical size dependence, whereas the spreading is larger in summer. The identification of further explanatory variables of this variability is left for future studies.

The analysis of the UHI intensity depending on the boundary temperature leads to the surprising phenomenon of intra-annual variations of the UHI effect. For many city clusters, the same background temperature comes with very different UHI intensities in spring and in fall. We attribute this phenomenon to the astronomical seasonality of cities and the meteorological seasonality of the surroundings (implying a phase shift). We identify 7 city cluster types which exhibit regional separation. These findings suggest a climatological basis for this new phenomenon. So far, it must be left unanswered but the explanation could be an interesting starting point for future work.

3

URBAN FORM AND HEAT [1]

ABSTRACT

Urban climate is determined by a variety of factors, whose knowledge can help to attenuate heat stress in the context of ongoing urbanization and climate change. We study the influence of city size and urban form on the Urban Heat Island (UHI) phenomenon in Europe and find a complex interplay between UHI intensity and city size, fractality, and anisometry. Due to correlations among these urban factors, interactions in the multi-linear regression need to be taken into account. We find that among the largest 5,000 cities, the UHI intensity increases with the logarithm of the city size and with the fractal dimension, but decreases with the logarithm of the anisometry. Typically, the size has the strongest influence, followed by the compactness, and the smallest is the influence of the degree to which the cities stretch. Accordingly, from the point of view of UHI alleviation small, disperse, and stretched cities are preferable. However, such recommendations need to be balanced against e.g. positive agglomeration effects of large cities. Therefore, trade-offs must be made regarding local and global aims.

KEYWORDS: Urban Heat Island, fractality, anisometry, city size

1 This chapter is based on the published paper Zhou, B., D. Rybski, and J. P. Kropp (2017). "The role of city size and urban form in the surface urban heat island". In: *Sci. Rep.* 7.1, p. 4791. DOI: 10.1038/s41598-017-04242-2

3.1 INTRODUCTION

Urban Heat Island (UHI) is a commonly observed phenomenon worldwide, describing an elevated temperature of urban areas compared to their surroundings. It arises from anthropogenic modification of natural landscapes and the consequent atmospheric and thermophysical changes in the urban boundary layer (Oke, 1987). Understanding UHI is of great relevance in the current discussion on sustainable urban design. In particular, heat waves have been observed more persistent and more frequent in the last decades (Coumou and Rahmstorf, 2012; Lettenmaier et al., 2014), and are projected to intensify in the future (Meehl and Tebaldi, 2004). Furthermore, heat waves are shown to pose an added stress on cities (Li and Bou-Zeid, 2013), raising serious concerns regarding general well-being and potential threats to human health, which in turn demands effective adaptation measures to alleviate the UHI.

The UHI effect arises from the anthropogenic modification of natural landscapes and the consequent atmospheric and thermophysical changes in the urban boundary layer (Oke, 1987). The formation of UHI can be mainly ascribed to an increased absorption and trapping of solar radiation in built-up urban fabrics associated with high thermal admittance of construction materials and the urban canyon structure. Anthropogenic heat release from transport and buildings in the purpose of heating and air conditioning further exacerbate the UHI. Other factors, such as population density, built-up density, and vegetation fractions can also directly or indirectly contribute to the formation of UHI. However, studies based on different spatial scales, more precisely, the vertical scales (urban screen, -canopy, -boundary levels) and the horizontal scales (mirco-, local, regional scales) may lead to varying results on the individual contributions of each factor (Arnfield, 2003).

UHI studies can be approximately categorized in two domains regarding the number of investigated cities. On the one hand, case study work focuses on one or a few cities and assesses the UHI characteristics with a high level of detail. On the other hand, ensemble or cross-sectional studies investigate a large number of cities aiming at achieving an understanding of common characteristics or fundamental differences arising among them. The availability of remote sensing surface skin temperature with global coverage has given rise to a number of systematic empirical studies of the latter type. In the following we focus on surface skin temperature and only mention the type explicitly (i.e. surface or 2 m) when necessary.

A global UHI study across more than 400 big cities (Peng et al., 2012) revealed that the average annual intensity during daytime is higher than

during nighttime and that the daytime intensity correlates negatively with the difference of vegetation cover and activity between urban and suburban areas. Similar diurnal patterns were found in an analysis of 32 Chinese cities (Zhou et al., 2014). A follow-up work by Zhou et al. (2015) based on the same Chinese cities suggested an exponential decay of the UHI along urban-rural gradients, the rate and extent exhibit site-specific diurnal and seasonal variations. In Europe, the UHI intensity of urban agglomerations exhibits a size dependency, and can typically reach a maximum of approx. 3 °C in summer and 0.5 °C in winter (Zhou et al., 2013).

A study based on 65 cities in North America found that the annual mean daytime and nighttime UHI are positively correlated with the precipitation and the logarithm of population, respectively (Zhao et al., 2014). It was suggested that the enhanced aerodynamic roughness of densely vegetated rural areas in the humid climate zone (with abundant precipitation) leads to less efficient convection, which hampered the heat transfer from urban to rural areas and resulted in an intensified UHI. This outcome at first glance seems to differ from previous studies by Lee and Baik (2010) and Lemonsu et al. (2013) based on air temperature, stating that a deficit of precipitation in the summer leads to stronger rural warming than in urban areas, i.e. a diminished UHI. However, there are substantial differences between these studies besides the data type. The positive correlation in Zhao et al. (2014) is regressed out of annual mean data (UHI intensity against precipitation) among scores of cities (cross-sectional), whereas the studies by Lee and Baik (2010) and Lemonsu et al. (2013) are based on data of individual case study cities across time (temporal).

Another global study comprehensively assessed the dependence of UHI on various urban intrinsic factors, regardless of geographic and climatic factorsClinton and Gong, 2013. Night light, urban area and vegetation are, inter alia, dominant ones accounting for the UHI or urban heat sinks, whereas population and urban structure were found to be of less relevance.

These studies have in common that land cover data is combined with remotely sensed surface skin temperature, i.e. urban land cover is used to define the physical extent of urban areas enabling to systematically extract the temperatures inside the cities and in their rural surroundings. To date, this methodology is an established standard protocol for robustly benchmarking the thermal stress across cities, and for deciphering statistical features of the UHI associated with biophysical and socio-economical indicators. These merits can scarcely be promised by the conventional case study work.

In order to gain an understanding of the UHI phenomenon and its relevance in terms of urban design, insights about the influencing factors are necessary. On the one hand, the UHI intensity of a city is subject to the empirical metrics and indicators used for quantifying the phenomenon (Schwarz et al., 2011). On the other hand, while analyzing its physical essence, it is determined by a variety of factors which can roughly be categorized into (i) external and (ii) intrinsic ones (Oke, 1982). External factors include location (lat./lon.) (Wienert and Kuttler, 2005), background climate (in particular wind) (Imhoff et al., 2010; Zhou et al., 2013), proximity to water courses (associated with sea- or lake-breeze circulation), etc., whereas intrinsic ones depict city-specific features (e.g., city size, land cover fractions, anthropogenic heat releases) which, despite being outcomes of long-run urbanization, can be regulated and reshaped.

How to alleviate the UHI effect is another issue of considerable interest. Local interventions (e.g. parks of various sizes, green and cool roofs) are shown to have a limited influence on local climate. The cooling distance, i.e. the maximum distance within which the cooling effect of such green spaces can still be detected, ranges from tens to hundreds meters (Feyisa et al., 2014; Zupancic et al., 2015). Possibilities to influence intrinsic properties – including the overall urban form – are very limited in cities of developed countries due to small growth rates or even negative ones. In contrast, dramatic urbanization is taking place in developing countries, so that insights about how the urban form affects UHI intensities could provide guidance for the large scale planning of cities, where there is a great demand of new infrastructure.

Thus, we search for traceable signatures between features of urban form and UHI intensity. We consider three features of urban form which break down the spatial shape of the urban extent into single values. First, *city size*, since it has been shown previously that larger cities tend to have higher UHI intensities. Second, the *fractal dimension* which represents an established measure to characterize the compactness of a city. Third, *anisometry* which we revealed as an important measure of city shape, quantifies to which extent a city's length is greater than its width. Examples include cities extending along valleys, rivers, country borders, etc. As we show below, interactions among the three indicators need to be taken into account which implies that the influence of each of them on the UHI intensity cannot be separated.

3.2 DATA AND METHODS

3.2.1 *Datasets*

CORINE urban morphological zones (UMZ) 2006 data at 250 m spatial resolution are used for delineating urban areas in Europe. For countries where raster UMZ data are not available, e.g. UK and Switzerland, we generated the UMZ data based on the CORINE Land Cover 2006 data following the method described in Simon et al. (2010). The processed UMZ data, containing binary urban/non-urban information for 38 European countries, are projected to the sinusoidal coordinate system which is consistent with that used in the LST data.

We used the MODIS Aqua 8-day composite (MYD11A2, Version 5) LST products for the summer months (June-July-August, JJA) from 2006 to 2013, in total 104 observations across 8 years. The data are at 926.6 m $\approx$ 1 km spatial resolution, and are measured at 13:30 (daytime) and 01:30 (nighttime) local solar time. In this study, we focus on the daytime LST, because the daytime surface UHI is more pronounced than that of the nighttime. Complementary results based on nighttime LST can be found in Appendix B.1. According to the pixel-wise LST error flag inherent in MYD11A2, we disregard pixels with LST error $>$ 2 K. We also omitted pixels with view zenith angle $>35^\circ$ to minimize the anisotropy bias caused by the view angle, while guaranteeing a sufficient data quantity for further analyses (Hu et al., 2014). Based on the processed LST data, multi-annual summer mean LST is calculated.

3.2.2 *Urban heat island (UHI) intensity*

We followed the methodology employed in previous studies (Peng et al., 2012; Zhou et al., 2013, 2016) to calculate the surface UHI intensity. Cities are defined via the City Clustering Algorithm (CCA) (Rozenfeld et al., 2008, 2011; Fluschnik et al., 2016) based on the UMZ data, with a clustering parameter $l = 250$ m, being in accordance with the spatial resolution. According to CCA, any pair of urban cells with a distance no larger than l are assigned to the same urban cluster. We defined an equal-area belt region around an identified city cluster as its rural or suburban reference, devoid of water courses and urban pixels of other clusters. The surface UHI intensity of an urban cluster is defined as the difference between average urban and rural temperature (Zhou et al., 2013, 2016), i.e. $\Delta T = T_C - T_B$. In contrast to previous studies (Zhou et al., 2013, 2016), here we base our analysis on temporally aggregated temperature data, namely multi-annual summer mean LST. Moreover, in

contrast to Zhou et al. (2013), here we disregard small city clusters and consider only the largest 5,000 clusters corresponding to cluster areas $S_C > 6.1\,km^2$.

3.2.3 *Fractal Dimension*

We used the box-counting algorithm to compute the fractal dimension D_f for each urban cluster (Bunde and Havlin, 1996). Therefore, we count the number of boxes N of size $r \times r$ necessary to fully cover the considered urban cluster. Assuming $N(r) \sim r^{-D_f}$, the linear regression to $\ln(N)$ vs. $\ln(r)$ provided the slope which corresponds to the fractal dimension D_f. The conventional method is to initialize r to the minimum cell size and stepwise double it until $N(r) = 1$. It turned out that this 2-based exponential sampling method led to a discreteness artefact and denser sampling was more robust.

Thus, we adopted a denser sampling strategy by incrementing r by 1 and omitting any point $(r,N(x))$ if the count $N(r) = N(r-1)$. Sampling can be seen in Fig. 3.1 (d–f).

3.2.4 *Anisometry*

We computed the anisometry (A) of city clusters similar to the method in Medalia and Hornik (1972). We defined the anisometry of a city cluster as the ratio of the city cluster's maximum Feret's diameter to its minimum Feret's diameter. The Feret's diameter is the distance between two parallels tangent to an object along a certain direction. In order to illustrate the relative stretch of clusters, we drew the equivalent ellipse of a city cluster by assigning the maximum and minimum Feret's diameters to the axes of the ellipse [see Fig. 3.1 (a–c)]. The ellipse centers at the centroid of a city cluster. Analog to the cluster size, we use the logarithms of anisometry ($\ln A$) throughout the study to reduce the skewness.

3.2.5 *Quantile regression*

Quantile regression is a method for estimating the impact of observed covariates on quantiles of the response variable (Koenker and Bassett, Jr., 1978; Koenker and Hallock, 2001). In contrast to ordinary least squares regression, quantile regression is particular applicable for the model with heterogeneous variance, e.g. in the presence of heteroscedasticity, where the former approach usually misestimates the real relationship or fails to detect the nonzero changes (Cade and Noon, 2003). Quantile

regression finds wide application in disciplines, where data are seldom normally distributed, e.g. ecology (Cade and Noon, 2003), climatology (Donner et al., 2012; Mueller and Seneviratne, 2012), etc. Assuming a regression function $Y = \beta X + \epsilon$. The estimators for the quantile τ, i.e. β_τ are obtained by minimizing the sum of asymmetrically weighted absolute residuals. The weights are given by the function ρ_τ (Koenker and Hallock, 2001).

$$\beta_\tau = \arg\min \sum_{i=1}^{n} \rho_\tau(Y_i - \beta X_i)$$

3.2.6 *Multi-linear regression*

We employed the general multi-linear model to quantify the relation between the UHI intensity ΔT and predictive variables – the logarithm of city size $\ln S_C$, fractal dimension D_f, and the logarithm of anisometry $\ln A$. We use the general ansatz

$$\begin{aligned}\Delta T = a + b\ \ln S_C + c\ D_f + d\ \ln A + e\ D_f\ \ln S_C + f\ D_f\ \ln A \\ + g\ \ln S_C\ \ln A + h\ D_f\ \ln S_C\ \ln A\ ,\end{aligned} \quad (3.1)$$

where $a, \ldots, h$ are eight parameters, and e.g. $D_f\ \ln S_C$ is the interaction between fractal dimension and city size. We used the forward and backward stepwise regression to determine the variables in the multi-linear model. The Bayesian Information Criterion was used to add and remove terms in the model, and to avoid data-overfitting.

3.3 RESULTS

Following the methodology employed in previous studies (Zhou et al., 2013, 2016), we combine land cover data with remote sensing temperature data and define the *surface UHI intensity* ΔT as the difference between the average temperature within the considered urban cluster and the average temperature within an equal area belt around it (see Methods Section for details). In contrast to Zhou et al. (2013), here we consider the 5,000 largest urban clusters in Europe and average the summer months (June, July, August) daytime observations from 2006 to 2013. In the following we investigate how the UHI intensity ΔT depends on (i) the size, (ii) the fractality, and (iii) the anisometry of the city clusters. Therefore, we need to measure the three quantities for all considered city clusters.

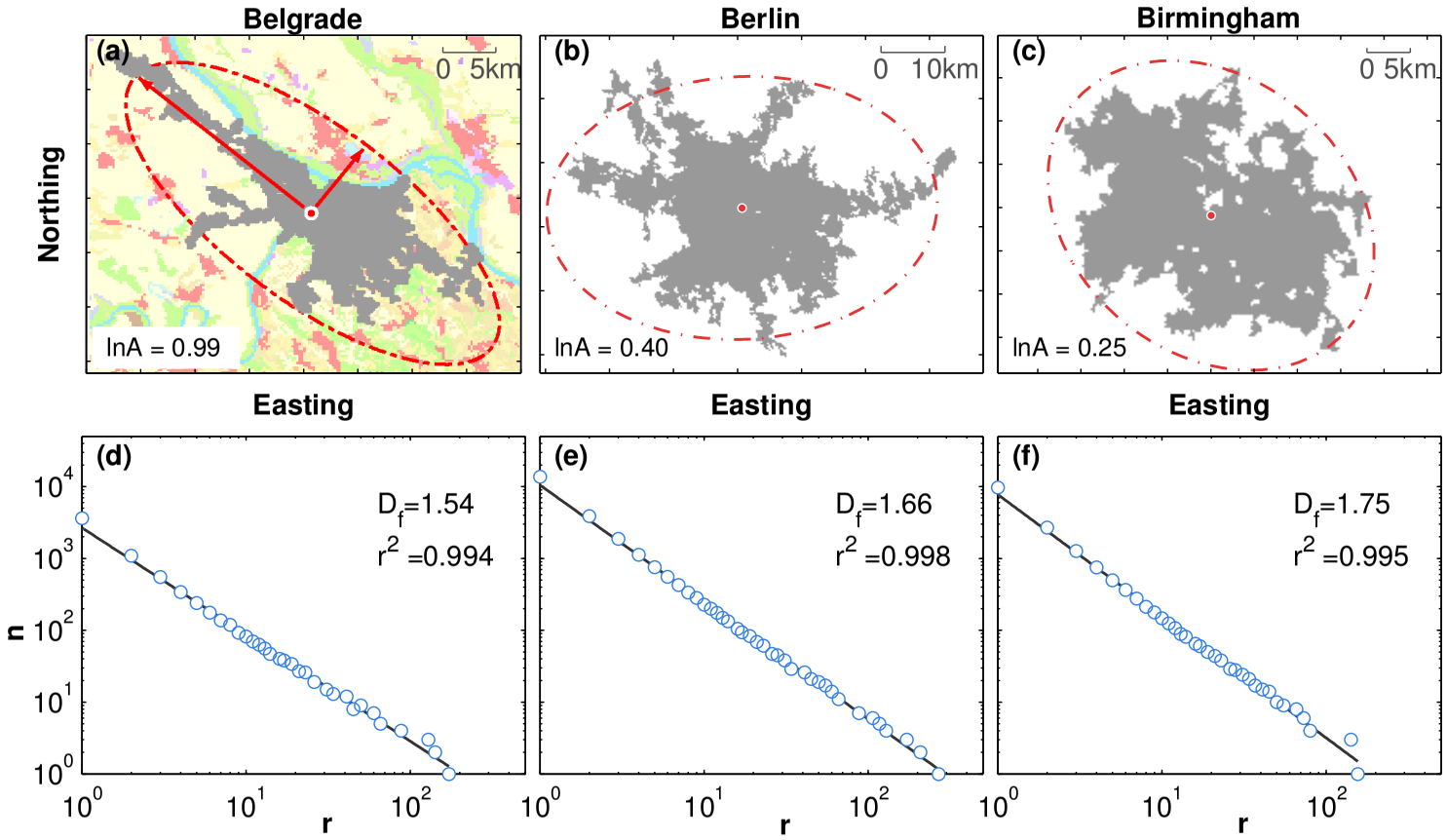

Figure 3.1: Example of city clusters and box-counting results leading to the fractal dimension (D_f), as well as the logarithm of anisometry ($\ln A$). The upper row, panels **(a)-(c)**, shows the city clusters as obtained applying CCA to the CORINE land cover data, for the cities of Belgrade, Berlin, and Birmingham. The red ellipse is the equivalent ellipse of the urban cluster, determined by following Medalia and Hornik (1972).The lower panels **(d)-(f)**, depicts the number of boxes necessary to cover the clusters as a function of the box size in double-logarithmic scale for the corresponding cities.The fractal dimension is obtained from the slope of linear regressions (straight lines).As can be seen from these examples, clusters vary in size, fractal dimension, and anisometry.

(i) The *city size* S_C is simply given by the number of cells constituting the city clusters multiplied by the area of each cell, $6.25 \times 10^{-2}\,\mathrm{km}^2$. Due to Zipf's law for cities (Auerbach, 1913; Zipf, 2012; Rozenfeld et al., 2011; Rybski, 2013; Fluschnik et al., 2016) there are many small cities and few large ones so that we use the logarithm of city size, $\ln S_C$, in order to reduce the skewness.

(ii) We compute the *fractal dimension* using the box counting method, assuming $n \sim r^{-D_f}$, where n is the number of (square) boxes of side length r necessary to cover the structure, see Methods Section. In Fig. 3.1 (a–c) we show 3 examples of city clusters differing in size and fractality. The corresponding box-counting results for varying r are shown in Fig. 3.1 (d–f) and linear regressions in the log-log scale provide the slopes which are an estimate of the fractal dimensions D_f. The fractal dimension D_f can be considered as a measure of compactness, i.e. compact cities have usually large values of D_f.

(iii) The *anisometry* A of a city cluster is defined as the eccentricity of the equivalent ellipse of the city cluster, i.e. the ratio of major axis to its minor axis, see Methods Section. It is a measure for the extent to which the city deviates from an approximate circular shape ($A \to 1$), i.e. to which extent it's length is greater than its width ($A > 1$). Figure 3.1 (a–c) also illustrates the anisometry by means of ellipses. As can be seen, the stretched shape of Belgrade is reflected in a higher value of A. Again, we use the logarithm, i.e. $\ln A$.

Figure 3.2 consists of scatter-plots where the daytime UHI intensity is plotted separately vs. the three quantities – binned values and regressions are included for illustrative purposes. In Fig. 3.2 (a), ΔT is displayed as a function of the city size. As expected and consistent with previous work (Oke, 1982; Park, 1986; Imhoff et al., 2010; Clinton and Gong, 2013; Zhou et al., 2013; Zhao et al., 2014), the UHI intensity increases with city size and doubling the city size leads to approximately 0.4 °C additional UHI intensity. Studies of UHI intensities in relation to population size go back to Oke (1973), who reported both a logarithmic and a power-law (exponent $\approx 1/4$) relation between UHI intensity and population. In Fig. 3.2 we also include quantile regressions and find that there is heteroscedasticity in the form of stronger spreading of ΔT among large cities.

In Fig. 3.2 (b) the influence of the fractal dimension on the UHI intensity is shown. In the range where most cities are found, ΔT typically increases by roughly 2 °C with increasing D_f. This finding suggests that

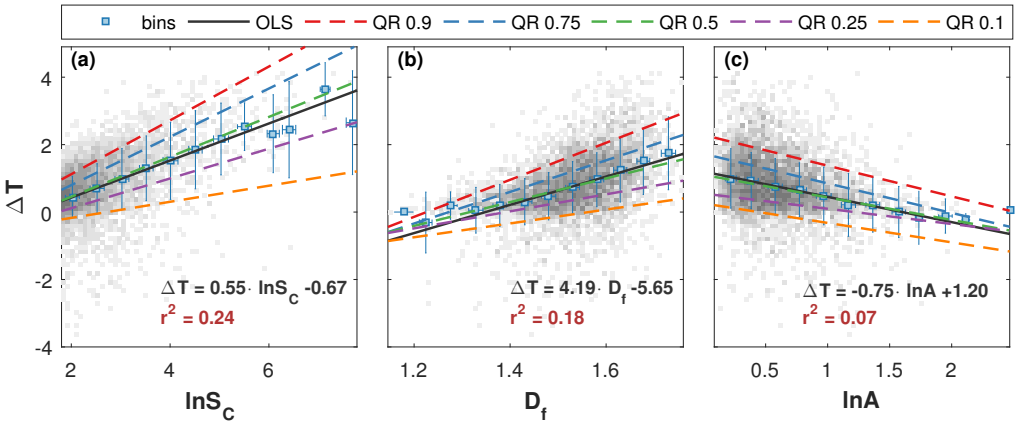

Figure 3.2: UHI intensity (ΔT) as a function of (a) logarithm of urban cluster size $\ln S_C$, (b) fractal dimension D_f, and (c) logarithm of anisometry $\ln A$, and quantile regressions (QR) as well as ordinary least square regression (OLS). The grey pixels indicate the number of cities that are covered by them (the darker, the higher the density). For visual purpose, the symbols represent averages in equal-width bins and their error-bars represent the standard deviations. The straight lines are linear regressions to raw data, whereas the dashed lines represent the results of quantile regressions. For the quantiles 0.1 and 0.9 we obtained the following slopes: (a) [0.24,0.80], (b) [2.05, 5.50], (c) [-0.58, -0.91].

more compact cities have more pronounced UHI intensities. The literature on UHI intensity and fractality is very limited. The fractal analysis of surface skin temperature related to vegetation abundance (Weng et al., 2004) cannot be easily compared with our results since here we study the urban cluster which leads to the UHI. In a more general sense, the influence of urban form has been studied for the example of Beijing metropolitan area (Yang et al., 2016), and it has been reported that, compared to a compact city, a dispersed one is efficient in reducing mean urban heat island intensity, but affects the thermal feedback at the regional scale. Last, in Fig. 3.2 (c) ΔT is plotted as a function of the anisometry. As one would expect from intuition, the UHI intensity decreases with increasing anisometry, by approximately 1.5 °C in the shown range. Thus, more circular cities seem to exhibit elevated UHI intensities. The above mentioned heteroscedasticity is also observed in Fig. 3.2 (b) and (c), and the spreading of ΔT is wider among cities with larger D_f and smaller $\ln A$.

Correlations among the three quantities $\ln S_C$, D_f, and $\ln A$ require a more complex analysis. While anisometry and cluster size are essentially uncorrelated with a Pearson correlation coefficient ρ of -0.05 [see Appendix B, Fig. B.2 (a)], fractal dimension and anisometry ($\rho = -0.61$) as well as cluster size and fractal dimension ($\rho = 0.30$) exhibit moderate cor-

relations, as shown in Appendix B, Fig. B.2 (b) and (c), respectively. On the one hand, cities with lower fractal dimension tend to exhibit higher anisometry, i.e. more compact cities also tend to be more circular. This correlation is the strongest among the three variables considered. On the other hand, larger cities tend to exhibit higher fractal dimensions, i.e. they are more compact. It has been reported previously (Shen, 2002; Encarnação et al., 2012; Rybski et al., 2013) that city size and fractal dimension are positively correlated, i.e. larger cities in terms of population or urbanized area have higher fractal dimensions.

Thus, we employ multi-linear regression in order to characterize the complex interplay between the UHI intensity and the three factors. Linearity, however, still represents an approximation – but a reasonable one – as will be discussed with the following example. The correlations between UHI intensity and city size S_C have been fitted according to a log-logistic function (Zhou et al., 2013)

$$\Delta T(S_C) = \frac{a}{1 + (S_C/b)^{-c}} \quad , \tag{3.2}$$

where the parameters a, b, c determine the saturation value, the inflection point, and the steepness, respectively. However, the sigmoid-shape of Eq. (3.2) takes only effect far from the inflection point, i.e. $S_C \ll b$ or $b \ll S_C$. (i) For small clusters [$\ln(S_C) \to -\infty$] the accuracy of ΔT is limited by the resolution of land surface temperature data ($\approx$1 km$\times$1 km). In order to have a reasonable estimate, both cluster and belt temperature should be based at least on a few gridded values. (ii) Due to Zipf's law for cities (see above), for large clusters [$\ln(S_C) \to \infty$] the sample of cities reduces considerably. As a consequence, there are simply too few data points carrying information on whether or not $\Delta T(S_C)$ saturates. Thus, it is justified to expand Eq. (3.2) in the mid-range. Since around the inflection point the logistic function $F(x) = 1/(1 + \exp(-x))$ can be approximated by $F(x) \approx 1/2 + 1/4x$ (Weisstein, 2016) , Eq. (3.2) can be approximated by the logarithmic function

$$\Delta T(S_C)/a \approx c/4 \cdot \ln(S_C/b) + 1/2 \quad \text{for } S_C \approx b \tag{3.3}$$

which corresponds to a linear polynomial of $\ln S_C$.

After having motivated the *linear* approximation, we finally apply the multi-*linear* regression. In the absence of correlations among the intrinsic urban factors a simple linear combination according to $\Delta T = a + b \ln S_C + c\, D_f + d\, \ln A$, where $a, \ldots, d$ are parameters, would be sufficient. Due to the correlations, all interaction terms need to be taken into account. By *interaction* the statistical correlations between 2 independent variables is meant as it occurs in multicollinearity. We performed

a stepwise linear regression with interactions (see Sec. 3.2.6) to all 5,000 considered city clusters and obtain

$$\Delta T = -1.86 - 0.85 \ln S_C + 1.11 D_f + 1.45 \ln A + 0.83 D_f \ln S_C - 1.17 D_f \ln A \tag{3.4}$$

with $R^2 = 0.34$, all fitting parameters carry the unit °C. According to the analysis, only six out of eight terms contribute statistically to ΔT. These are the offset, the three urban factors, and the interaction terms between fractal dimension and size as well as between fractal dimension and anisometry. Consistent with the absence of correlations between size and anisometry [see Appendix B, Fig. B.2 (a)], the corresponding interaction term is missing. Similarly, the three-point-correlation term proportional to $D_f \ln S_C \ln A$ statistically does not add information.

As a consequence of the remaining interaction terms, the (linear) dependence of ΔT on e.g. D_f has a varying slope depending on the considered values of $\ln S_C$ and $\ln A$. For fixed values, e.g. $\ln S_C = 5$ and $\ln A = 0.5$, Eq. (3.4) simplifies to $\Delta T(D_f) = -5.38 + 4.67 D_f$. However, for other values of $\ln S_C$ and $\ln A$ both, slope and intercept, are different. A similar effect occurs for $\Delta T(\ln S_C)$ and $\Delta T(\ln A)$. Due to this complex interplay, it can hardly be visualized in two dimensions how the UHI intensity depends on all of the three intrinsic urban factors.

Following the above example, Figure 3.3 illustrates the linear dependencies of the UHI intensity on one urban factor when the other two are kept constant. Therefore, we fix two of the factors, simplify Eq. (3.4) to a linear form depending only on the third factor, and extract slope and intercept. Then we rasterize the two fixed factors, repeat the procedure, and display the slope and intercept as shown in Fig. 3.3.

In Fig. 3.3 (a) we observe that $\Delta T(D_f)$ is steepest for large cities with small anisometry and less steep for small cities with large anisometry. The diagonal stripes are due to the interactions of D_f with $\ln S_C$ and $\ln A$. In Fig. 3.3 (b), $\Delta T(\ln S_C)$ has its largest slope for compact cities, i.e. large D_f, which only occurs in combination with small anisometry. In this case, the slope only changes along D_f (horizontal stripes) – interactions with $\ln A$ have not been found. Lastly, the slope of $\Delta T(\ln A)$ is mostly negative [Fig. 3.3 (c)], with the steepest negative slopes observed for cities with a large fractal dimension. The vertical stripes illustrate the interactions with D_f, i.e. there would be no stripes in the absence of interactions.

At this point we still do not know which of the three factors has the strongest influence. The reason is that due to different ranges (e.g. D_f is roughly within 1.2 and 1.8, while $\ln A$ is roughly in the range between 0 and 2.5), the parameters obtained in Eq. (3.4) are not comparable. Thus,

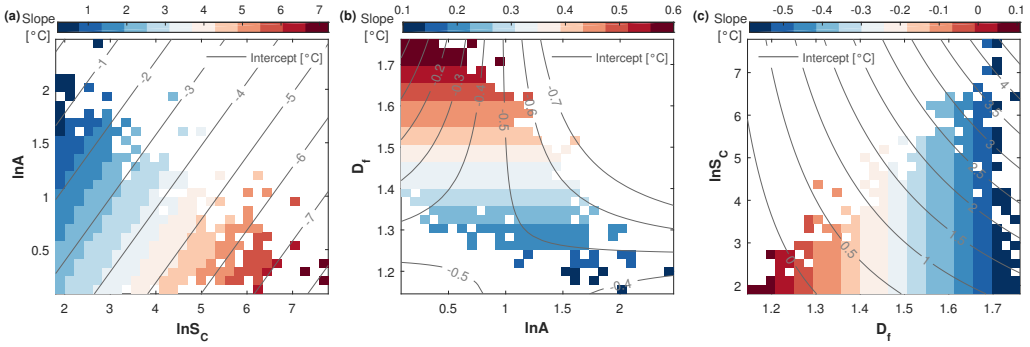

Figure 3.3: Visualization of Eq. (3.4) as obtained from multi-linear regression for $\Delta T(\ln S_C, D_f, \ln A)$. The panels display the slope (colors) and the intercept (countour lines) of the linear relation between ΔT and one urban factor given the other two urban factors are kept constant. For fixed values of $\ln S_C$ and $\ln A$, Eq. (3.4) simplifies to (a) $\Delta T = \text{slope} \cdot D_f + \text{intercept}$. Rastering through the relevant ranges of $\ln S_C$ and $\ln A$ we show for each combination the corresponding slope and intercept. Analogously, panels (b) and (c) represent $\Delta T = \text{slope} \cdot \ln S_C + \text{intercept}$ and $\Delta T = \text{slope} \cdot \ln A + \text{intercept}$, respectively. Combinations which do not occur in the data are kept white. Please note that the range of values covered by the color bar differs among the panels; the figure illustrates the regression, Eq. (3.4) – not the actual data.

we repeat the multi-linear regression, but normalize the data previously to zero mean and unit standard deviation, e.g. $D_f^* = (D_f - \langle D_f \rangle)/\sigma_{D_f}$ where $\langle D_f \rangle$ is the mean and σ_{D_f} the standard deviation. Then we obtain

$$\Delta T = 0.71 + 0.33\ \ln S_C^* + 0.23\, D_f^* - 0.10\ \ln A^* + 0.06\, D_f^*\ \ln S_C^* - 0.03\, D_f^*\ \ln A^* \tag{3.5}$$

whereas the 95% confidence interval of the parameters is ± 0.03 or smaller. Now we can insert the average values $\langle \ln S_C^* \rangle$ and $\langle \ln A^* \rangle$ as typical values (which are both zero due to normalization) and obtain $\Delta T = 0.71 + 0.23\, D_f^*$. Accordingly, from analogous considerations for the other factors, we see that city size has the strongest influence ($0.33\ \ln S_C^*$), followed by fractality ($0.23\, D_f^*$), and smallest is the influence of anisometry ($-0.10\ \ln A^*$). Consistent with Fig. 3.2, ΔT increases with $\ln S_C^*$ as well as with D_f^* and decreases with $\ln A^*$. However, due to the above discussed interaction, the ranking is only valid for typical cities in our sample and including further small cities could affect the overall outcome. Moreover, we perform a rather basic normalization and we cannot exclude that the skewed distributions could affect the resulting parameters.

Since it has been argued that the UHI intensity based on daytime LST are overestimated (Mohan and Kandya, 2015), we also included an analysis based on nighttime LST in Appendix B.1.2. Due to overall weaker

intensities, the dependencies on the city size, fractality, and anisometry are less pronounced. Nevertheless, the relative contributions are consistent with the daytime results.

Certainly, the regression Eq. (3.4) and (3.5) can hardly capture the huge variations of urban form and heat island intensities for entire Europe. For instance, Berlin ($S_C = 854.69\,km^2$, $D_f = 1.66$ and $\ln A = 0.4$) is the largest city among the ones shown in Fig. 3.1, the measured and predicted temperatures are 3.12 °C and 3.34 °C. For Belgrade ($S_C = 227.56\,km^2$, $D_f = 1.54$ and $\ln A = 0.99$) and Birmingham ($S_C = 606.38\,km^2$, $D_f = 1.75$ and $\ln A = 0.25$), the measured ΔT are 1.39 °C and 3.75 °C; the predicted ΔT are 1.82 °C and 3.82 °C, respectively. The three examples suggest that the predictive power of the global regression model, i.e. based on the full sample of cities, is rather limited, which could be due to regional inhomogeneities.

Therefore, we adopted two different sampling strategies to assess the robustness of the results against the regional inhomogeneities. We first divided the study area into 9 zones of similar number of cities and applied the multi-linear regression in Eq. (3.5), independently. As shown in Fig. 3.4 (a), city size dominates in most cases, followed by fractal dimension, whereas in South Europe anisometry has a larger impact on the UHI. Second, we created subsamples of varying number of cities with and without replacement and applied stepwise regression to the subsamples. Figure 3.4 (b) and (c) reveal that as the sample size increases, our model in Eq. (3.5) tends to appear more frequently. We conclude that our model has a good global performance, while at local scale the model should be used with certain precaution.

3.4 DISCUSSION

In summary, we explore the recently established methodology, which systematically combines urban land cover and remote sensing surface skin temperature, in order to characterize the UHI intensities of a vast number of cities. Studying the largest 5,000 European urban agglomerations, we find a complex interplay among the correlations with intrinsic urban factors. Among the three considered large scale urban features, typically city size has the strongest influence, followed by the fractality – and the anisometry presents the weakest influence. That is, in general, the larger, the more compact (high fractal dimension), and the less stretched (small anisometry) the cities are, the stronger their UHI intensity tends to be.

Our empirical findings on the dependence of the UHI intensity on the city size and form could be attributed to the scale effect of convection

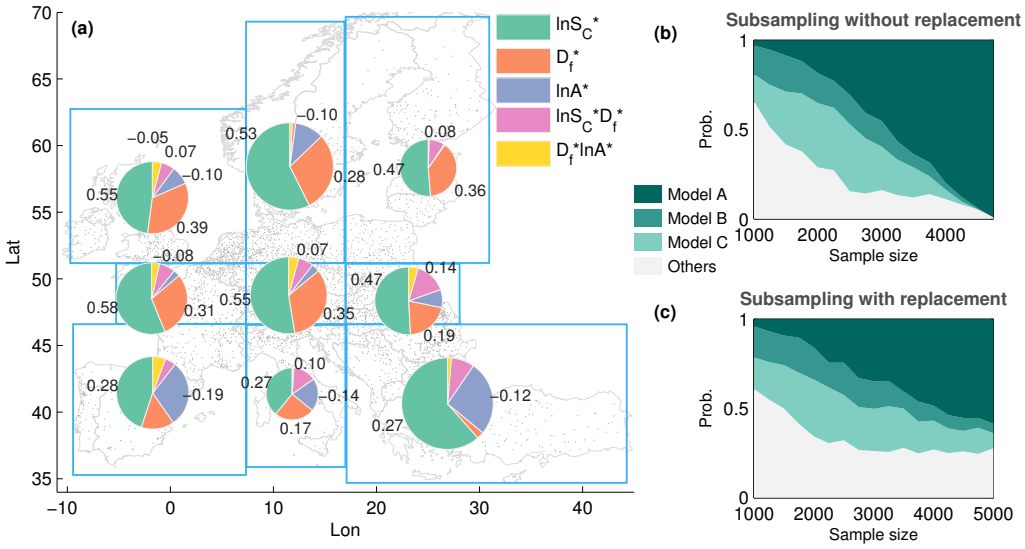

Figure 3.4: Robustness of multi-linear regression under spatial and random sampling. In panel (a) we divide the study area into 9 partitions (blue rectangles) of similar size and separately apply linear regression according to Eq. (3.5) to the normalized quantities. The pie-charts depict the resulting coefficients (for negative values the absolute value has been taken). The area of the pie-charts is proportional to the number of cities in the partition. Only statistically significant coefficients (at 95 % level) are labeled. City size dominates in most cases, followed by fractal dimension, whereas in the south the anisometry becomes important. In panels (b) and (c) the results of stepwise regression on randomly sampled cities (500 repetitions) without and with replacement, respectively, are displayed. In both cases, as the sample size increases, Model A i.e. Eq. (3.5) becomes the most probable model. Model B and C give better estimates under small sample size, and have the forms $\Delta T \sim \ln S_C + D_f + \ln A + D_f \ln S_C$ [i.e. f, g, h $\simeq 0$ in Eq. (3.1)] and $\Delta T \sim \ln S_C + D_f + \ln A + \ln S_C \ln A$ [i.e. e, f, h $\simeq 0$ in Eq. (3.1)], respectively.

(Sakai et al., 2009). As derived in Appendix B.3, by adopting an idealized urban configuration, the UHI intensity is approximately proportional to $S_C^{(1-aD_f)(1-m)}$ with $a \approx 0.43$ and $1 - m > 0$. For a fixed fractal dimension, as the urban area increases, the heat convection (quantified by the convection heat transfer coefficient h) diminishes, resulting in a higher surface temperature. Analogously, for a fixed surface area S_C, an increasing fractal dimension D_f weakens the convection and leads to a higher surface temperature.

Our results can be relevant for urban policy and planning in the context of global warming and local UHI adaptation.

1. Avoid large cities.
   How the UHI intensity depends on city size is in particular relevant in world regions of ongoing urbanization. Policies could be developed for incentives to also populate medium size and small cities, i.e. thereby to control the exponent of Zipf's law for cities (Auerbach, 1913; Zipf, 2012; Rozenfeld et al., 2011; Rybski, 2013; Fluschnik et al., 2016), which relates the relative frequency of large and small cities.

2. Avoid compact cities.
   More compact urban clusters have larger fractal dimensions (Makse et al., 1998). Qualitatively, it is comprehensible that urban sprawl and polycentric form lead to smaller fractal dimensions. Urban planning can influence these features of urban form.

3. Avoid rotund cities (i.e. approximately rotational invariance).
   It is plausible that stretched cities have lower UHI intensities since the distances to the city border are shorter, in favor of enhanced atmospheric convection. Thus, from an UHI alleviation perspective, cities extending along natural or artificial topographic lines are preferable over those developing mostly around their center.

Certainly, such recommendations need to be opposed to other advantages and disadvantages. In particular, keeping cities small and the consequent ameliorated urban climate should be balanced against positive agglomeration effects of large cities such as shorter trip lengths (Louf and Barthelemy, 2014). Scattered and anisometric cities come along with more traffic, which has negative side effects, including increased anthropogenic heat and CO_2 emissions. Thus, trade-offs on the *local* scale need to be made, when implementing urban factors. Moreover, from a *global* point of view it has been argued that compact cities are preferred because of their potentials in reducing energy consumption and CO_2

emissions (Martilli, 2014). However, as mentioned above such recommendations should also be adjusted according to regional specificities (see Fig. 3.4).

Our work adds to previously gained understanding on how compact urban form increases the UHI intensity and on the problems of transferring such insights into spatial planning (Debbage and Shepherd, 2015; Schwarz and Manceur, 2015). Thus, our results also contribute to the ongoing discussion on the effectiveness of urban forms – in particular, single-centric (compact city) vs. poly-centric city (dispersed city) – as a means for alleviating heat islands as a negative impact of urbanization (Yang et al., 2016).

This study is also an example on how concepts from fractal geometry are of use in city science. For three decades, it has been argued that cities are fractal in form (Batty and Longley, 1987a,b; Batty and Longley, 1994), and the relation between fractal structures and urban areas has received widespread attention (Encarnação et al., 2012). The fractal dimension of urban agglomerations is a measure of their compactness. Thus, in this study we contribute to the view on cities from a fractals perspective and postulate that the correlations between cluster size and fractal dimension are a manifestation of multi-fractality at the regional scale.

Last but not least, our work opens a perspective for future studies in various directions. First, since here we solely investigate surface skin temperature, an apparent question to be raised is to what extent similar correlations of UHI intensities with urban form also appear considering air temperature. Due to data limitations this can hardly be verified empirically, so that numerical modeling (De Ridder et al., 2015) could represent an alternative. Second, we focus on large scale features of urban form, i.e. intrinsic factors. It could be interesting to test whether the consideration of external factors, foremost wind, would improve the characterization of the influence of intrinsic factors on the UHI intensities. Third, we study ensemble data, i.e. quantify correlations among the sample of cities, and do not consider temporal dynamics. It is important to verify if our findings also hold for an individual city under growth scenarios reflecting the features of urban form (Yang et al., 2016). Lastly, can numerical models reproduce our findings or lead at all to comparable results (Zhou et al., 2016)?

4

ASSESSING SEASONALITY IN THE SURFACE URBAN HEAT ISLAND OF LONDON [1]

ABSTRACT

This paper assesses the seasonality of the Urban Heat Island (UHI) effect in the Greater London Area. Combining satellite based observations and urban boundary layer climate modeling with UrbClim model, we are able to address the seasonality of UHI intensity, based on both land surface temperature (LST) and 2 m air temperature, for four individual times of the day (LT0130, LT1030, LT1330, LT2230) and the daily means derived from them. An objective of this paper is to investigate whether the UHI intensities based on both quantities exhibit similar hysteresis-like trajectory that is observed for LST when plotting the UHI intensity against the background temperature. The results show that the UrbClim model can satisfactorily reproduce both the observed urban-rural LSTs and 2 m air temperatures, as well as their differences and the hysteresis in the surface UHI. However, the hysteresis-like seasonality is largely absent in both the observed and modeled 2 m air temperatures. A conducted sensitivity simulation of the UHI intensity to incoming solar radiation suggests that the hysteresis of the LST can mainly be attributed to the seasonal variation in incoming solar radiation.

KEYWORDS: Urban Heat Island, seasonality, London, UrbClim, Model,

1 This chapter is based on the published paper Zhou, B., D. Lauwaet, H. Hooyberghs, K. De Ridder, J. P. Kropp, and D. Rybski (2016). "Assessing Seasonality in the Surface Urban Heat Island of London". In: *J. Appl. Meteorol. Clim.* 55.3, pp. 493–505. DOI: 10.1175/JAMC-D-15-0041.1 ©American Meteorological Society. Used with permission

4.1 INTRODUCTION

As climate change and urbanization globally continue, studies addressing their reciprocal impacts are gaining growing importance (Kalnay and Cai, 2003; Parker, 2010; UN-Habitat, 2011). The Urban Heat Island (UHI) effect, observed as an elevated temperature of urban areas relative to rural ones, relates to both challenges, and is a persistent focus of urban climate and environmental studies (Arnfield, 2003; Stewart and Oke, 2012). The UHI effect emerges through (1) land surface modification (reduced albedo, less vegetation, increased roughness and thermal admittance) which favors heat storage and trapping in the city (Oke, 1982), and (2) anthropogenic heat release (from vehicles, buildings, and human metabolism) (Ichinose et al., 1999; Sailor and Lu, 2004). It can also be caused partially by (3) increased incoming long-wave radiation as a consequence of air pollution (Rouse et al., 1973). However, air pollutants mostly have a minor or even negligible influence on the UHI, which has been demonstrated through field measurements (Nunez et al., 2000) and modelling (Estournel et al., 1983; Oke et al., 1991).

Conventionally, the UHI intensity is assessed by using 2 m air temperature data obtained from urban and rural weather stations. The air temperature based UHI intensity usually reaches its maximum on clear, calm nights and could be as much as 12 °C (Oke, 1987). Since the 1970s, remotely sensed surface skin temperature data have been used to study urban climate, including the UHI effect. Constant development in sensor technologies and better understandings of atmospheric physics have remarkably enhanced both, the quality and the quantity, of data, making a multi-scale investigation of urban climate possible (Tomlinson et al., 2011). In the last decades, UHI studies based on thermal remote sensing have increased the knowledge on (1) spatial patterns of UHI and its correlation with diverse contributing variables, e.g. sky view factor and vegetation; (2) urban surface energy balance; and, to a lesser extent, (3) surface-air relations (Voogt and Oke, 2003; Weng, 2009).

However, the surface skin temperature, in general, differs from the 2 m air temperature (Norman and Becker, 1995; Jin and Dickinson, 2010). Prigent et al. (2003) compared the surface skin temperature with in situ measured air temperatures. They found a positive difference between the surface skin temperature and the air temperature during daytime and a negative difference at night, which they attributed mainly to a quicker response of surface temperatures to solar radiation. Dense vegetation and high soil moisture can diminish the difference by altering the partitioning of surface heat fluxes in favor of the latent heat flux. More-

over, the surface skin temperature and the 2 m air temperature converge under cloudy conditions (Prigent et al., 2003; Gallo et al., 2011).

To systematically quantify the UHI intensity, land cover data has been employed to define the spatial extent of cities as contiguous urban clusters (following Rozenfeld et al., 2008), surrounded by a non-urban belt of equal area (Peng et al., 2012). Combining this urban/non-urban definition with remote sensed Land Surface Temperature (LST) data, Zhou et al. (2013) calculated the UHI intensity – defined as the average temperature in the urban cluster minus the average temperature in the non-urban surroundings (background temperature) – in an automated and systematic manner for all European agglomerations.

One of the findings Zhou et al. (2013) present is the region-specific seasonality of the surface UHI intensity occurring in a large number of cities. Plotting the UHI intensity as a function of the background temperature exhibits a clockwise loop with higher intensities in spring than in fall. The causes of this hysteresis are unclear, and it is unknown if a similar phenomenon also takes place for 2 m air temperature.

Table 4.1 lists some previous works which documented the seasonal variation of UHI intensities. These studies attribute the seasonality mainly to climate and synoptic conditions, e.g. monsoon, wind speed, relative humidity, cloudiness and vegetation, and to a lesser extent to anthropogenic heat release. However, conclusions such as to what extent each factor determines the seasonality are difficult to generalize, as the studies differ considerably in terms of data used (T_{air} versus surface skin temperature), data acquisition method (automobile traverse, remote sensing and weather station observation), UHI intensity metrics (daily maximum versus mean), and choice of rural reference (station-dependent or fairly arbitrary), as well as the time span of observation (from one-year to multi-year).

Nevertheless, there are still some features in common: During the day, UHI intensities based on the surface skin temperature measured by satellites are found to be the highest in the wet summer season and weaker in the dry season, whereas the air temperature based UHI intensities show less obvious seasonal variations. Weaker UHI intensities are usually observed in windier and cloudier months, i.e. the UHI is inversely related to wind speed and cloudiness, as summarized by Arnfield (2003). Recently, Schatz and Kucharik (2014) investigated explicitly the seasonality of UHI in Madison, Wisconsin, by using a densely deployed sensor network. They emphasize the key role of vegetation and snow-cover conditions in shaping the seasonality of UHI intensity, whereas factors such as wind and clouds only fluctuate the seasonality to a certain extent. These find-

Study	City	Year	Seasonal variation
Jauregui (1997)[1]	Mexico City, Mexico	1994	Maximum nighttime UHI intensity (~5 °C) occurred in the dry season (Dec/Jan) and declined to a minimum (~2 °C) during the wet months (Aug/Sept). Daytime UHI intensity reached a maximum in July (~3 °C) and diminished to a minimum (~1 °C) in December.
Figuerola and Mazzeo (1998)[1]	Buenos Aires, Argentina	1994-97	Maximum UHI intensities were frequently found >4 °C in winter and spring with weak wind and low cloudiness, while, under strong wind and cloudiness, UHI intensities in winter fell dramatically. As the temperature increased in summer, negative UHI intensities occurred more frequently.
Runnalls and Oke (2000)[1]	Vancouver, Canada	1992-94	The nighttime UHI intensity was greatest in the fall, followed by summer, winter, and spring.
Unger et al. (2001)[1]	Szeged, Hungary	1999-2000	Bimodal with maximum UHI intensity (~4 °C) in mid-spring (Apr/May) and late summer (Aug/Sept), largely diminished in winter (~1.5 °C).
Wilby (2003)[1]	London, UK	1961-90	Nighttime UHI intensity peaked in August (~2.2 °C) and reached its minimum in January (~1.1 °C). No remarkable seasonality in the daytime UHI intensity was observed.
Kim and Baik (2005)[1]	Seoul, Korea	2001-02	Strong nighttime and morning UHI intensity in fall and winter (>4 °C), least developed in summer. No obvious seasonal pattern for daytime UHI intensity.
Tran et al. (2006)[2]	Tokyo, Japan	2001-02	Daytime UHI intensity reached its peak (~12 °C) around Jul-Aug, followed by a decline until Jan-Feb (~3 °C).

Study	City	Year	Seasonal variation
Roth (2007)[1,3]	(Sub)tropical cities		In the cities under review, a pronounced seasonal variation of nighttime UHI intensities was found, which was attributed to the dry (maximum) and wet (minimum) seasons.
Zhou and Shepherd (2009)[1]	Atlanta, USA	1984-2007	UHI intensity reached its peak in spring (Apr/May), depending on the chosen rural station, respectively at 3 °C and 3.7 °C, and decreased to 1.43 °C and 2.6 °C in Aug.
Pongrácz et al. (2010)[2]	Munich, Germany Milan, Italy Warsaw, Poland Budapest, Hungary	2001-03	The daytime UHI intensities reached their peak in summer (Jun/Jul) and diminished in winter (Nov-Feb). Nocturnal UHI intensities remained stable (around 2-3 °C) between Mar and Oct, and weakened in winter except in Milan, where a maximum UHI intensity of 4 °C occurred in Jan/Feb.
Cui and Foy (2012)[1,2]	Mexico City, Mexico	2006	For both skin and air temperatures, maximum nighttime UHI intensities (up to 10 °C appeared during the cold dry season (Nov-Feb), while the minima (>5 °C) occurred during the wet season (Jul-Oct). The skin temperature based daytime UHI intensities were found strongest (~ 12 °C) in the wet season, and weakest (even negative) in the dry season, whereas the air temperature based ones had low and relatively invariant values across seasons.

[1] Air temperature based. [2] Surface skin temperature based. [3] Review article.

Table 4.1: Selected publications which reported seasonal variations of UHI intensity.

ings are consistent with earlier works (Imhoff et al., 2010; Peng et al., 2012).

However, little effort has been made to address seasonality by integrating observations with increasingly more sophisticated urban climate modeling. In this work, we modeled the urban climate of London by the urban boundary layer climate model UrbClim (De Ridder et al., 2015). Combined with a standardized methodology for quantifying the UHI (Zhou et al., 2013), we were able to assess the hysteresis of this example.

In brief, the aim of this study is to verify (1) if the model can reproduce the hysteresis in the surface temperatures of London, (2) if the hysteresis effect also occurs in the 2 m air temperature and (3) if the phase shift between astronomical and meteorological cycle is a plausible explanation for the observed hysteresis effect.

4.2 NUMERICAL MODEL, EXPERIMENT SET-UP, AND MODEL EVALUATION

4.2.1 *The UrbClim model*

The model simulations in this study were performed with the urban boundary layer climate model UrbClim, designed to cover agglomeration-scale domains at a very high spatial resolution (De Ridder et al., 2015). UrbClim consists of a land surface scheme containing urban physics coupled to a 3-D atmospheric boundary layer module.

The *land surface scheme* is based on the soil-vegetation-atmosphere transfer scheme of De Ridder and Schayes (1997), but is extended to account for urban surface physics. This urbanization is accomplished by representing the urban surface as a rough impermeable slab, with appropriate values for the albedo, emissivity, thermal conductivity, and volumetric heat capacity. The main feature of the extension of the scheme is the inclusion of a parameterization of the inverse Stanton number, which is known to be much higher in urban areas (Kanda et al., 2007; De Ridder et al., 2012). Further details can be found in De Ridder et al. (2015).

The land surface scheme takes part of its input variables (wind speed, temperature and specific humidity close to the surface) from values simulated in the atmospheric boundary layer model, a 3-D model of the lower atmosphere, extending to a constant height of 3 km.

The *atmospheric boundary layer module* is tied to synoptic-scale meteorological fields through the lateral and top boundary conditions, to ensure that the synoptic forcing is properly taken into account. This model is represented by conservation equations for horizontal momentum (considering zonal and meridional wind speed components u and v, respectively), potential temperature, specific humidity, and mass (involving the vertical wind speed component w). Pressure fields are not calculated

internally, but prescribed from a large-scale host model from which UrbClim receives its boundary conditions, hence only the synoptic-scale pressure gradient is accounted for. By doing so we avoid the complexities associated with a full mesoscale meteorological model. More importantly, it allows the use of much longer time increments in the numerical solver and a lower model top (since no absorbing layer is required to damp gravity waves), which makes the model much faster.

The large-scale driving model specifies the lateral and top boundary conditions, the synoptic-scale pressure gradient, and the down-welling radiation and precipitation – the variables required by the land surface scheme. This one-way nesting approach allows the UrbClim model to account for the effect of synoptic weather on local climate (De Ridder et al., 2015).

Terrain elevation data are taken from the GMTED2010 dataset (Danielson and Gesch, 2011), which has a global coverage and is freely available. The spatial distribution of land cover types, needed for the specification of required land surface parameters, is taken from the 2006 CORINE land cover data for Europe (Büttner et al., 2007).

The urban land cover percentage is specified using the urban soil scaling raster data files distributed by the European Environment Agency. Maps of vegetation cover fraction are obtained from the Normalized Difference Vegetation Index (NDVI) acquired by the MODIS instrument on-board the TERRA satellite platform. Vegetation cover fraction is specified as a function of the NDVI, using the linear relationship proposed by Gutman and Ignatov (1998), and then interpolated to the model grid.

Model grid cells featuring exclusively non-urban land use types are divided into vegetation and bare soil (the complementary fraction). In the case of grid cells containing urban land use, the urban fraction as derived from the urban soil sealing raster data takes precedence over the NDVI-based fractional vegetation cover data in case both sum to over 100 %. In case they sum to less than that, the remaining fraction is assigned to bare soil.

Each of the surface types within a grid cell has its own energy balance and corresponding temperature, although the model employs aggregated values for both the aerodynamic and the thermal roughness length parameters. The urban surface cover has an associated very low thermal roughness length which strongly inhibits the turbulent transfer of heat from the urban substrate to the atmosphere, so that a relatively large share of the available radiant surface energy flux is converted to storage heat rather than to turbulent sensible heating of the atmosphere. This, together with the typically high values of thermal inertia of urban materials, leads to the large storage heat flux values typically observed

(or estimated as a residual of the surface energy balance) over urban areas (Piringer et al., 2007).

The urban substrate is represented as a massive slab, which is discretized in six vertical layers, and its specific volumetric heat capacity ($2 \times 10^6\,J\,m^{-3}\,K^{-1}$) and thermal conductivity ($2\,W\,m^{-1}\,K^{-1}$) values are in line with values found in the literature for urban areas (see, e.g. , Oke, 1987; Pielke, 2002). Evaporation from the urban surface is included by implementing a fractional surface wetness parameter, which accounts for the amount of water stored on the urban substrate, calculated as the difference between precipitation on the urban fraction and evaporation of the stored water. The maximal fraction of wet surface is set as 0.14, with a maximum storage capacity of $1.17\,kg\,m^{-2}$. Both parameters have been estimated recently by Wouters et al. (2015).

The evolution of the temperature profile in the soil is calculated using the same heat diffusion equations as those used for the urban slab. The main difference is that, for soil, the volumetric heat capacity and thermal conductivity are functions of soil moisture content, as in De Ridder and Schayes (1997). Water transport in the soil is described by means of Richards' equation (Garratt, 1992), accounting for infiltration of rain water in the soil and the uptake of soil water by plant roots. Here also, the reader is referred to De Ridder and Schayes (1997) for more details.

4.2.2 *Experiment set-up*

The model described above was applied to simulate a 7-year period (2006-12) for the wider urban agglomeration of London, driven by meteorological data from the ERA-Interim reanalysis dataset of the European Centre for Medium-range Weather Forecasting (ECMWF).

The domain was configured with 161×161 grid cells in the horizontal direction, using a spatial resolution of 1 km, equal to the resolution of the MODIS data. In the vertical direction, 20 levels were specified, with the first level 10 m above the displacement height, the resolution smoothly decreasing upward to 250 m at the model top located at 3 km height. This vertical discretization closely matched that of the ECMWF model (De Ridder et al., 2015).

The simulation was initialized on 1 December 2005 at LT0000. Initial soil temperature and soil moisture data were taken from the ERA-Interim reanalysis. The sea temperatures in the model were treated separately, and they were adopted from the ERA-Interim reanalysis during the whole simulated period and not calculated internally.

In order to assess the sensitivity of the observed hysteresis effect in the surface UHI of London to the annual cycle of the incoming short-

wave radiation, a sensitivity experiment was carried out. In this scenario, referred to as SR experiment, the input short-wave radiation from the ERA-Interim reanalysis was rescaled with a daily factor so the clear-sky maximum radiation was always equal to the value of 21 March, when it almost equaled its annual mean value. Thus, all year round, the daily cycle of incoming short-wave radiation under clear sky conditions remained constant, eliminating the annual cycle. Note that we did not change the temporal variation of the incoming radiation. Cloudy conditions remained cloudy. The values only were rescaled.

4.3 DATA AND UHI INTENSITY CALCULATION

We used the same UHI intensity definition as explored by Zhou et al. (2013). The idea is to define a city by its physical extent, i.e. via urban land cover. Overlaying the city delineation (and an equal area belt around it) and the heat map, the average temperatures in the city and its surroundings are calculated so that the difference between city and background temperatures (i.e. the belt temperatures) provides the intensity. A similar methodology has been used in prior research (Peng et al., 2012).

In detail, the calculation of the UHI intensity, ΔT, consists of the following steps:

1. We applied the City Clustering Algorithm (Rozenfeld et al., 2008, 2011) to CORINE land cover data at 250 m resolution. The algorithm assigns any two urban cells to the same urban cluster if their distance is lower or equal to a threshold distance l. As in Zhou et al. (2013), we used $l = 500$ m and obtained the London city cluster [Fig. 4.1 (a)].

2. A belt of approximately equal size as the cluster was determined by consecutively enclosing layers of non-urban land use, avoiding other urban cells (Zhou et al., 2013, Supplementary Material).

3. Based on the gridded temperature fields, we calculated the average temperatures in the cluster, T_C and in the belt, T_B. The temperature is either LST from MODIS or modeled 2 m air temperatures as described in Sec. 4.2. The UHI intensity was then calculated as $\Delta T = T_C - T_B$. In any case, the resolution is 1 km, consistent with that used in MODIS. Figure 4.1 (b) shows, as an example, the annual mean 2 m air temperature map from the UrbClim model.

The 2006 CORINE land cover data used in this study includes 38 European Environmental Agency member states (Büttner et al., 2007). The

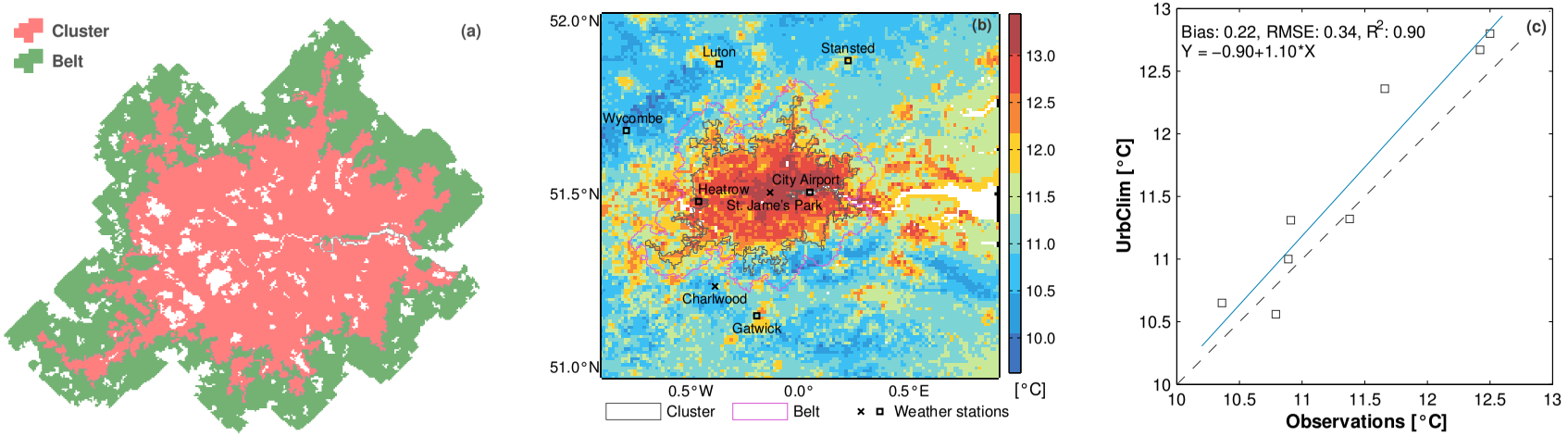

Figure 4.1: City cluster and belt for the Greater London Area and gridded temperature field. (a) City cluster identified by city clustering algorithm with $l = 500\,\mathrm{m}$. The belt is of the same area as the cluster. (b) Modeled annual mean 2 m temperature for the year 2011. The locations of the measurement stations are indicated by black squares, whereas the stations 'St. James Park' and 'Charlwood' are indicated by black crosses. (c) Comparison between observed and modeled annual mean 2 m air temperatures.

44 distinguished land surface classes include artificial land coverage and are reclassified into urban and non-urban in accordance with Simon et al. (2010).

We used the MOD11A2 and MYD11A2 Version 5 data, from MODIS Terra and Aqua platforms, respectively. Determined by overpass times, the Terra satellite provides twice-daily data at around local time (LT) 1030 and LT2230, whilst the Aqua data are collected at LT1330 and LT0130. Both data are aggregated into a 8 day temporal resolution, which corresponds to 46 observations annually. Wan (2008) validated LST V5 data with in situ measurements, indicating an accuracy better than 1 °C in most cases.

By averaging the four periods MODIS data for each observation, we obtained gridded temperature fields of daily means. To minimize bias caused by cloud contamination inherent in the data, we based our calculation of each grid cell only on complete data. Gridded daily means based on incomplete data are omitted. Unless specified differently, we use daily averages for our analyses hereafter. Moreover, we disregarded observations where either cluster or belt were affected by at least 50 % cloud cover. Finally, we had 276 valid observations (86 % of the total) from 2006 to 2012 (the UrbClim simulations were run over the same period).

We plotted the UHI intensity, ΔT, as a function of the background temperature, T_B, and calculated the monthly averages of both quantities. In order to better assess the hysteresis, we performed a second order Fourier approximation of both times series, in agreement with Zhou et al. (2013).

4.4 RESULTS

4.4.1 *Observed and modeled 2 m air temperature comparison*

The UrbClim model has already been successfully validated regarding its energy fluxes, 2 m air temperatures, and urban-rural temperature differences for the cities of Ghent (Belgium) and Toulouse (France) (De Ridder et al., 2015). The LST in the UrbClim land surface scheme, too, have been validated in the past with satellite data. In De Ridder (2006), the urban parameterization is tested for the city of Paris, and the simulated LST compared favorably to observed values obtained from thermal infrared satellite imagery. Afterwards, the land surface scheme was coupled to a mesoscale atmospheric model and applied to both Paris and the German Ruhr area, again yielding good comparisons between sim-

ulated and observed LST from thermal infrared satellite imagery (De Ridder et al., 2008, 2012).

Regarding the London domain in this study, we were able to obtain 2 m air temperature measurement data from a location inside the city center (St. James Park, 51.504° N 0.129° W) and in the rural surroundings (Charlwood, 51.144° N 0.230° W) for the period 2010-12. Unfortunately, the urban station is located inside a park, which is known to be cooler than a true urban environment, so the measurements do not capture the full extent of the London UHI effect. In order to obtain comparable statistics as in the LST analysis, the data were aggregated into a 8 day temporal resolution which corresponded to 46 observations each year. The error statistics of the UrbClim model for both locations are shown in Tab. 4.2. The overall performance of the model is good, with a bias of only a few tenths of a degree, root mean square errors below 1 °C, and correlation coefficients above 0.98.

However, the focus of this evaluation is on the model's ability to reproduce observed urban-rural temperature differences. The simulated temperature differences agree fairly with the observed ones, with a negligible bias, a root mean square error below 0.5 °C, and correlation coefficients up to 0.7.

In order to evaluate the model's ability to reproduce the spatial pattern of 2 m air temperatures, measurement data from 6 additional locations in and around the city were gathered for the year 2011. The locations of the measurement stations are shown in Fig. 4.1 (b), with the annual mean 2 m air temperature from the UrbClim model in the background. Figure 4.1 (c) depicts the linear relationship between modeled and observed values, with a bias of 0.22 and a coefficient of determination (R^2) of 0.90, suggesting the model can properly reproduce the observation regarding its annual mean spatial pattern.

4.4.2 *Observed and modeled land surface temperature comparison*

We calculated the LST UHI intensity for London from measurements as detailed in Sec. 4.3, which we compare in the following with the results of the UrbClim model (see Sec. 4.2). Empirical and modeled temperatures have spatial and temporal overlap, and we calculate the UHI intensities in the analogous manner.

First, we want to analyze if the UrbClim model reproduces the hysteresis-like seasonality in the LST. Therefore, the UHI intensity, ΔT, is plotted versus the background temperature, T_B. For both quantities, the raw data in 8 day resolution is aggregated to monthly means.

year	Tu			Tr			ΔT		
	Bias	RMSE	CORR	Bias	RMSE	CORR	Bias	RMSE	CORR
2010	0.08	0.73	0.99	0.01	0.64	0.99	0.07	0.29	0.70
2011	0.26	0.93	0.99	0.17	0.91	0.98	0.17	0.42	0.59
2012	0.12	0.87	0.99	0.05	0.98	0.98	0.07	0.36	0.65

Table 4.2: Error statistics for the simulated (versus observed) urban (St. James Park, Tu) and rural (Charlwood, Tr) 2 m air temperatures and their differences (ΔT). The quantities given are the bias, root mean square error (RMSE), and correlation coefficient (CORR).

Figure 4.2 exhibits the raw values, the monthly means with standard deviations, and second order Fourier approximation. Figure 4.2a-b shows the LST results for the MODIS data and the UrbClim model, respectively. In the case of the measured data, the monthly background temperature ranges between slightly over than 0 °C and almost 20 °C, whereas the UHI intensity is between somewhat lower than 1 °C and almost 3 °C. The modeled data shows similar ranges, although slightly smaller UHI intensity in summer and slightly higher background temperature in winter.

Despite considerable spreading of the 8 day values, the monthly values exhibit the characteristic clockwise course in both Figs. 4.2 (a) and (b), which imply a phase shift between the UHI intensity and the background temperature. The UHI intensity reaches its peak around the summer solstice, i.e. in the strongest incoming solar radiation, while the maximum values of background temperature occur around the end of July and the beginning of August. As can be seen in Fig. 4.2 (a), the typical UHI intensity in May is, by approximately one degree, larger than in September. The modeled data in Fig. 4.2 (b) shows a similar effect, although a bit less pronounced in May/September. Overall, the hysteresis-like seasonality in the modeled LST matches the observed pattern for London. The dif-

	T_C	T_B	ΔT
Bias	0.18	0.21	-0.03
RMSE	1.19	1.23	0.40
CORR	0.99	0.98	0.86

Table 4.3: Error statistics for the simulated 8 day averaged LST versus observed MODIS LST for urban cluster (T_C), belt (T_B) and their differences (ΔT).

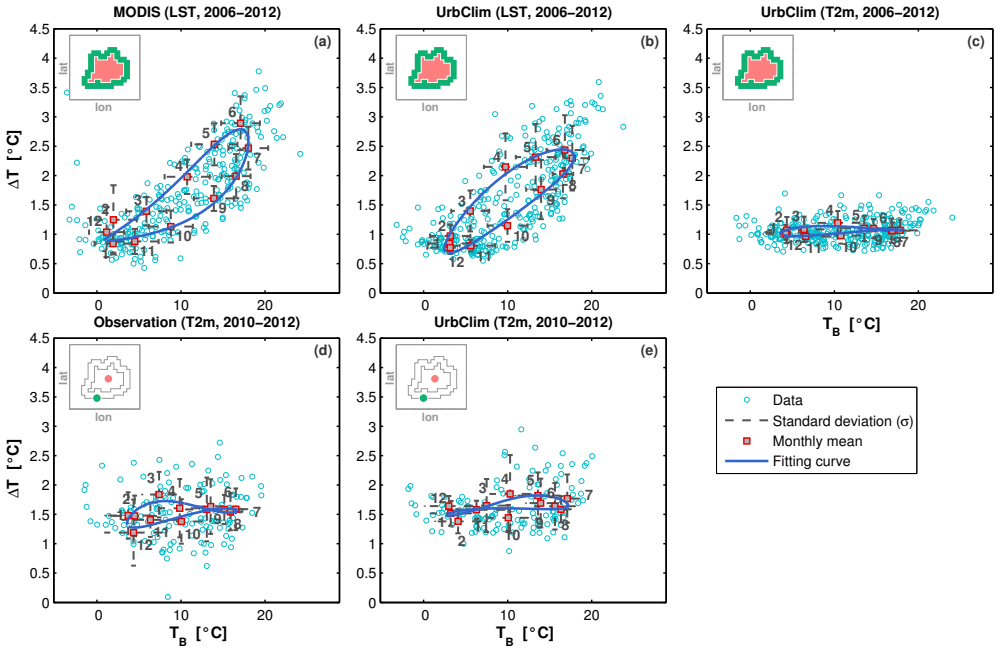

Figure 4.2: Seasonality of UHI intensity for the London city cluster based on empirical MODIS (LST), observations (2 m temperatures), and modeled UrbClim results (both). The inset icons denote how the UHI intensity (ΔT) is calculated, i.e. based either on the mean temperature difference between urban area and its surrounding [(a)-(c)], or on the temperature difference between St. James Park (urban) and Charlwood (rural) [(d), (e)]. The UHI intensity, ΔT, is plotted as a function of the background temperature, T_B. The numbers (1-12) within the plot correspond to months of the year. The panels (a), (b) show the results for land surface temperatures, whereas the panels [(c)-(e)] are for the 2 m air temperatures. The comparison between the observed and modeled 2 m air temperatures [(d), (e)] is based on data from 2010 to 2012.

ferences in the shape of the Fourier approximations are minor compared to the spreading of the raw data and the resulting standard deviations.

The simulated 8 day averaged LST agree with the observations, both for the city cluster and the belt (Tab. 4.3). The UrbClim model also performs well in simulating the LST based UHI, with a bias of -0.03 and a correlation coefficient of 0.86.

4.4.3 *Modeled land surface and 2 m air temperature comparison*

The described hysteresis-like seasonality has been reported and reproduced (Sec. 4.4.2) only for land surface temperature so far. Next, we want to verify if the phenomenon occurs also in the 2 m air temperature.

First, we investigate if the hysteresis is present in the measurement data from the stations St. James Park and Charlwood for the years 2010-2012 and if the UrbClim model shows comparable results. Afterwards, we focus on the full modeled period (2006-12) to make a comparison with the LST analysis. The comparison between measurements and model results regarding a potential hysteresis-like seasonality is presented in Figs. 4.2 (d) and (e). A hysteresis-like seasonality is absent in both the observations and the model results, as all year round the UHI intensity for 2 m air temperatures is between 1 and 2 °C.

Figures 4.2 (b) and (c) show the results for the modeled LST and 2 m air temperature, respectively. Here, we calculate the daily mean temperature by averaging the four times of the day. While the background temperature, T_B, exhibits a similar range in both cases, it is apparent that the modeled 2 m air temperature is not significantly different between the seasons. The maximum deviation of approximately 0.2 °C occurs between April and October (Fig. 4.2 (c)). In comparison to the size of the spreading, this effect can be neglected.

As we do not observe any significant hysteresis-like seasonality in the daily mean 2 m air temperature in both the model and the observations, we can conclude that it must be a phenomenon that is restricted to land surface temperature. In other words, the UHI intensities derived from LST and air temperature constitute different seasonalites.

In Fig. 4.2 (c), ΔT is approximately constant throughout the year. Under the climate conditions, relatively high UHI episodes can occur, even in winter, during dry and sunny periods. Since sunny episodes and rainfall events are possible all over the year, ΔT is almost constant.

4.4.4 *Seasonality of daytime and nighttime UHI intensities*

Figure 4.3 shows the seasonality of air temperature based UHI for both daytimes and nighttimes. It is generally known that the nighttime UHI is larger than the daytime UHI for air temperatures (Oke, 1987). The UHI intensity reaches its peak of about 2 °C at LT0130 in spring (April/May), whereas the minimum UHI intensity occurs at LT1330 (about 0.5 °C). On clear sky days, during the daytime, the surface is heated by solar radiation, and the boundary layer becomes unstable, favoring convection and turbulent mixing. This mixing hampers the formation of a strong near-surface UHI since a lot of warm air is transported upwards to the atmosphere. After the sunset the surface cools and the boundary layer becomes stable, favoring stronger near-surface temperature gradients. The difference in cooling rate between urban and rural area intensifies further the UHI. This process might explain the bimodal seasonality at

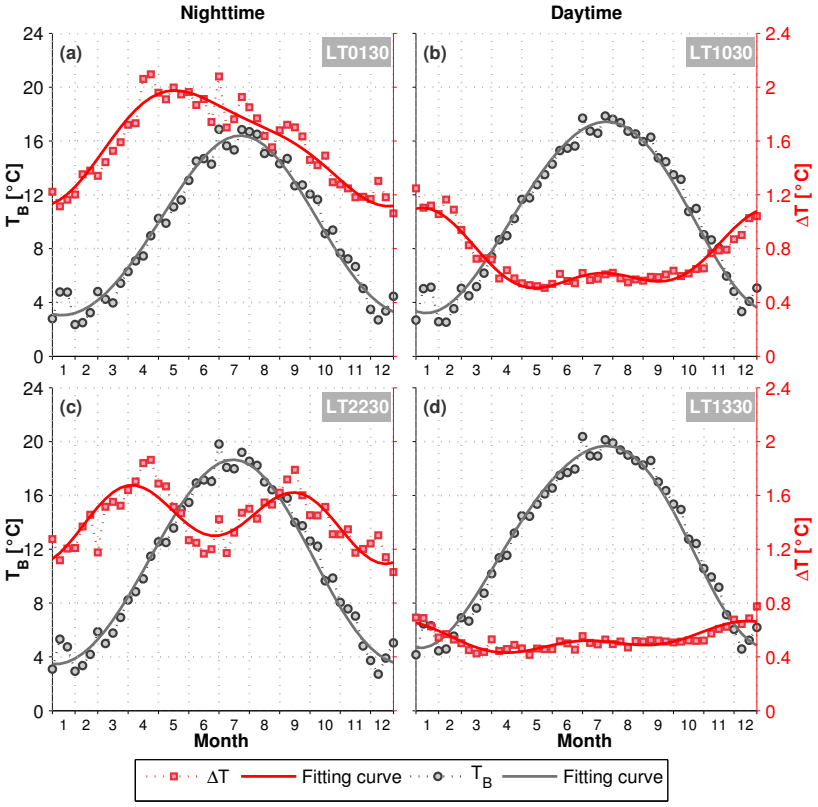

Figure 4.3: The seasonality of modeled air temperature. Background temperatures (T_B) and UHI intensities (ΔT) are shown for 4 local times of the day (a) LT0130, (b) LT1030, (c) LT1330 and (d) LT2230, which are consistent with the MODIS overpass times. The data are fitted by second order Fourier approximation.

LT2230. Due to the late sunset time (about LT2120) in June and July, the stabilization of the boundary layer occurs after LT2230. The UHI intensity reaches its peak several hours after sunset, and at LT0130 is approximately 0.4 °C larger than at LT2230 in June/July.

Table 4.4 shows the partial correlation matrix of UHI intensities for different times of the day. For LST based UHI intensities, from both observation and simulation, highly positive correlations are found between individual times of the day (Tab. 4.4 (a) and (b)). For air temperature based UHI intensities, high correlations are found solely between daytime UHI intensities (LT1030 and LT1330), and between nighttime UHI intensities (LT0130 and LT2230), whereas non-significant and even negative correlations are found between daytime and nighttime UHI intensities. This difference suggests that the LST based UHI intensities exhibit similar seasonalities at various times during the day, while this consistency across times does not exist with respect to air temperature based UHI intensities.

(a) ΔT_{LST}^{MODIS}

	LT0130	LT1030	LT1330	LT2230
LT0130	0.62			
LT1030	0.63	0.89		
LT1330	0.71	0.65	0.65	
LT2230				

(b) $\Delta T_{LST}^{UrbClim}$

	LT0130	LT1030	LT1330	LT2230
LT0130	0.92			
LT1030	0.94	0.95		
LT1330	0.95	0.87	0.93	
LT2230				

(c) $\Delta T_{T_{2m}}^{UrbClim}$

	LT0130	LT1030	LT1330	LT2230
LT0130	-0.26			
LT1030	-0.11*	0.66		
LT1330	0.74	-0.04*	-0.03*	
LT2230				

* $p > 0.01$

Table 4.4: Correlations between UHI intensities of four individual times, based on (a) MODIS observed LST (ΔT_{LST}^{MODIS}), (b) UrbClim simulated LST ($\Delta T_{LST}^{UrbClim}$), and (c) UrbClim simulated 2 m air temperature ($\Delta T_{T_{2m}}^{UrbClim}$). For LST based UHI intensities, from both observation and simulation, highly positive correlations are found between individual times of the day, whereas for air temperature based UHI intensities, correlations are non-significant or even negative between different times.

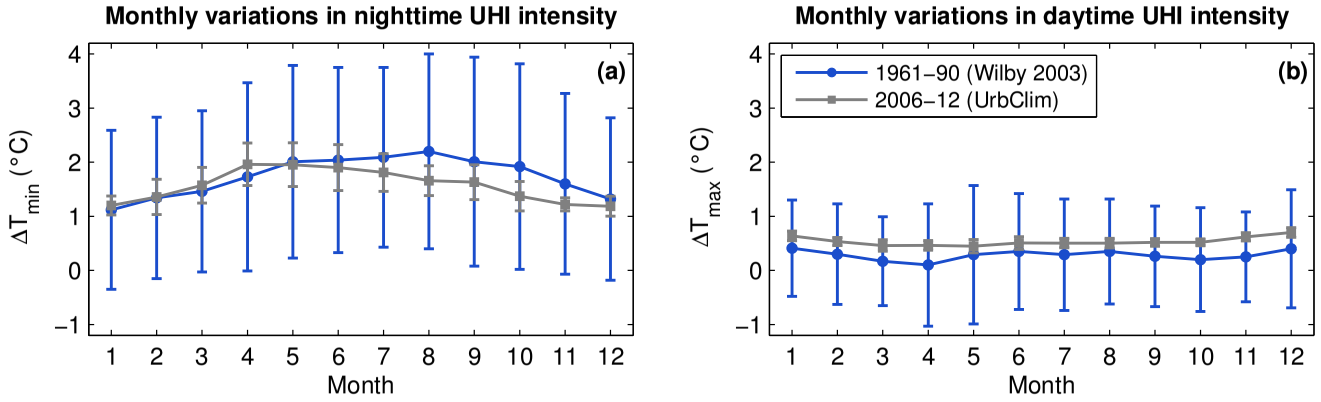

Figure 4.4: Monthly variations in (a) nighttime and (b) daytime UHI intensities based on 2 m air temperature modeled by UrbClim in comparison with the results by Wilby (2003), where observational temperature data of two weather stations from 1961 to 1990 were used to calculate the UHI intensities. Vertical bars denote standard deviations.

When averaging to daily mean, the air temperature based UHI seasonality is attenuated. This could explain why the LST based daily mean UHI exhibits a pronounced seasonality throughout the study period, whereas a similar trend is absent for the air temperature based UHI.

A previous study conducted by Wilby (2003) assessed both daytime and nighttime UHI intensities based on 2 m air temperature data observed from 1961 to 1990 at two weather stations (St. James Park and Wisley, 30 km from London). He reported a maximum nighttime UHI intensity in August (2.2 °C) and a minimum in January (1.1 °C), whereas there was no remarkable seasonality in the daytime UHI intensity. We recalculated the UHI intensity in a similar way to Wilby (2003), i.e. defining the nighttime UHI intensity $\Delta T_{min} = \min(T_C^t) - \min(T_B^t), t \in \{LT0130, LT2230\}$, and the daytime UHI $\Delta T_{max} = \max(T_C^t) - \max(T_B^t), t \in \{LT1030, LT1330\}$. As can be seen from Figs. 4.4 (a) and (b), in the present study the daytime UHI intensities have low values (about 0.5 °C) throughout the year, while the nighttime UHI intensity reaches its maximum in April/May (about 2.0 °C). Considering the difference in studying period, UHI definition and large data spreading in the previous study, it is reasonable to conclude that our findings are consistent and well comparable with the previous ones.

4.4.5 *Sensitivity to the annual cycle in the radiation*

We found that UrbClim reproduces the hysteresis-like seasonality in the LST based UHI and that the effect is largely absent in the 2 m air temperature UHI (Sec. 4.4.3). Next, we want to investigate a possible mechanism behind the hysteresis-like seasonality. It has been hypothesized that the phenomenon is due to the phase shift between astronomical and meteorological seasons: the land surface temperature in the city follows the astronomical seasons driven by solar radiation and the temperature in the surroundings follows the meteorological seasons corresponding to the regional climate (Zhou et al., 2013).

Here, we test this hypothesis by performing a model run with manipulated external driving. As detailed in Sec. 4.2.2, in the sensitivity experiment the clear-sky maximum short-wave radiation (SR experiment) is kept constant throughout the year. In Fig. 4.5, we compare the LST UHI intensities of MODIS with the ones obtained from the SR experiment. While in Fig. 4.2 the daily averages are plotted, in Fig. 4.5 we study the 4 times of the day separately.

During the day times it can be seen that the hysteresis shape greatly diminishes in the manipulated model run and only small UHI intensities in the LST remain, in contrast to the unaltered data observed with large

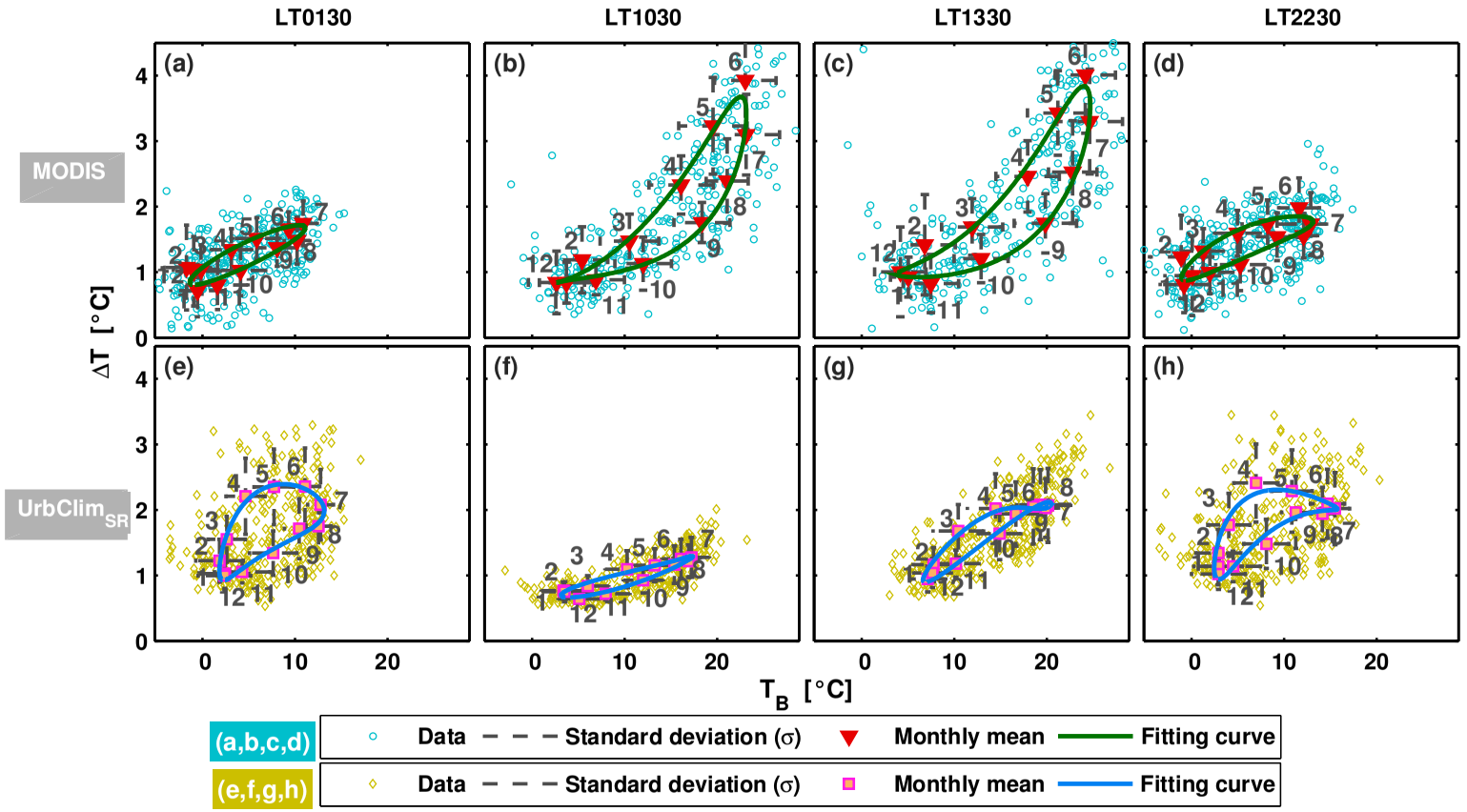

Figure 4.5: Hysteresis of UHI intensity for the London city cluster comparing the empirical MODIS values with the ones obtained from the constant short-wave radiation (SR) experiment as explained in Sec. 4.2.2. Analogous to Fig. 4.2 the UHI intensity (ΔT) is plotted as a function of the background temperature (T_B) for MODIS [(a)-(d), upper] and UrbClim SR experiment[(e)-(h), lower]. The numbers (1-12) within the plot correspond to months of the year. The columns show the results for the four times of the day, i.e. LT0130 [(a), (e)], LT1030 [(b), (f)], LT1330 [(c), (g)], and LT2230 [(d), (h)].

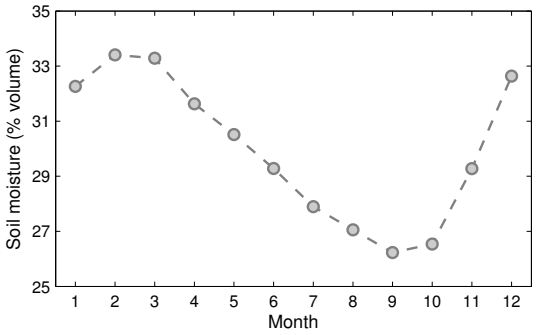

Figure 4.6: Monthly means of soil moisture for London, derived from NOAA Climate Prediction Center soil moisture data at a 0.5° × 0.5° grid.

maximum ΔT of approximately 4 °C in June. During the night times however, the UHI intensities of the SR experiment still exhibit a slight hysteresis shape, in contrast to the night times of the MODIS data where the phenomenon does not occur. This remaining hysteresis at night could be due to a combination of the higher soil moisture and colder deep soil temperatures in spring, compared to autumn, keeping the rural LST low and therefore increasing the UHI effect. Indeed, observations indicate a seasonality in the soil moisture content in the London region, which results in larger thermal admittance and a decrease of warming rate in the rural areas in spring compared to autumn. Figure 4.6 shows the 7-year (2006-12) monthly mean soil moisture for the Greater London Area, obtained from the NOAA Climate Prediction Center (CPC) soil moisture data (Fan, 2004). However, the UrbClim model appears to be too sensitive to this effect, as it can not be seen in the nighttime MODIS data. During daytime the seasonality of soil moisture plays a minor role in the hysteresis effect, as the astronomical seasonality is dominant.

4.5 SUMMARY AND DISCUSSION

In this paper we have analyzed the seasonal variation of UHI intensities by combining satellite-based observations from MODIS and simulations with the urban boundary layer climate model UrbClim. Based on both LST and 2 m air temperature, the seasonality of UHI intensity from 2006 to 2012 has been investigated. Although both are supposed to describe the magnitude of city warming compared to the surrounding, they constitute different seasonalities. We find that the model reproduces the hysteresis effect in the surface UHI intensities. In the observed and modeled 2 m air temperature, the phenomenon is largely absent, suggesting that the seasonality is due to peculiarities of the LST. Both, observed and simulated, LST based UHI intensities exhibit consistent seasonality across the different times of the day. However, the seasonality of UHI in-

tensities based on air temperature is rather a function of the time of the day.

A sensitivity test has been conducted by rescaling the incoming shortwave radiation so that the clear-sky maximum radiation is always equal to the value of 21 March. In this case the surface UHI intensity is considerably reduced, supporting that the hysteresis is due to a delay between the meteorological seasonality, driving the background temperature, and the astronomical seasonality, driving the city temperature.

In future work it could be of interest to relate this perception with the earlier findings by Runnalls and Oke (2000). They suggested that seasonalities of UHI intensity could be mainly attributed to the difference in thermal admittance between urban and rural areas, which determines the warming and cooling rate of each part. For urban areas, the thermal admittance could be seen as constant throughout the year. The warming rate of urban areas is proportional to the solar radiation during the daytime, while its cooling rate due to infrared emission is almost constant during the nighttime. In the non-urban area, where the thermal admittance is highly subject to soil moisture and vegetation, the warming and cooling rates exhibit pronounced seasonal variations. Around the summer solstice the urban warming rate reaches its maximum, and so is the difference between urban and rural warming. As a consequence of this difference, the UHI intensity peaks in June/July.

Our results indicate that the seasonality of the soil moisture in the London region can contribute to seasonal variations of the UHI intensity. Although this effect is less pronounced in the case of London, but we expect that larger differences (e.g. in more semi-arid conditions) could contribute significantly to hysteresis-like curves in other regions.

5

SYNTHESIS

5.1 GENERAL ACHIEVEMENTS

This work at hand has presented a general framework to systematically quantify the UHI effect using a standardized approach based on *City Clustering Algorithm (CCA)*, whereby cities are defined as clusters of maximum spatial continuity derived from CORINE land use data, with their rural hinterland being defined analogously. By combining land use data with spatially explicit surface skin temperatures from MODIS sensors, the UHI intensity can be calculated in a consistent and robust manner. This facilitates monitoring, benchmarking, and categorizing UHI intensities across scales. In light of this innovation, the relationship between city size and surface UHI intensity has been systematically investigated, as well as the contributions of urban form indicators, inter alia fractality and anisometry, to the UHI intensity. Simulating the UHI in the Greater London area using an urban boundary layer model – UrbClim, the seasonal variations of UHI have been assessed from both screen (air temperature) and skin (surface skin temperature) levels. These outcomes are of particular relevance for the overall spatial planning and regulation at meso- and macro levels. They help harness the benefits of rapid urbanization, while proactively minimizing its ensuing thermal stress.

In the following sections, the contributions of each chapter to answering the research questions raised in Sec. 1.3 will be highlighted and discussed in a broader perspective. Some caveats and challenges will be addressed, followed by final remarks and the outlook for future work.

5.2 ANSWERS TO THE RESEARCH QUESTIONS

Research Question 1

How can one systematically quantify the intensity of UHI across scales despite the complexity and diversity of urban systems?

To overcome the problem resulted from the inconsistent definition of urban/rural areas, the CCA has been applied to delineate city clusters (as detailed in Sec. 2.3). Since the CCA is based on the remotely sensed land use data, the quality of land use data is crucial for its overall performance. So far, land use mapping using remote sensing has been achieved with simultaneously a high spatial resolution (varying from 30 m to 1 km) and classification accuracy (Schneider et al., 2009; Friedl et al., 2010; Gong et al., 2013; Ban et al., 2014). This goes along with an observing network composed of tens of commercial and non-commercial satellites, which ensures a frequent update of land cover data at a global scale. All this together renders the land use data-based CCA an approach of global applicability enabling tracking the dynamics of urban land use at an appropriate pace.

However, the CCA and the analogous algorithm to define the rural surroundings are by no means an invariable approach. The choice of underlying land use data and the setting of inherent parameters (e.g., threshold distance, l, and boundary/cluster ratio) can remarkably affect the functionality of the algorithms and the ensuing results (Fluschnik et al., 2016). In practice, medium-resolution land use data as used in this work are preferred, because they can avoid the conjunction of distant cities through highway traffic networks resolved in high-resolution data, at the same time attaining an optimum spatial accuracy.

Moreover, as shown in Fig. C.1, a large value of l (in this case, 3-fold of the spatial resolution of land cover data) has resulted in an overestimation of urban area in Paris and the formation of a super-cluster agglomerated from several scattered cities. As a consequence, the computed UHI intensities are smaller than in the scenarios with smaller l.

Peng et al. (2012) analyzed the impact of boundary/cluster ratio on the derived UHI intensities, suggesting that conclusions remained unchanged under different boundary/cluster ratios. This is consistent with our experiment, taking Berlin as an example (Figs. C.2 and C.3). The UHI intensity increases with the ratio, i.e. larger boundary/cluster ratio leads to a pronounced UHI intensity. Nevertheless, the UHI intensities between varying ratios exhibit a pronounced temporal correlation. Therefore, we consider the impact caused by this factor to be small.

Due to the fascinating nature of CCA, there is, in parallel with the conduction of the research underlying this dissertation, a boom of literature that adopted this approach in studying the surface UHI, both globally (Clinton and Gong, 2013) and regionally (Zhou et al., 2014). One of the recent findings is an exponential decay of UHI along the urban-rural gradient (Zhou et al., 2015). To check its general validity, we presented in Appendix D two variants for defining the buffers: 1) equal-ratio and

2) equal-distance. We demonstrate that the conclusion by Zhou et al. (2015) is equivalent to the established two-dimensional Gaussian model proposed by Streutker (2002, 2003).

Furthermore, the CCA is not confined to population and land cover data. It can be extended, e.g. to remotely sensed nighttime light data which have increasingly been seen as a good proxy for tracking human activities (Imhoff et al., 1997; Elvidge et al., 1999; Levin and Zhang, 2017).

Research Question 2

How does the city size determine the surface UHI intensity in the era of Earth Observation?

The relationship between surface UHI intensity and city size is an issue of great importance from the viewpoint of UHI alleviation. This work has systematically investigated the relationship between city size measured by surface area and surface UHI intensity based on MODIS LST products. Two kinds of relationships are revealed: i) a log-logistic relationship [Eq. (2.1)], and ii) a log-linear relationship (in Sec. 3.3). These seemingly inconsistent relationships are obtained under different assumptions: the former one is derived using a full sample of city clusters identified in Europe totaling ~ 130,000, whereas the latter is based on a subsample of the largest 5,000 city clusters in Europe (corresponding to cluster areas S_C >6.1 km^2). More specifically, the log-logistic relationship approximates the log-linear one when taking cities in the mid-range into account.

According to Eq. (2.1) it can be deduced that small city clusters ($S_C \to 0$) are supposed not to show warmth relative to their vicinity, whereas the UHI intensity for large cities ($S_C \to \infty$) saturates at a certain value. This deduction seems quite plausible from a physical perspective, given the fact that the energy to support the UHI is finite; and the increased urban-rural temperature gradient intensifies the convection (Oke, 1973). However, this log-logistic relationship has a limited usage due to the following two reasons.

i) The computation of temperature for both city clusters and its vicinity should be based on a minimum number of LST values to obtain a plausible estimation relative to the accuracy of LST data.

ii) Zipf's law postulates an extremely low probability of emergence of huge cities, which makes it difficult to verify the value of saturation [parameter α in Eq. (2.1)].

In contrast, the log-linear relationship applies in particular to cities in the mid-range. This is consistent with the results of Imhoff et al.

(2010), who suggested, however, a larger slope and a positive intercept for cities in North America. This discrepancy can be ascribed to a more pronounced UHI in North America than in Europe (Oke, 1973) and a different definition of rural reference.

Moreover, the log-linear relationship implies a differentiated impact of urbanization on cities of varying size with respect to the ensuing change in thermal conditions. Under the same area increase, smaller cities are expected to experience a more severe temperature increase than larger ones. This is of particular relevance for developing countries where rapidly growing population and accelerating urbanization are resulting in considerable urban dynamics in the form of newly emerging cities, merge of small and mid-sized cities together, and rise of megacities. As urbanization is increasingly viewed as inevitable and ultimately desirable, it seems difficult to balance efficiency gains against the rapidity of urban growth. To compensate the consequence of an intensifying UHI, city-level adaptation strategies (e.g. cool pavements and roofs, green infrastructure) should top the priority list of sustainable urban planning and practices. These measures are expected to bring about both economic and health benefits and to synergize the global mitigation efforts (Estrada et al., 2017).

Research Question 3

How does the urban form determine the surface UHI intensity?

A complex interplay has been revealed between UHI intensity and urban form indicators considered in this work. In general, there is a positive correlation between UHI intensity and fractality, whereas the UHI intensity negatively correlates with anisometry (Fig. 3.2). These correlations are more pronounced during daytime than nighttime, as comparably observed between Fig. 3.2 and Fig. B.1.

Quantitatively, the relationship of UHI intensity with city size and urban form indicators can be described using multiple linear regression [Eq. (3.4)]. Performing the same analysis on the normalized data, we are able to identify the relative contributions of each indicator on the UHI intensity: City size is found to have the strongest influence on the UHI intensity, followed by the fractality and the anisometry.

However, their relative contributions to the UHI intensity depict a pronounced regional heterogeneity. As shown in Fig. 3.4, in the Mediterranean region, the anisometry has a much stronger influence than in any other regions, although city size is still the dominating factor. This reveals a distinct urbanization pathway in the Mediterranean region. While growing in size, cities in the Mediterranean region have tended to expand in an anisometric manner. This may be subject to the char-

acteristic geographical conditions of this region, in particular considering many cities are situated along coastlines. As a consequence, the increased anisometry, together with the cooling effect of sea breezes can to some extent compensate the intensifying UHI alongside the increased city size.

Relating city size and form with the scale effect of convection (Sakai et al., 2009), this work also provided a theoretical explanation about the interplay among the UHI intensity, city size and form (see Appendix B.3). Ideally, for a fixed fractal dimension, an increase in urban surface diminishes the heat convection, thus resulting in a higher surface temperature. Analogously, for a fixed urban area, an increasing fractal dimension weakens the convection and leads to a higher surface temperature.

These findings suggest that small, less fractal/ sprawling, and stretched cities perform better in harnessing negative effects of the UHI, which is consistent with previous studies (Clinton and Gong, 2013; Yang et al., 2016). However, UHI alleviation measures based on such findings should be discussed in a broader context of climate change, taking the global climate mitigation goal into account. In view of that compact cities are more capable of creating co-benefits of efficiency gains and reduction in per capita CO_2 emissions (Martilli, 2014), a multi-scale loss/gain analysis of urban planning measures is necessary to reconcile local and global adaptations in cities (Georgescu et al., 2015).

Undoubtedly, other urban form indicators such as the configuration and composition of cities could also be utilized to study the interplay between UHI and urban form, as addressed in Chow et al. (2011) and Schwarz and Manceur (2015). However, this work demonstrates one of the early works in assessing the UHI from a fractal perspective and is expected to stimulate further research to scrutinize the UHI combining the burgeoning new science of city (Batty, 2008).

Research Question 4

How does the UHI intensity vary seasonally at both screen and skin levels?

By plotting the surface UHI intensity as a function of the background temperature, a remarkable diversity has been observed among city clusters, not only from the correlation perspective, but also regarding the seasonal variations these two variables present. From the former viewpoint, this work revealed that for most European cities, a background temperature increase resulted in an intensifying surface UHI. The minimum and maximum surface UHI intensities occurred in winter and summer, perspectively. In contrast, the *Urban Cool Island* or *Oasis Effect* was also widely observed in cities predominantly located in the Mediter-

ranean region. During the summer, mean surface temperatures within those city clusters could be even lower than in their rural surroundings.

On the other hand, the time series of surface UHI intensities and background temperatures can be jointly illustrated using hysteresis-like curves, as detailed in Sec. 2.4.2. For many city clusters, the same background temperature comes with a higher UHI intensity in spring contrasted with a discernibly lower UHI intensity in fall (Fig. 2.3). This implies a phase shift between the time series of UHI intensity and background temperatures. Due to an abundance of construction materials of high thermal inertia in cities, the urban surface temperature is much influenced by the annual cycle of solar radiation. Its increase decelerates after the summer solstice. In comparison, in the vegetated rural surroundings, the temperature tends to follow the meteorological seasonality. All this together results in a maximum surface UHI intensity occurring approximately at the summer solstice.

We extended the analysis on the seasonality to the screen level, taking the Greater London area as an example. According to the model results, the pronounced seasonality/hysteresis observed at the skin level was absent at the screen level. In London, the air temperature-based UHI intensity was quite stable and remained about 1.5 °C throughout the years investigated (2010-2012), as shown in Figs. 4.2 (d) and (e). We ascribe the vanishing seasonality foremost to the comparably weak diurnal variation of air temperatures both in cities and rural surroundings, leading to smaller UHI intensities in value. Meanwhile, the UHI intensity at the skin level exhibits similar seasonality at various times during the day, whereas the air temperature based UHI intensity demonstrates distinct seasonalities across times (see Fig. 4.3 and Tab. 4.4). The latter process depends considerably upon the stability of boundary layer. When averaging to daily means, the seasonality based on the air temperature is attenuated and therefore can hardly be observed.

The relationship between near-surface air temperature and surface skin temperature has long been recognized as a key to link the UHI at screen and skin levels. However, the high correlation observed in previous studies (Prihodko and Goward, 1997; Gallo et al., 2011) and in Figs. A.4 (b) and (d) are attributable in large part to the seasonal cycle embedded in the both temperatures. Therefore, it may be inadequate to claim a good performance of a model merely targeting a high correlation between observed and simulated temperatures throughout a long period, while it is incapable of reproducing the diurnal and seasonal cycles of the UHI intensity. By contrast, the work at hand sheds light on the assessment of seasonality from both observation and modeling perspectives.

Research Question 5

What is a plausible scheme to classify cities according to their UHI characteristics, and what is their geographical pattern?

This work develops a data-driven scheme to classify cities according to their UHI characteristics (as detailed in Sec. 2.4.2). The time series of UHI intensities and background temperatures are broken down into quantifiable harmonics obtained from the second order Fourier approximation. Based on the harmonics, cities can be classified using typical clustering models (e.g. K-means clustering algorithm). Although urban form does influence the UHI intensity, as addressed in this work, and can also be used to classify cities (Huang et al., 2007; Schwarz, 2010), classification schemes based on the relatively static urban form indicators fail to capture the temporal characteristics of the UHI.

As depicted in Fig. 2.4, seven groups were identified. The spatial distribution of these groups demonstrates a pronounced regional heterogeneity, which well coincides with the climate zones. Two findings are worthy of particular mention.

i) The fact that large cities across different climate zones are predominantly classified into the same group (Group 6 in Fig. 2.4) may indicate that the UHI effect in large cities may go beyond geographical constraints and exhibit some common features globally.

ii) The method applied is able to distinguish inland and coastal cities in the Mediterranean region, although their seasonalities resemble each other in shape. The difference can be mainly ascribed to the proximity to water courses and the ensuing enhanced convection in the form of sea breeze.

Simple though the solution is, this approach provides a data-driven alternative to classify cities with regard to the UHI characteristics. To date, we are increasingly aware that cities are seldom an isolated system, yet are connected and sorted by commonalities and disparities. Understanding the essential differences as well as the common features that coexist among cities is, therefore, of great importance in the context of the ongoing discussion about sustainability. For practitioners in urban planning, the classification delivers a very first screening of measures to know whether the measures for alleviating the UHI targeting a certain city can be further transferred and implemented in their own cases.

5.3 CONSTRAINTS AND CAVEATS

Despite the advances this work has made in broadening the insights into the surface UHI, there are still several constraints and caveats that need to be mentioned.

Firstly, one should bear in mind that the accuracy of MODIS LST data of better than 1 K was obtained in optimum conditions (Wan, 2008). Validation field campaigns were conducted over homogeneous land cover, such as lakes and agricultural fields. This gives rise to concern that the de facto accuracy may be lower, in particular for urban pixels which are characterized by a remarkable inhomogeneity. Though the latest Version 6 LST products of MODIS are evaluated to be much better than the previous versions (Wan, 2014), the problem associated with the inhomogeneity of urban areas remains unsolved. The uncertainty may exceed the calculated UHI intensity in the worst case. However, the utilization of 8-day LST composites and averaging data over years could significantly reduce the uncertainty caused by the low accuracy.

Secondly, a majority of this work focuses on the UHI intensity – the temperature difference between city clusters and their rural surroundings. Based on the empirical findings, alleviation measures are suggested with the aim of reducing the UHI intensity. However, these measures do not necessarily result in a decrease of overall temperatures (Schwarz and Manceur, 2015). Therefore, it is more proper to consider lowering UHI intensities and overall temperatures at the same time, while conceiving of UHI mitigation strategies.

In this work, it leaves unanswered how the UHI will develop under the impact of global climate change. This is due to the fact that high-resolution spatially explicit temperature projections are generally not available. Dynamically downscaled projections typically available at a spatial resolution of ~3 km are too coarse to resolve urban scale features (Grossman-Clarke et al., 2017), whereas statistical downscaling is highly reliant on a sufficient amount of past observations (Trzaska and Schnarr, 2014). As a trade-off, the downscaled temperature projections obtained by using the computationally inexpensive UrbClim model (Lauwaet et al., 2015) can be utilized in the future work to fill this research gap.

Furthermore, this work does not employ any Digital Elevation Model (DEM) to eliminate the influence of elevation, which applies in particular to cities located in mountainous regions or those extending across varied landscapes. These shortcomings need to be properly addressed in the future work.

5.4 FINAL REMARKS AND FUTURE WORK

This work as a whole has complemented and advanced a number of previous work by virtue of the enormous amount of cities considered. Such a large sample size achieved through the utilization of an innovative automated city clustering algorithm enables this work to systematically and statistically scrutinize the UHI. The log-linear relationship between city size and UHI intensity suggested by Oke (1973) and Imhoff et al. (2010) has been confirmed and extended to a log-logistic relationship, when taking a wider range of small-sized cities into account. The contribution of urban form to the UHI has been assessed and discussed from a fractal perspective. This attempt is expected to open up new avenues for understanding the UHI from a broader context, for instance, from the urban scaling perspective. In addition, the efforts in classifying cities according to their UHI characteristics have highlighted the importance of regional climates in determining the UHI.

Despite the broad range of issues covered in this work, there are still an array of interesting questions and critical thinking which remain to be addressed. Prospectively, I would like to raise three points for future consideration.

i) It is promising to extend the analyses performed in this work to a broader scale as a response to the accelerating urbanization worldwide. Particular attention will be paid to cities in the Global South. They are expected to bear the brunt of negative impacts of climate change, including a deteriorating thermal well-being. How their UHIs developed in the past and proceed under future climate change scenarios will be the main focus of the envisaged work.

ii) The UHI exhibits a good agreement with human activities and the anthropogenic heat resulting therefrom (Ichinose et al., 1999; Sailor and Lu, 2004). However, anthropogenic heat release data are conventionally estimated at a city level, restricting the investigation of its influence on the UHI at a regional or global scale. Yet, human activities can be estimated increasingly by means of remotely sensed nighttime light data (Elvidge et al., 1999) which are seen as a good proxy for the anthropogenic heat release (Dong et al., 2016). Combining thermal and nighttime light remote sensing is anticipated to fill the gap as to what extent anthropogenic heat release influences the UHI at a global scale. This may also help to explain the seasonality observed in cities at high latitudes [see Fig. 2.4 (i)].

iii) The urban/rural binarism delivers a simple yet intuitive solution to study urban-related issues. However, this approach is far from flaw-free, since the difference between urban and rural areas looks scarcely like a cliff. Instead, it is characterized by a gradual change in building/street morphology, functionality, and surface cover, etc. The classification scheme – Local Climate Zones (LCZ) proposed by Stewart (2011) and Stewart and Oke (2012) seems a promising candidate to deal with this ambiguity. This new-rising scheme may refine the classification approach proposed in this study to gain a better understanding the commonalities among cities.

A

APPENDIX CHAPTER 02

This Supplementary Material consists of the following additional details and results:

- Boundary Generation Algorithm
- Summertime mean land surface temperature (LST) of Greater London and surroundings
- Exemplary comparison of LST and 2 m air temperature as well as the corresponding urban heat island (UHI) intensities
- Largest city cluster, Flemish Diamond

A.1 BOUNDARY GENERATION ALGORITHM

The boundary of a cluster refers to the area surrounding it. The area of the boundary is specified to be of approximately equal size as the cluster area, i.e. $S_B^{(i)} \simeq S_C^{(i)}$. After each city cluster has been identified, the boundaries are constructed under the following constraints:

- Every cluster must have at least one boundary layer.
- A non-urban cell can serve as boundary cell for more than one cluster.

The boundary of a considered city cluster is then built layer by layer as follows:

1. An arbitrary non-urban grid cell adjacent to the considered city cluster is the first cell marked as belonging to the layer.
2. Iteratively, for a non-urban cell, if any of its 4-connected cells is a confirmed layer cell, and any of its 8-connected cells is an urban cell of the same cluster, then the cell is attributed to the layer.

3. The procedure is continued until no more cells can be attributed to this layer.
4. The next layer is built by iteratively adding a non-urban cell, if any of its 4-connected cells is a confirmed cell of the previous layer.
5. Successively, further layers are added and the procedure is stopped if the total number of boundary cells (i.e. the sum of layer cells) is lager than the number of cluster cells. The boundary stops growing when $S_B^{(i)} \geqslant S_C^{(i)}$.

After finishing the iterative generation of layers which together form the boundary, it has to be decided whether the area including the last layer is closest to the area of the cluster or if the area excluding the last layer is closer. If b_j is the number of boundary cells created in the jth layer, the total size of the boundary with n layers is $S_B^{(i)} = \sum_{j=1}^{n} b_j$. To decide whether the nth layer should remain in the boundary, the following criterion must be fulfilled:

$$\ln \sum_{j=1}^{n} b_j - \ln S_C \leqslant \ln S_C - \ln \sum_{j=1}^{n-1} b_j \,,$$

$$\Rightarrow \sum_{j=1}^{n-1} b_j \sum_{j=1}^{n} b_j \leqslant S_C^2, \tag{A.1}$$

i.e. the geometric mean of boundary sizes with $n-1$ and n layers must be less than the cluster size. Otherwise, the nth boundary layer is omitted, and only $n-1$ layers are used to represent the boundary, as illustrated in Fig. A.1 (d) and (e). The algorithm is illustrated in Fig. A.1 for a cluster with 349 cells and the procedure stops with 4 layers, whereas a boundary consisting of 3 layers is chosen with 311 cells.

A.2 SUMMER MEAN LAND SURFACE TEMPERATURE (LST) OF GREATER LONDON AND SURROUNDINGS

Figure A.2 shows the summertime (June-July-August) mean land surface temperature averaged over 6 years (2006-2011), as obtained from MODIS MYD11A2 data (see data Section in the main article). Similar to the results shown in the main article [Fig. 2.1 (b)], the urban cluster identified by City Clustering Algorithm (CCA) (Rozenfeld et al., 2008, 2011) agrees well with the heat pattern and vice versa. Due to the cooling effect of vegetation, parks within the city and around can be seen due to their lower temperatures.

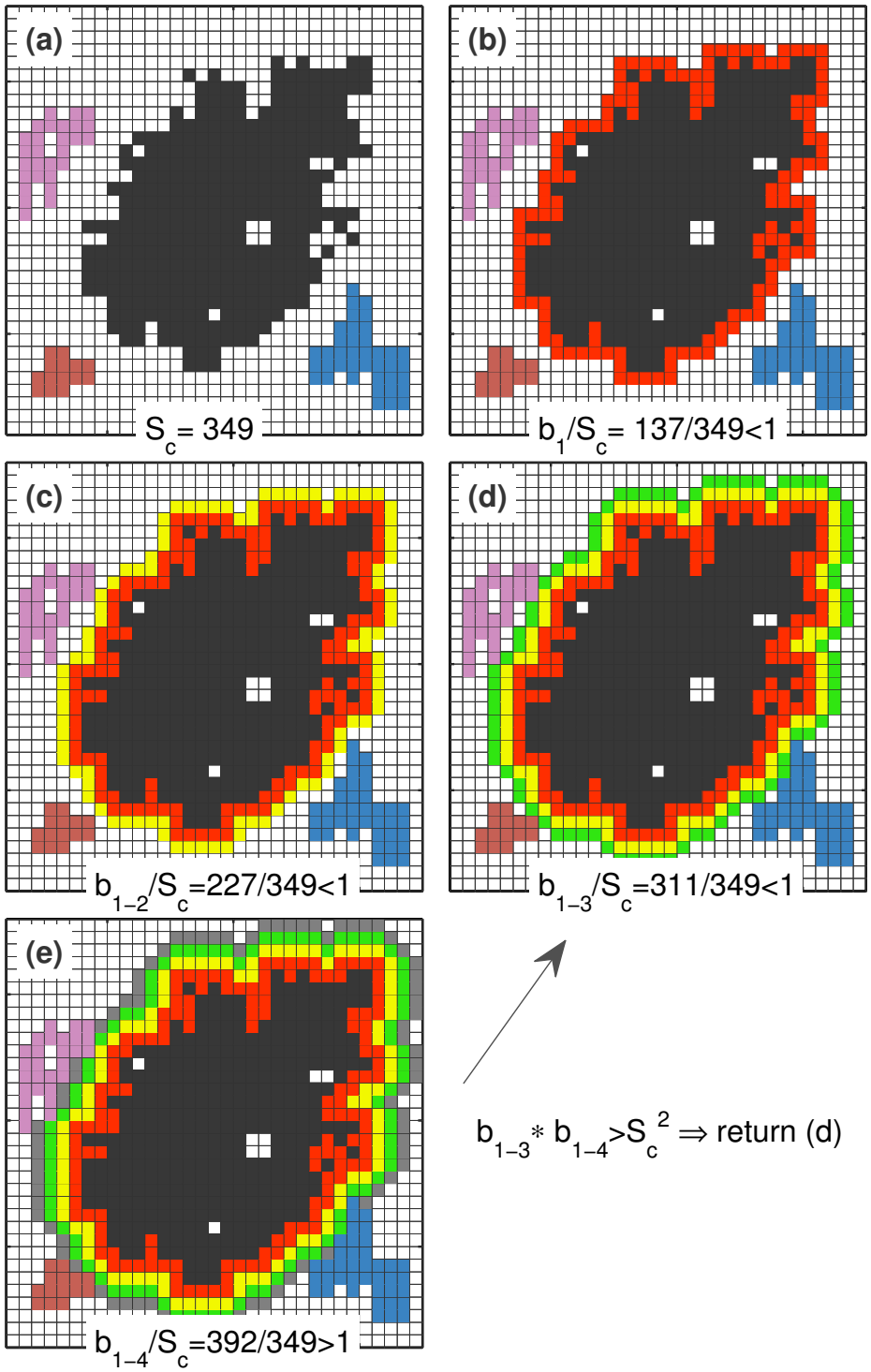

Figure A.1: Illustration of the boundary generation algorithm. (a) The various clusters have been identified, as indicated with colors. The considered cluster in the center (grey) has 349 grid cells. (b)-(e) The boundary is built by consequently forming layers around the considered city cluster, devoid of urban cells of other clusters. Closed inner non-urban pixels are not taken into account. The boundary stops growing when the boundary is larger than the cluster. To decide whether the last generated layer should remain as the boundary, the criterion in Eq. (A.1) is applied, resulting finally in a boundary consisting of three layers in this example.

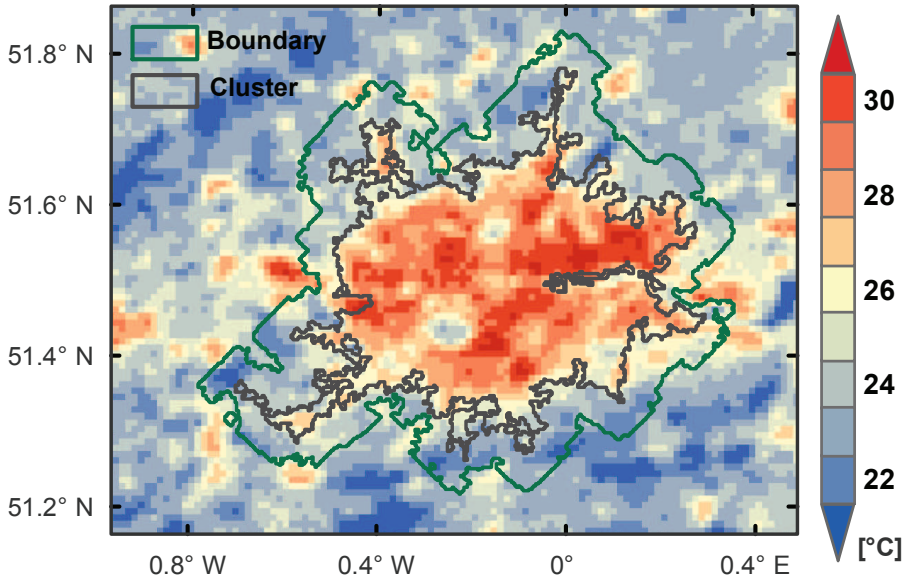

Figure A.2: 6-year (2006-2011) summer (June-August) mean land surface temperature for the Greater London area derived from MYD11A2 datasets, i.e. LST at approximately 13:30 local time. The city cluster and the urban heat distribution are in agreement. The blue pixels within the cluster are zones with relatively lower temperatures within the urban cluster, where the land cover is characterized by a large share of green areas.

A.3 EXEMPLARY COMPARISON OF LST AND 2 M AIR TEMPERATURE AS WELL AS THE CORRESPONDING UHI INTENSITIES

The comparison of UHI intensities is based on

- MODIS LST as detailed in the data Section of the main article and
- 2 m air temperature records from the German Weather Service (DWD).

Berlin is chosen as an example to conduct the comparison. The air temperature records from the weather stations in Berlin and vicinity are in hourly resolution, covering 2006 to 2010. The data from 12:30 CET to 14:30 CET, about the overpass time of Aqua satellite, are averaged and then aggregated into 8-day resolution which are in accordance with the temporal resolution of the MODIS data. Figure A.3 shows the stations used for this comparison, among which Alexanderplatz, Tegel, Dahlem, Buch, Tempelhof, Schönefeld are within the city cluster of Berlin. The remaining three stations – Potsdam, Köpenick, and Lindenberg – are used to represent the boundary, since they are located in non-urban space. Analogous to the definition of LST-based UHI intensity, the UHI

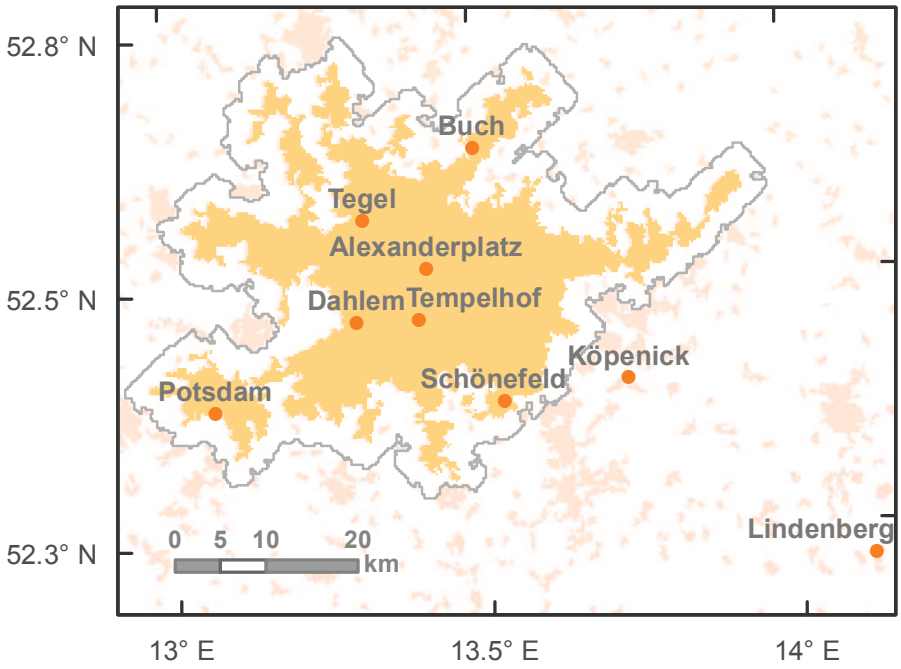

Figure A.3: Locations of weather stations in Berlin and vicinity, where 2 m air temperature are measured. The orange area represents the cluster for Berlin, while its boundary is outlined with grey line. The pink areas are other clusters near Berlin. To obtain the UHI intensity, we calculate the urban temperature through averaging the data from Alexanderplatz, Tegel, Dahlem, Buch, Tempelhof, Schönefeld, whereas the rural temperature is calculated form the records measured at Potsdam, Köpenick, and Lindenberg.

intensity obtained from the 2 m air temperature is defined as the mean temperature difference between urban stations and non-urban stations ("boundary"). Figure A.4 (a), (c) and (e) shows the time series of cluster temperatures (T_C), boundary temperatures (T_B), and the difference between them (ΔT), respectively, retrieved from LST and 2 m air temperatures. Strong correlations are found between the different temperature measurements [Fig. A.4 (b) and (d)], as suggested earlier by Prihodko and Goward (1997). However, the UHI intensity derived from these two methods shows no correlations [Fig. A.4 (f)]. The LST based UHI intensity shows apparent seasonal cycles, whereas the same seasonality can hardly be seen for the UHI intensity derived from air temperature data [Fig. A.4 (e)]. By contrast, the air temperature based "midday" UHI intensity fluctuates around 0 °C.

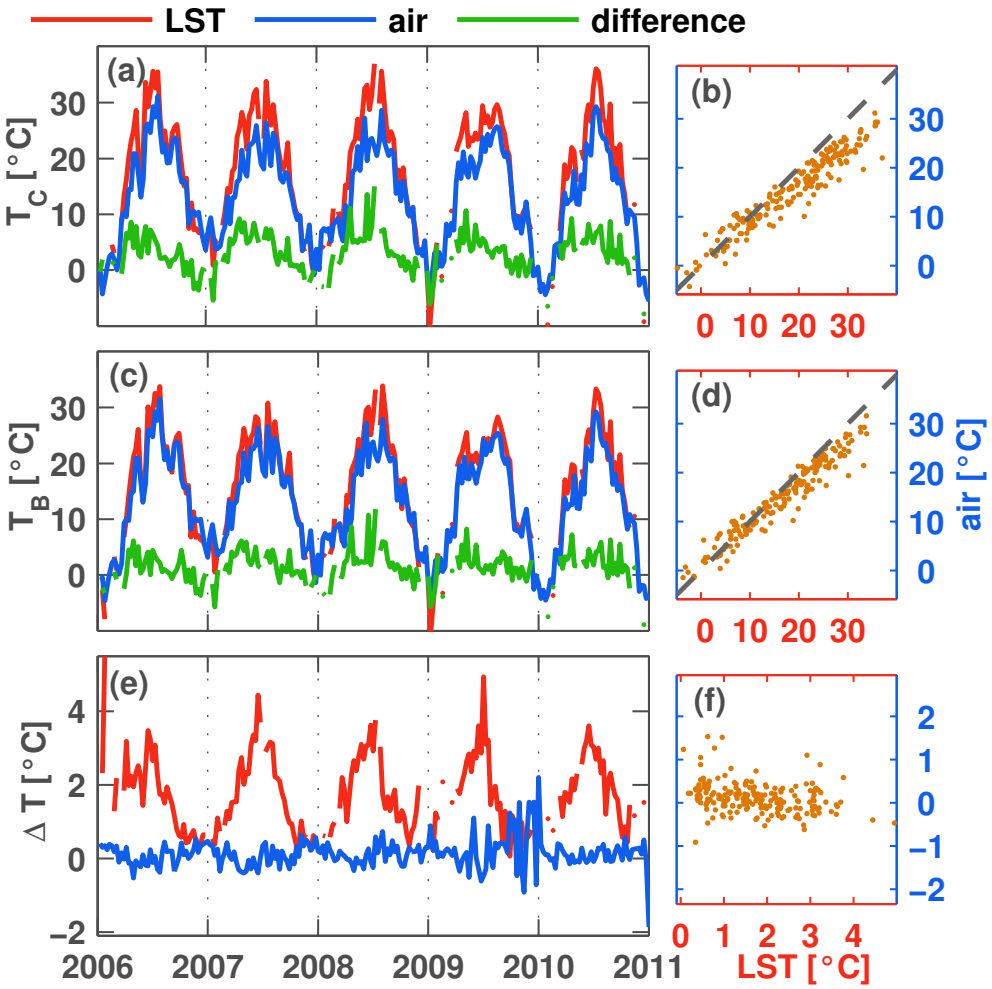

Figure A.4: Comparison of LST and 2 m air temperature as well as the resulting UHI intensities. The cluster records are shown in panel (a) calculated from LST (red) and air temperature (blue). The difference of both is green. Panel (b) is the scatter plot of air temperatures with LST. The analogous for the boundary is depicted in panel (c) and (d). Panel (e) shows the resulting UHI intensities. There is an apparent seasonal variability for the LST based UHI intensity, whereas the air temperature based UHI is relatively stable throughout the year. No significant correlations can be found between them, as seen in panel (f).

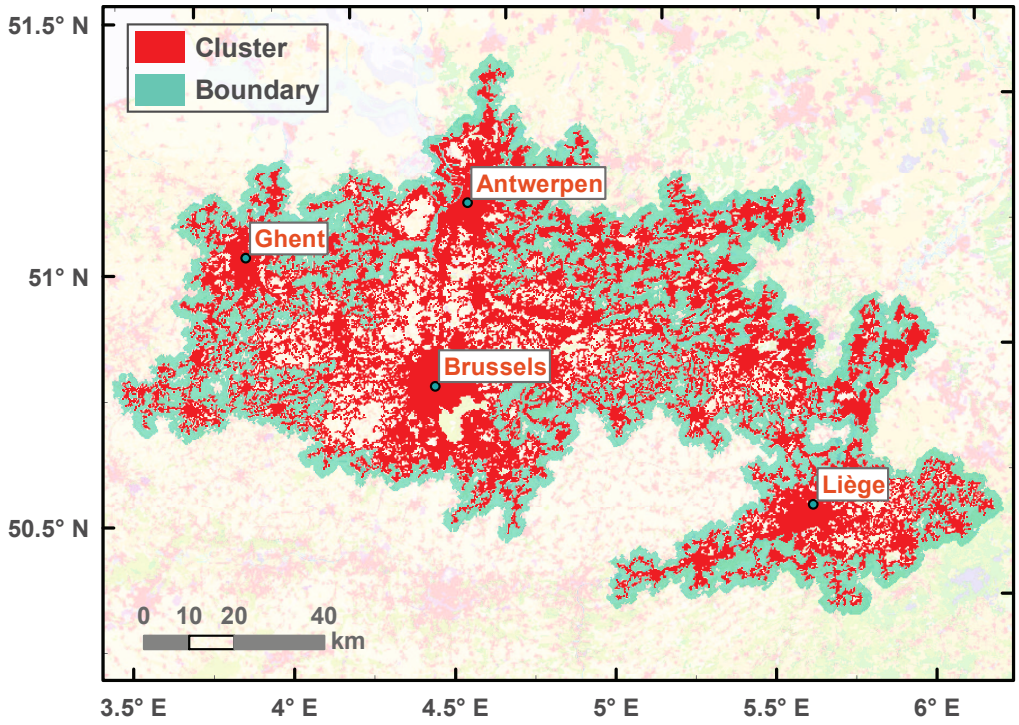

Figure A.5: Urban cluster (red) and boundary (green) identified by CCA for the largest cluster in the scope of this study. The cluster contains mainly the Flemish Diamond (a multi-centered urban agglomeration of Brussels, Ghent, Antwerp and Leuven) and Liège, characterized by scattered urban areas. Cluster and boundary are to some extent interwoven, which should not harm the analysis, since the temperature corresponds well with the land cover as seen in Fig. A.2.

A.4 LARGEST CITY CLUSTER, FLEMISH DIAMOND

Figure A.5 depicts the largest city cluster as identified in this study for comparison with Greater London in Fig. 2.1.

B

APPENDIX CHAPTER 03

This Supplementary Information includes

1. Analyses on the nighttime UHI
2. Correlations between variables
3. Linking heat transfer coefficient, area, and fractal dimension.

B.1 ANALYSES ON THE NIGHTTIME UHI

B.1.1 *Bivariate regression*

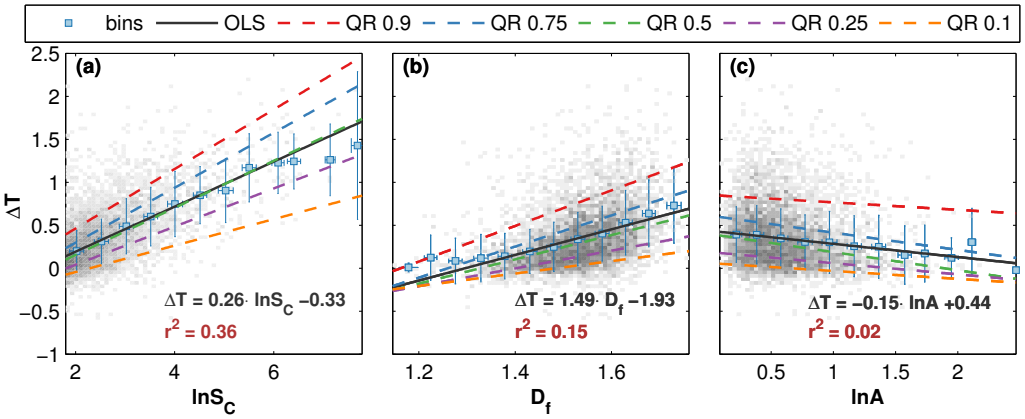

Figure B.1: Nighttime surface UHI intensity (ΔT) as a function of (a) logarithm of urban cluster size $\ln S_C$, (b) fractal dimension D_f, and (c) logarithm of anisometry $\ln A$. Compared to Fig. 3.2 in Chapter 2, the absolute values of regression slopes are smaller.

B.1.2 *Multi-linear regression*

The result obtained from a step-wise multi-linear regression based on 5,000 city clusters, without normalizing the dependent variables – $\ln S_C$, $\ln A$, D_f.

$$\Delta T = -1.03 - 0.10 \ln S_C + 0.11 D_f + 0.53 \ln A + 0.21 D_f \ln S_C - 0.33 D_f \ln A \qquad (R^2 = 0.41) \quad \text{(B.1)}$$

Analogous to Eq. (3.4) in Chapter 3.

The relation based on normalized dependent variables

$$\Delta T = 0.33 + 0.17 \ln S_C^* + 0.09 D_f^* + 0.01 \ln A^* + 0.01 D_f^* \ln S_C^* - 0.01 D_f^* \ln A^* \qquad (R^2 = 0.41) \quad \text{(B.2)}$$

Analogous to Eq. (3.5) in Chapter 3.

Since the nighttime surface UHI is generally weaker than that during daytime (which can be seen from the value range of the Y-axis), the parameters obtained from the multi-linear regression are also correspondingly smaller. However, these results are consistent with the findings in Chapter 3, i.e. city size exerts the strongest influence (0.17 $\ln S_C^*$), followed by fractality (0.09 D_f^*), and anisometry (0.01 $\ln A^*$).

B.2 CORRELATIONS BETWEEN $\ln S_C$, D_F AND $\ln A$

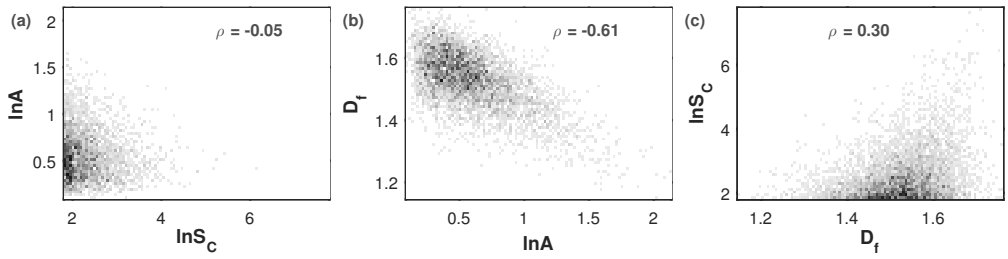

Figure B.2: Correlations among intrinsic urban factors (a) $\ln A$ vs. $\ln S_C$, (b) D_f vs. $\ln A$, and (c) $\ln S_C$ vs. D_f. The grey pixels indicate the number of cities that are covered by them (the darker, the higher the density). The Pearson correlation coefficient ρ is provided in each panel.

B.3 LINKING HEAT TRANSFER COEFFICIENT, AREA, AND FRACTAL

Energy balance of urban surfaces

The energy balance of urban surface can be written as

$$\begin{aligned} Q^* &= K\downarrow - K\uparrow + L\downarrow - L\uparrow \\ &= Q_H + Q_E + Q_G \end{aligned}$$

where

K short-wave radiation (arrows indicate incoming and outgoing),

Q^* net all-wave radiation,

Q_H sensible heat flux,

L long-wave radiation (arrows indicate incoming and outgoing),

Q_E latent heat flux,

Q_G conduction to or from soil.

Regardless of the anthropogenic heat release, surface temperature ($T_{surface}$) is mainly determined by the sensible heat flux Q_H, as $Q_H = h\Delta T = h(T_{surface} - T_{air})$, where h is the convection transfer coefficient. To simplify the problem, we idealize the urban surface as a flat horizontal isotropic plate, without taking into account the surface roughness. The convection heat transfer coefficient h – more precisely, how h is related to object size – is crucial to study the scale effect of the surface temperature (Sakai et al., 2009).

Convection heat transfer coefficient h

The convection heat transfer coefficient h can be expressed by using the dimensionless Nusselt number Nu (the ratio of convective to conductive heat transfer),

$$h = Nu \cdot k/L \tag{B.3}$$

where

h convection heat transfer coefficient [W m^{-2} K^{-1}],

L characteristic length [m],

k thermal conductivity [W m^{-1} s^{-1}].

Empirically, the Nusselt number for a flat plate under turbulent forced convection can be expressed as

$$Nu = C \cdot Re^m \cdot Pr^n \tag{B.4}$$

where

C $\simeq 0.0296$ (Johnson and Rubesin, 1948),

Re Reynolds number [dimensionless],

Pr Prandtl number [dimensionless],

m ≈ 0.8 (empirical number, Johnson and Rubesin, 1948),

n $\approx 2/3$ (empirical number, Johnson and Rubesin, 1948).

The Prandtl number is defined as the ratio of momentum diffusivity to thermal diffusivity,

$$Pr = \frac{c_p \mu}{k} \tag{B.5}$$

where

c_p [J kg^{-1} K^{-1}],

μ dynamic viscosity [N S m^{-2}],

k thermal conductivity [W m^{-1} s^{-1}].

The Reynolds number is defined as the ratio of inertial forces to viscous forces

$$Re = \frac{\rho v L}{\mu} \tag{B.6}$$

where

ρ density [kg m^{-3}],

v wind speed [m s^{-1}].

Combining Eqs. (B.3) to (B.6) we obtain (Sakai et al., 2009)

$$\begin{aligned} h &= C k^{1-n} \rho^m \mu^{n-m} v^m c_p^n L^{m-1} \\ h &\sim L^{m-1} \quad (m - 1 < 0). \end{aligned} \tag{B.7}$$

According to Lovejoy (1982) and Batty and Longley (1994), the perimeter P of an object is given by the area (S) raised to the power of $\widehat{D_f}/2$, i.e.

$P \sim S^{\widehat{D_f}/2}$, where $\widehat{D_f}$ is the fractal dimension of the perimeter. Thus, the characteristic length is $L = S/P \sim S^{1-\widehat{D_f}/2}$. Equation (B.7) can be rewritten as

$$h \sim S^{(1-\widehat{D_f}/2)(m-1)} \quad (1 \leqslant \widehat{D_f} \leqslant 2, 1-m > 0). \tag{B.8}$$

To illustrate the influence of surface area S and fractal dimension D_f, we consider a constant influx of solar radiation. For a fixed fractal dimension, the convection transfer coefficient h decreases with increasing surface area S, resulting in a higher surface temperature. Analogously, for a fixed surface area S, the convection transfer coefficient h decreases with increasing fractal dimension D_f, resulting in a higher surface temperature.

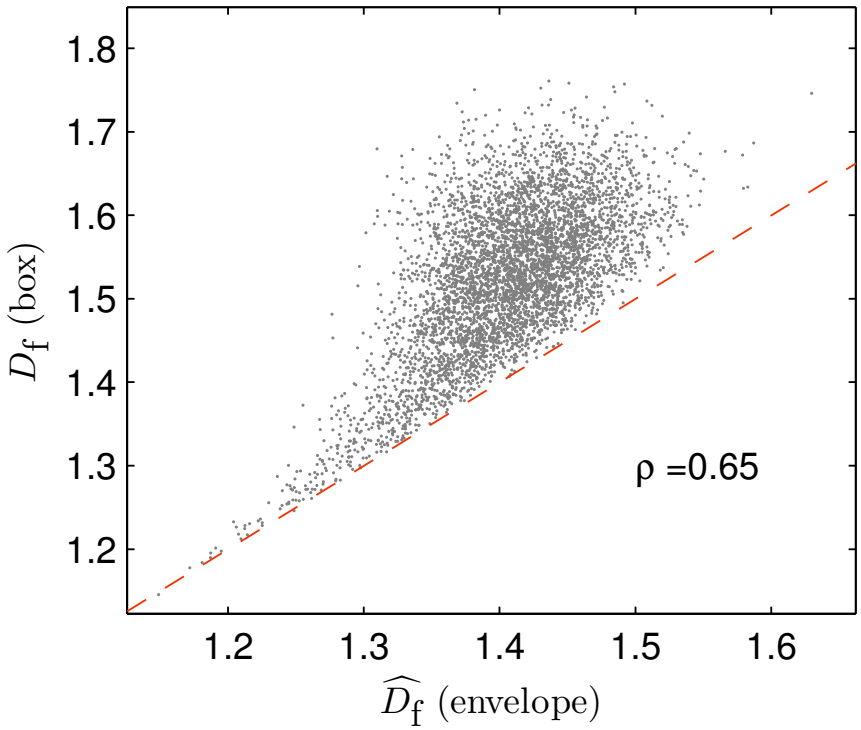

Figure B.3: The box fractal dimension D_f versus the envelope fractal dimension $\widehat{D_f}$. It can be seen that the box fractal dimension is always larger than the envelope fractal dimension.

It is worth mentioning that the fractal dimension $\widehat{D_f}$ of the perimeter, also called as envelope fractal dimension, is different from the fractal dimension calculated in this study. The latter one is also known as box fractal dimension. We estimated both the envelope and box fractal dimensions by applying the box counting method to the urban outline

(envelope) and urban area, respectively (Batty and Longley, 1994). As shown in Fig. B.3, the box fractal dimension is always larger than the envelope fractal dimension. Analyzing our data, we obtained empirically $P \sim S^{aD_f}$, with $a \approx 0.43$. Since the term $1 - a\,D_f$ in Eq. (B.8) is still positive, the conclusions are not affected.

C

INFLUENCE OF CCA PARAMETERS ON THE SURFACE UHI INTENSITY

This Appendix addresses the influence of the CCA parameters – i) threshold distance l, and ii) ratio of boundary area to cluster area – on the calculated UHI intensities, taking Paris and Berlin as examples, respectively.

As shown in Fig. C.1, with the increase of l to 3-fold of the cell size, i.e. 750 m, the city cluster of Paris includes more urban areas extending from the northern edge of Paris. The UHI intensities based on this scenario are smaller than the other two scenarios throughout the year. The scenarios S01 ($l = 250$ m) and R02 ($l = 500$ m) depict slight difference both with respect to the identified cluster form and the derived UHI intensity.

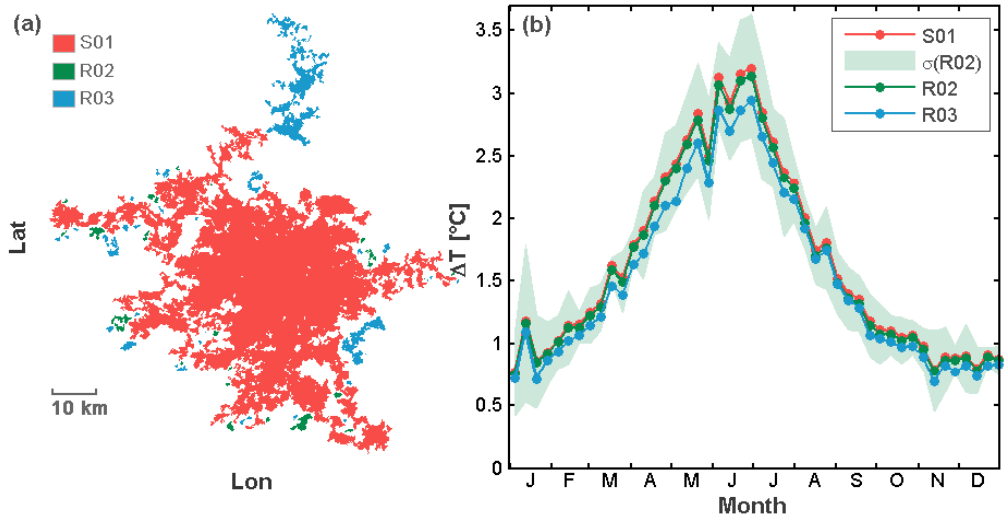

Figure C.1: Influence of CCA-burning distances on the UHI intensity. (a) Paris identified with CCA-burning distances $l = 250$ m (S01), 500 m (R02), 750 m (R03). (b) Time series of mean ΔT over 8 years from 2006 to 2013. The green band indicates the standard deviation for R02. The standard deviations for S01 and R03 are of the same order, and are not shown here.

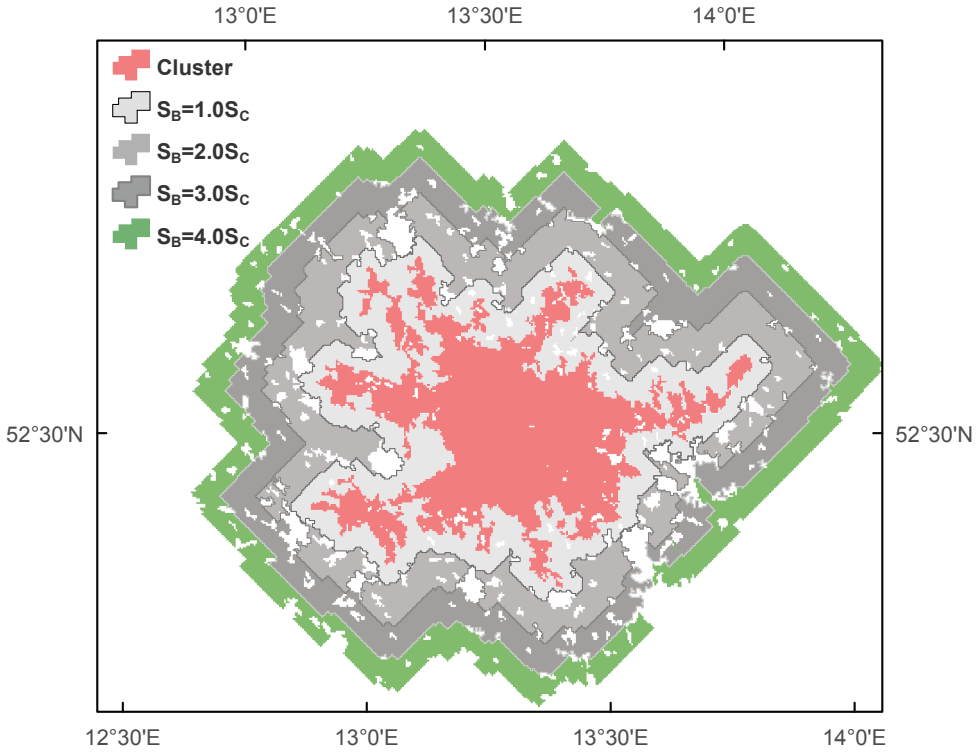

Figure C.2: The city cluster of Berlin, identified with $l = 500m$, with boundaries of different size, ranging from 1.0 to 4.0 S_C. The boundaries are defined in a cumulative way where the outer larger boundaries include the inner smaller ones.

Figure C.2 illustrates the city cluster of Berlin and its boundaries of varying sizes. The UHI intensities based on each setting are shown in Fig. C.3. As observed, the larger the ratio is, the more pronounced is the UHI intensity. This applies for most cities situated in temperate climate zones, where the vegetated/arable boundary areas exhibit lower temperature than cities. Including a larger area into the boundary further lowers the mean temperature of boundaries, thereby increasing the UHI intensity. This is also consistent with the findings in Appendix D that the background temperature follows a pronounced decay.

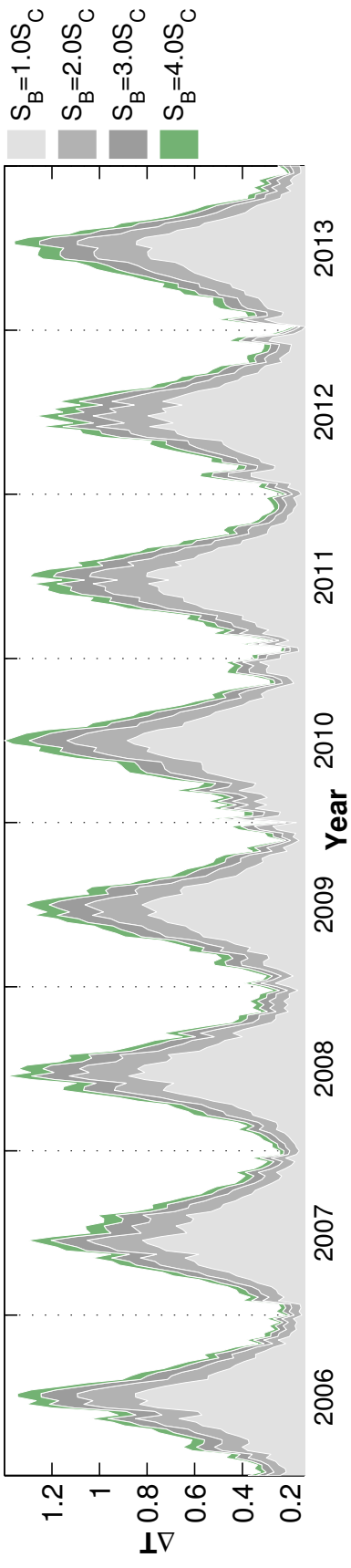

Figure C.3: The time series of ΔT calculated under varying boundary/cluster ratios in the case of Berlin. As observed, the larger the ratio is, the more pronounced is the UHI intensity.

D

DECAY OF SURFACE SKIN TEMPERATURE UNDER TWO APPROACHES OF BUFFER DEFINITION

In this Appendix an analytical relation of the surface temperature decay from a city outwards under two different approaches of buffer definition is derived.

Assuming an ideal city centered at point (x_0, y_0). The surface skin temperature field above the city, as first proposed by Streutker (2002), follows a two-dimensional Gaussian function g,

$$g(x,y) = A \exp\left(-\left(\frac{(x-x_0)^2}{2\sigma_x^2} + \frac{(y-y_0)^2}{2\sigma_y^2}\right)\right),$$

where A is the amplitude and σ_x, σ_y are the x and y spatial extents of the Gaussian surface. To further simplify the problem, we let $x_0 = y_0 = 0$ and $\sigma_x = \sigma_y = \sigma$, and idealize the urban area as a circle with radius R_0, as shown in Fig. D.1. The urban area is then $D = \{(x,y) \in \mathbb{R}^2 : x^2 + y^2 \leqslant R_0^2\}$. Transformed into polar coordinates, $D = \{(\rho,\phi) \in \mathbb{R}^2 : 0 \leqslant \rho \leqslant R_0, 0 \leqslant \phi \leqslant 2\pi\}$,

$$g(\rho,\phi) = A \exp(-\frac{\rho^2}{2\sigma^2}) \tag{D.1}$$

The mean temperature of the city T_0 is

$$T_0 = \frac{\iint_D g(\rho,\phi)\rho \, d\rho d\phi}{\iint_D \rho \, d\rho d\phi} \tag{D.2}$$

$$= \frac{\int_0^{2\pi}\int_0^{R_0} Ae^{-\frac{\rho^2}{2\sigma^2}} \rho \, d\rho d\phi}{\int_0^{2\pi}\int_0^{R_0} \rho \, d\rho d\phi}. \tag{D.3}$$

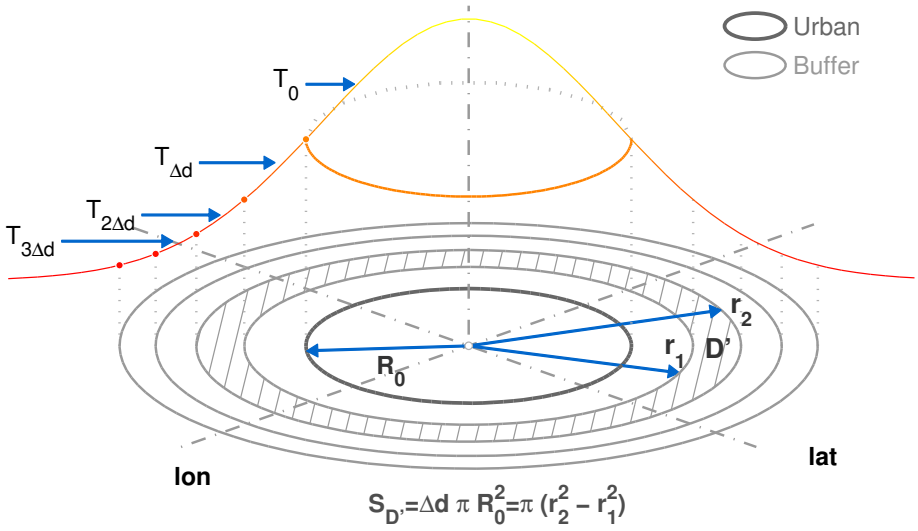

Figure D.1: Schematic of an ideal city and its non-urban buffers overlapped with a Gaussian surface temperature field defined in Eq. (D.1), firstly proposed by Streutker (2002).

Making the substitution $u = -\frac{\rho^2}{2\sigma^2}$, we obtain $du = -\frac{\rho}{\sigma^2}d\rho$.

$$\begin{aligned} T_0 &= \frac{-A\sigma^2 \int_0^{-\frac{R_0^2}{2\sigma^2}} e^u \, du \int_0^{2\pi} d\phi}{\pi R_0^2} \\ &= \frac{2\pi A\sigma^2(1 - e^{-\frac{R_0^2}{2\sigma^2}})}{\pi R_0^2} \\ &= \frac{2A\sigma^2(1 - e^{-\frac{R_0^2}{2\sigma^2}})}{R_0^2} \end{aligned} \tag{D.4}$$

After the city cluster has been identified, there are two approaches to defining the surrounding buffers – circular rings around the city cluster, namely

i) Equal-ratio buffer definition,

ii) Equal-distance buffer definition.

In i), two adjacent buffers are of the same area, whereas they are of the same width in ii).

D.1 EQUAL-RATIO BUFFER DEFINITION

Zhou et al. (2015) delineated the exponential decay of surface skin temperature away from urban areas using a equal-ratio buffer definition. d represents the distance from the urban area in units [*multiple of urban area*]. The non-urban buffer zones extend themselves layer by layer outwards with an increment of Δd [in Zhou et al. (2015), $\Delta d = 0.5$], i.e. each buffer zone is Δd of the urban area by size. If $d = 0$ denotes no buffer, equivalent to the urban area D. The buffer zone with $d = \{\Delta d, 2\Delta d, \dots\}$ away from the urban outline is $D' = \{(\rho, \phi) \in \mathbb{R}^{+2} : r_1 \leqslant \rho \leqslant r_2, 0 \leqslant \phi \leqslant 2\pi, r_2^2 - r_1^2 = \Delta d R_0^2, r_2^2 = (d+1)R_0^2\}$.

The mean temperature of the buffer zone D', T_d is presented as,

$$
\begin{aligned}
T_d &= \frac{-A\sigma^2 \int_{-\frac{r_1^2}{2\sigma^2}}^{-\frac{r_2^2}{2\sigma^2}} e^u \, du \int_0^{2\pi} d\phi}{\pi(r_2^2 - r_1^2)} \\
&= \frac{2A\sigma^2(e^{-\frac{r1^2}{\sigma^2}} - e^{-\frac{r_2^2}{2\sigma^2}})}{r_2^2 - r_1^2} \qquad \text{(D.5)} \\
&= \frac{2A\sigma^2(e^{-\frac{r1^2}{2\sigma^2}} - e^{-\frac{r_2^2}{2\sigma^2}}) \cdot e^{\frac{r_2^2}{2\sigma^2}}}{(r_2^2 - r_1^2) \cdot e^{\frac{r_2^2}{2\sigma^2}}} \\
&= \frac{2A\sigma^2(e^{\frac{\Delta d R_0^2}{2\sigma^2}} - 1)}{\Delta d R_0^2 e^{\frac{(d+1)R_0^2}{2\sigma^2}}} \\
&= \frac{2A\sigma^2(e^{\frac{\Delta d R_0^2}{2\sigma^2}} - 1)}{\Delta d R_0^2 e^{\frac{R_0^2}{2\sigma^2}}} e^{-\frac{R_0^2}{2\sigma^2} d} \\
&= A' e^{-\frac{R_0^2}{2\sigma^2} d}. \qquad \text{(D.6)}
\end{aligned}
$$

As Δd, A, R_0 are predefined or city-specific constants, $A' = 2A\sigma^2 \frac{(e^{\frac{\Delta d R_0^2}{2\sigma^2}} - 1)}{\Delta d R_0^2 e^{\frac{R_0^2}{2\sigma^2}}}$ is a constant. The mean temperature away from the urban decays exponentially, with a decay rate of $-\frac{R_0^2}{2\sigma^2}$. This relation has been empirically described in Chinese cities (Zhou et al., 2015).

D.2 EQUAL-DISTANCE BUFFER DEFINITION

In the equal-distance buffer definition, each buffer is generated consecutively with a predefined radical increment Δl outwards. Buffer area with a distance l from the urban outskirts can be written as $L' = \{(\rho, \phi) \in \mathbb{R}^{+2} : r_1 \leqslant \rho \leqslant r_2, 0 \leqslant \phi \leqslant 2\pi, r_2 - r_1 = \Delta l, r_2 = R_0 + l\}$. Analogously, as deduced above, the mean tempearture of L' is the same as Eq. (D.5),

$$
\begin{aligned}
T_l &= \frac{2A\sigma^2(e^{-\frac{r1^2}{2\sigma^2}} - e^{-\frac{r_2^2}{2\sigma^2}})}{r_2^2 - r_1^2} = \frac{2A\sigma^2(e^{-\frac{(r2-\Delta l)^2}{2\sigma^2}} - e^{-\frac{r_2^2}{2\sigma^2}})}{(r_2 + r_1)(r_2 - r_1)} \\
&= \frac{2A\sigma^2 e^{-\frac{(r_2 - \frac{\Delta l}{2})^2}{2\sigma^2}}[e^{(\frac{r_2\Delta l}{2\sigma^2} - \frac{3\Delta l^2}{8\sigma^2})} - e^{(-\frac{r_2\Delta l}{2\sigma^2} + \frac{\Delta l^2}{8\sigma^2})}]}{(2r_2 - \Delta l)\Delta l} \\
&= \frac{2A\sigma^2 e^{-\frac{(r_2 - \frac{\Delta l}{2})^2}{2\sigma^2}} e^{-\frac{\Delta l^2}{8\sigma^2}}[e^{(\frac{r_2\Delta l}{2\sigma^2} - \frac{\Delta l^2}{4\sigma^2})} - e^{(-\frac{r_2\Delta l}{2\sigma^2} + \frac{\Delta l^2}{4\sigma^2})}]}{2r_2\Delta l - \Delta l^2} \\
&= \frac{2A\sigma^2 e^{-\frac{\Delta l^2}{8\sigma^2}} e^{-\frac{(r_2 - \frac{\Delta l}{2})^2}{2\sigma^2}} 2\sinh(\frac{r_2\Delta l}{2\sigma^2} - \frac{\Delta l^2}{4\sigma^2})}{2r_2\Delta l - \Delta l^2} \\
&\approx \frac{A\sigma^2 e^{-\frac{\Delta l^2}{8\sigma^2}} e^{-\frac{(r_2 - \frac{\Delta l}{2})^2}{2\sigma^2}} \frac{2r_2\Delta l - \Delta l^2}{\sigma^2}}{2r_2\Delta l - \Delta l^2} \\
&\approx A' e^{-\frac{(r_2 - \frac{\Delta l}{2})^2}{2\sigma^2}} \\
&\approx A' e^{-\frac{(l + R_0 - \frac{\Delta l}{2})^2}{2\sigma^2}},
\end{aligned}
\tag{D.7}
$$

where, $A' = Ae^{-\frac{\Delta l^2}{8\sigma^2}}$. As shown in Eq. (D.7), the exponential decay of T_l with l does not apply here. However, the relationship can be described by the first order Gaussian model, i.e. the T_l decays approximately with l^2. In comparison to the equal-ratio buffer definition, the surface temperature based on the equal-distance buffer definition exhibits a more pronounced decrease.

BIBLIOGRAPHY

Akaike, H (1973). "Information theory as an extension of the maximum likelihood principle". In: *Second International Symposium on Information Theory*. Ed. by B. N. Petrov and F Csaki. Vol. 19. Budapest: Akademiai Kiado, pp. 267–281.

Akbari, H., M. Pomerantz, and H. Taha (2001). "Cool surfaces and shade trees to reduce energy use and improve air quality in urban areas". In: *Sol. Energy* 70.3, pp. 295–310. DOI: 10.1016/S0038-092X(00)00089-X.

Akbari, H. (2005). "Energy Saving Potentials and Air Quality Benefits of Urban Heat Island Mitigation". In: *Sol. Energy*, pp. 1–19.

Arnfield, A. J. (2003). "Two decades of urban climate research: A review of turbulence, exchanges of energy and water, and the urban heat island". In: *Int. J. Climatol.* 23.1, pp. 1–26. DOI: 10.1002/joc.859.

Arnfield, a. J. and C. Grimmond (1998). "An urban canyon energy budget model and its application to urban storage heat flux modeling". In: *Energy Build.* 27.1, pp. 61–68. DOI: 10.1016/S0378-7788(97)00026-1.

Auerbach, F. (1913). "Das Gesetz der Bevölkerungskonzentration". In: *Petermanns Geogr. Mitteilungen* 59.74, pp. 73–76.

Ban, Y., A. Jacob, and P. Gamba (2014). "Spaceborne SAR data for global urban mapping at 30m resolution using a robust urban extractor". In: *ISPRS J. Photogramm. Remote Sens.* 103, pp. 28–37. DOI: 10.1016/j.isprsjprs.2014.08.004.

Batty, M. and P. A. Longley (1987a). "Fractal-based description of urban form". In: *Environ. Plann. B* 14.2, pp. 123–134. DOI: 10.1068/b140123.

— (1987b). "Urban shapes as fractals". In: *Area* 19.3, pp. 215–221. URL: http://www.jstor.org/stable/20002475.

Batty, M. and P. Longley (1994). *Fractal Cities: A Geometry of Form and Function*. San Diego, CA and London: Academic Press Inc.

Batty, M. (2008). "The Size, Scale, and Shape of Cities". In: *Science (80-.).* 319.5864, pp. 769–771. DOI: 10.1126/science.1151419.

Best, M. J. and C. S. B. Grimmond (2015). "Key Conclusions of the First International Urban Land Surface Model Comparison Project". In: *Bull. Am. Meteorol. Soc.* 96.5, pp. 805–819. DOI: 10.1175/BAMS-D-14-00122.1.

Bettencourt, L. M. and G. West (2010). "A unified theory of urban living." In: *Nature* 467.7318, pp. 912–913. DOI: 10.1038/467912a.

Brazel, A., N. Selover, R. Vose, and G. Heisler (2000). "The tale of two climates — Baltimore and Phoenix urban LTER sites". In: *Clim. Res.* 15, pp. 123–135. DOI: 10.3354/cr015123.

Bruse, M. and H. Fleer (1998). "Simulating surface-plant-air interactions inside urban environments with a three dimensional numerical model". In: *Environ. Model. Softw.* 13.3-4, pp. 373–384. DOI: 10.1016/S1364-8152(98)00042-5.

Bunde, A. and S. Havlin (1996). *Fractals and Disordered Systems*. Berlin: Springer.

Büttner, G., T. Soukup, and A. Sousa (2007). *CLC2006 technical guidelines*. Tech. rep. 17. Available at: http://www.eea.europa.eu/publications/technical_report_2007_17. (Accessed: 11th May 2016). EEA.

Cade, B. S. and B. R. Noon (2003). "A gentle introduction to quantile regression for ecologists". In: *Front. Ecol. Environ.* 1.8, pp. 412–420. DOI: 10.1890/1540-9295(2003)001[0412:AGITQR]2.0.CO;2.

Chandler, T. J. (1967). "Night-time temperatures in relation to Leicester's urban form". In: *Meteorol. Mag.* 96, pp. 244–250.

Chow, W. T. L., R. L. Pope, C. A. Martin, and A. J. Brazel (2011). "Observing and modeling the nocturnal park cool island of an arid city: horizontal and vertical impacts". In: *Theor. Appl. Climatol.* 103.1-2, pp. 197–211. DOI: 10.1007/s00704-010-0293-8.

Clinton, N. and P. Gong (2013). "MODIS detected surface urban heat islands and sinks: Global locations and controls". In: *Remote Sens. Environ.* 134, pp. 294–304. DOI: 10.1016/j.rse.2013.03.008.

Coceal, O. and S. E. Belcher (2005). "Mean winds through an inhomogeneous urban canopy". In: *Boundary-Layer Meteorol.* 115.1, pp. 47–68. DOI: 10.1007/s10546-004-1591-4.

Coumou, D. and S. Rahmstorf (2012). "A decade of weather extremes". In: *Nat. Clim. Chang.* 2.7, pp. 1–6. DOI: 10.1038/nclimate1452.

Cui, Y. Y. and B. de Foy (2012). "Seasonal Variations of the Urban Heat Island at the Surface and the Near-Surface and Reductions due to Urban Vegetation in Mexico City". In: *J. Appl. Meteorol. Climatol.* 51.5, pp. 855–868. DOI: 10.1175/JAMC-D-11-0104.1.

Danielson, J. J. and D. B. Gesch (2011). *Global multi-resolution terrain elevation data 2010 (GMTED2010)*. U.S. Geological Survey Open-File Report 2011-1073.

Dash, P., F.-M. Göttsche, F.-S. Olesen, and H. Fischer (2002). "Land surface temperature and emissivity estimation from passive sensor data: Theory and practice-current trends". In: *Int. J. Remote Sens.* 23.13, pp. 2563–2594. DOI: 10.1080/01431160110115041.

de Munck, C., G. Pigeon, V. Masson, F. Meunier, P. Bousquet, B. Tréméac, M. Merchat, P. Poeuf, and C. Marchadier (2013). "How much can air conditioning increase air temperatures for a city like Paris, France?" In: *Int. J. Climatol.* 33.1, pp. 210–227. DOI: 10.1002/joc.3415.

De Ridder, K. (2006). "Testing Brutsaert's temperature roughness parameterization for representing urban surfaces in atmospheric models". In: *Geophys. Res. Lett.* 33.13, p. L13403.

De Ridder, K. and G Schayes (1997). "The IAGL Land Surface Model". In: *J. Appl. Meteor.* 36.2, pp. 167–182.

De Ridder, K. et al. (2008). "Simulating the impact of urban sprawl on air quality and population exposure in the German Ruhr area. Part I: reproducing the base state". In: *Atmos. Environ.* 42.30, pp. 7059–7069.

De Ridder, K., C. Bertrand, G. Casanova, and W. Lefebvre (2012). "Exploring a new method for the retrieval of urban thermophysical properties using thermal infrared remote sensing and deterministic modeling". In: *J. Geophys. Res.* 117, p. D17108.

De Ridder, K., D. Lauwaet, and B. Maiheu (2015). "UrbClim – A fast urban boundary layer climate model". In: *Urban Clim.* 12, pp. 21–48. DOI: 10.1016/j.uclim.2015.01.001.

Debbage, N. and J. M. Shepherd (2015). "The urban heat island effect and city contiguity". In: *Comput. Environ. Urban Syst.* 54.October, pp. 181–194. DOI: 10.1016/j.compenvurbsys.2015.08.002.

Dong, Y., A. Varquez, and M. Kanda (2016). "Global anthropogenic heat flux database with high spatial resolution". In: *Atmos. Environ.* 150, pp. 276–294. DOI: 10.1016/j.atmosenv.2016.11.040.

Donner, R. V., R. Ehrcke, S. M. Barbosa, J. Wagner, J. F. Donges, and J. Kurths (2012). "Spatial patterns of linear and nonparametric long-term trends in Baltic sea-level variability". In: *Nonlinear Proc. Geoph.* 19.1, pp. 95–111. DOI: 10.5194/npg-19-95-2012.

Elvidge, C. D., K. E. Baugh, J. B. Dietz, T. Bland, P. C. Sutton, and H. W. Kroehl (1999). "Radiance Calibration of DMSP-OLS Low-Light Imaging Data of Human Settlements". In: *Remote Sens. Environ.* 68.1, pp. 77–88. DOI: 10.1016/S0034-4257(98)00098-4.

Encarnação, S., M. Gaudiano, F. C. Santos, J. A. Tenedório, and J. M. Pacheco (2012). "Fractal cartography of urban areas". In: *Sci. Rep.* 2.527. DOI: 10.1038/srep00527.

EPA (2001). *Our built and natural environments: A technical review of the interactions between land use, transportation, and environmental quality*. Tech. rep. URL: https://www.epa.gov/sites/production/files/2014-03/documents/our-built-and-natural-environments.pdf.

Estournel, C., R. Vehil, D. Guedalia, J. Fontan, and A. Druilhet (1983). "Observations and Modeling of Downward Radiative Fluxes (Solar

and Infrared) in Urban/Rural Areas". In: *J. Clim. Appl. Meteorol.* 22.1, pp. 134–142. DOI: 10.1175/1520-0450(1983)022<0134:OAMODR>2.0.CO;2.

Estrada, F., W. J. W. Botzen, and R. S. J. Tol (2017). "A global economic assessment of city policies to reduce climate change impacts". In: *Nat. Clim. Chang.* 7.6, pp. 403–406. DOI: 10.1038/nclimate3301.

Ewing, R. and F. Rong (2008). "The impact of urban form on US residential energy use". In: *Hous. Policy Debate* 19.1, pp. 1–30. DOI: 10.1080/10511482.2008.9521624.

Fan, Y. (2004). "Climate Prediction Center global monthly soil moisture data set at 0.5° resolution for 1948 to present". In: *J. Geophys. Res.* 109.D10, p. D10102. DOI: 10.1029/2003JD004345.

Ferguson, G. and A. D. Woodbury (2007). "Urban heat island in the subsurface". In: *Geophys. Res. Lett.* 34.23, pp. 2–5. DOI: 10.1029/2007GL032324.

Feyisa, G. L., K. Dons, and H. Meilby (2014). "Efficiency of parks in mitigating urban heat island effect: An example from Addis Ababa". In: *Landsc. Urban Plan.* 123.March, pp. 87–95. DOI: 10.1016/j.landurbplan.2013.12.008.

Figuerola, P. I. and N. A. Mazzeo (1998). "Urban-rural temperature differences in Buenos Aires". In: *Int. J. Climatol.* 18.15, pp. 1709–1723. DOI: 10.1002/(SICI)1097-0088(199812)18:15<1709::AID-JOC338>3.0.CO;2-I.

Fischer, E. M. and C. Schär (2010). "Consistent geographical patterns of changes in high-impact European heatwaves". In: *Nat. Geosci.* 3.6, pp. 398–403. DOI: 10.1038/ngeo866.

Fluschnik, T., S. Kriewald, A. G. C. Ros, B. Zhou, D. E. Reusser, J. P. Kropp, and D. Rybski (2016). "The size distribution, scaling properties and spatial organization of urban clusters: a global and regional percolation perspective". In: *Int. J. Geo-Information* 5.7, p. 110. DOI: 10.3390/ijgi5070110.

Fouillet, A, G Rey, F Laurent, G Pavillon, S Bellec, C Guihenneuc-Jouyaux, J Clavel, E Jougla, and D. Hémon (2006). "Excess mortality related to the August 2003 heat wave in France." In: *Int. Arch. Occup. Environ. Health* 80.1, pp. 16–24.

Frank, L., J. Sallis, T. Conway, J. Chapman, B. Saelens, and W. Bachman (2006). "Many Pathways from Land Use to Health and Air Quality". In: *J. Am. Plan. Assoc.* 72.No. I, pp. 75–87. DOI: 10.1080/01944360608976725.

Friedl, M. A., D. Sulla-Menashe, B. Tan, A. Schneider, N. Ramankutty, A. Sibley, and X. Huang (2010). "MODIS Collection 5 global land cover: Algorithm refinements and characterization of new datasets".

In: *Remote Sens. Environ.* 114.1, pp. 168–182. DOI: 10.1016/j.rse.2009.08.016.

Fukui, E. (1957). "Increasing temperature due to the expansion of urban areas in Japan". In: *J. Meteor. Soc. Japan* 75th anniv, pp. 336–341.

Gago, E. J., J. Roldan, R. Pacheco-Torres, and J. Ordóñez (2013). "The city and urban heat islands: A review of strategies to mitigate adverse effects". In: *Renew. Sustain. Energy Rev.* 25, pp. 749–758. DOI: 10.1016/j.rser.2013.05.057.

Gallo, K., R. Hale, D. Tarpley, and Y. Yu (2011). "Evaluation of the relationship between air and land surface temperature under clear- and cloudy-sky conditions". In: *J. Appl. Meteorol. Climatol.* 50.3, pp. 767–775. DOI: 10.1175/2010JAMC2460.1.

Gamba, P. and M. Herold (2009). *Global Mapping of Human Settlement*. Ed. by P. Gamba and M. Herold. Vol. 20090662. Remote Sensing Applications Series. CRC Press. DOI: 10.1201/9781420083408.

Garratt, J. R. (1992). *The Atmospheric Boundary Layer*. Cambridge University Press, p. 316.

Georgescu, M., G. Miguez-Macho, L. T. Steyaert, and C. P. Weaver (2009). "Climatic effects of 30 years of landscape change over the Greater Phoenix, Arizona, region: 1. Surface energy budget changes". In: *J. Geophys. Res.* 114.D5, p. D05110. DOI: 10.1029/2008JD010745.

Georgescu, M, M Moustaoui, A Mahalov, and J Dudhia (2011). "An alternative explanation of the semiarid urban area oasis effect". In: *J. Geophys. Res.* 116.

Georgescu, M, a Mahalov, and M Moustaoui (2012). "Seasonal hydroclimatic impacts of Sun Corridor expansion". In: *Environ. Res. Letters* 7.3, p. 034026. DOI: 10.1088/1748-9326/7/3/034026.

Georgescu, M, W. T. L. Chow, Z. H. Wang, A Brazel, B Trapido-Lurie, M Roth, and V Benson-Lira (2015). "Prioritizing urban sustainability solutions: coordinated approaches must incorporate scale-dependent built environment induced effects". In: *Environ. Res. Lett.* 10.6, p. 61001. DOI: 10.1088/1748-9326/10/6/061001.

Gong, P. et al. (2013). "Finer resolution observation and monitoring of global land cover: first mapping results with Landsat TM and ETM+ data". In: *Int. J. Remote Sens.* 34.7, pp. 2607–2654. DOI: 10.1080/01431161.2012.748992.

Grazi, F., J. J.C.J. M. van den Bergh, and J. N. van Ommeren (2008). "An Empirical Analysis of Urban Form, Transport, and Global Warming". In: *Energy J.* 29.4, pp. 97–122. DOI: 10.2307/41323183.

Grimmond, C. S. B. et al. (2010). "The International Urban Energy Balance Models Comparison Project: First Results from Phase 1". In: *J. of*

Appl. Meteorol. Climatol. 49, pp. 1268–1292. DOI: 10.1175/2010JAMC2354.1.

Grimmond, C. S. B. et al. (2011). "Initial results from Phase 2 of the international urban energy balance model comparison". In: *Int. J. Climatol.* 31.2, pp. 244–272. DOI: 10.1002/joc.2227.

Grossman-Clarke, S., S. Schubert, and D. Fenner (2017). "Urban effects on summertime air temperature in Germany under climate change". In: *Int. J. Climatol.* 37.2, pp. 905–917. DOI: 10.1002/joc.4748.

Gutman, G. and A. Ignatov (1998). "The derivation of the green vegetation fraction from NOAA/AVHRR data for use in numerical weather prediction models". In: *Int. J. Remote Sensing* 19.8, pp. 1533–1543. DOI: 10.1080/014311698215333.

Holderness, T., S. Barr, R. Dawson, and J. Hall (2013). "An evaluation of thermal Earth observation for characterizing urban heatwave event dynamics using the urban heat island intensity metric". In: *Int. J. Remote Sens.* 34, pp. 864–884. DOI: 10.1080/01431161.2012.714505.

Howard, L. (1833). *The climate of London*. Vol. 1. Gent, p. 221.

Hu, L., N. A. Brunsell, A. J. Monaghan, M. Barlage, and O. V. Wilhelmi (2014). "How can we use MODIS land surface temperature to validate long-term urban model simulations?" In: *J. Geophys. Res. Atmos.* 119.6, pp. 3185–3201. DOI: 10.1002/2013JD021101.

Hu, L., A. Monaghan, J. A. Voogt, and M. Barlage (2016). "A first satellite-based observational assessment of urban thermal anisotropy". In: *Remote Sens. Environ.* 181, pp. 111–121. DOI: 10.1016/j.rse.2016.03.043.

Huang, J., X. Lu, and J. M. Sellers (2007). "A global comparative analysis of urban form: Applying spatial metrics and remote sensing". In: *Landsc. Urban Plan.* 82.4, pp. 184–197. DOI: 10.1016/j.landurbplan.2007.02.010.

Ichinose, T., K. Shimodozono, and K. Hanaki (1999). "Impact of anthropogenic heat on urban climate in Tokyo". In: *Atmos. Environ.* 33.24-25, pp. 3897–3909. DOI: 10.1016/S1352-2310(99)00132-6.

Imhoff, M. L., W. T. Lawrence, D. C. Stutzer, and C. D. Elvidge (1997). "A technique for using composite DMSP/OLS 'city lights' satellite data to map urban area". In: *Remote Sens. Environ.* 61.3, pp. 361–370. DOI: 10.1016/S0034-4257(97)00046-1.

Imhoff, M. L., P. Zhang, R. E. Wolfe, and L. Bounoua (2010). "Remote sensing of the urban heat island effect across biomes in the continental USA". In: *Remote Sens. Environ.* 114, pp. 504–513. DOI: 10.1016/j.rse.2009.10.008.

IPCC (2014). *Climate Change 2013 - The Physical Science Basis*. Ed. by Intergovernmental Panel on Climate Change. Cambridge: Cambridge University Press, p. 33. DOI: 10.1017/CBO9781107415324.

Jabareen, Y. R. (2006). "Sustainable Urban Forms: Their Typologies, Models, and Concepts". In: *J. Plan. Educ. Res.* 26.1, pp. 38–52. DOI: 10.1177/0739456X05285119.

Jain, A. K. and R. C. Dubes (1988). *Algorithms for Clustering Data*. Vol. 355. Englewood Cliffs, New Jersey: Prentice Hall, p. 320.

Jauregui, E. (1997). "Heat island development in Mexico City". In: *Atmos. Environ.* 31.22, pp. 3821–3831. DOI: 10.1016/S1352-2310(97)00136-2.

Jin, M. and R. E. Dickinson (2010). "Land surface skin temperature climatology: benefitting from the strengths of satellite observations". In: *Environ. Res. Lett.* 5.4, p. 044004. DOI: 10.1088/1748-9326/5/4/044004.

Johnson, H. and M. Rubesin (1948). *Aerodynamic Heating and Convective Heat Transfer*. American Society of Mechanical Engineers, p. 10.

Kalnay, E. and M. Cai (2003). "Impact of urbanization and land-use change on climate." In: *Nature* 423.6939, pp. 528–31. DOI: 10.1038/nature01675.

Kanda, M., M. Kanega, T. Kawai, R. Moriwaki, and H. Sugawara (2007). "Roughness Lengths for Momentum and Heat Derived from Outdoor Urban Scale Models". In: *J. Appl. Meteor. Climatol.* 46.7, pp. 1067–1079. DOI: 10.1175/JAM2500.1.

Kanda, M. (2007). "Progress in Urban Meteorology :A Review". In: *J. Meteorol. Soc. Japan* 85B, pp. 363–383. DOI: 10.2151/jmsj.85B.363.

Kato, S. and Y. Yamaguchi (2005). "Analysis of urban heat-island effect using ASTER and ETM+ Data: Separation of anthropogenic heat discharge and natural heat radiation from sensible heat flux". In: *Remote Sens. Environ.* 99.1-2, pp. 44–54. DOI: 10.1016/j.rse.2005.04.026.

Kim, Y.-H. and J.-J. Baik (2005). "Spatial and Temporal Structure of the Urban Heat Island in Seoul". In: *J. Appl. Meteorol.* 44.5, pp. 591–605. DOI: 10.1175/JAM2226.1.

Koenker, R. and G. Bassett, Jr. (1978). "Regression Quantiles". In: *Econometrica* 46.1, pp. 33–50. URL: http://www.jstor.org/stable/1913643.

Koenker, R. and K. F. Hallock (2001). "Quantile Regression". In: *J. Econ. Perspect.* 15.4, pp. 143–156. DOI: 10.1257/jep.15.4.143.

Kusaka, H. and F. Kimura (2004). "Thermal Effects of Urban Canyon Structure on the Nocturnal Heat Island: Numerical Experiment Using a Mesoscale Model Coupled with an Urban Canopy Model". In: *J. Appl. Meteorol.* 43.12, pp. 1899–1910. DOI: 10.1175/JAM2169.1.

Lagouarde, J. P., A. Hénon, M. Irvine, J. Voogt, G. Pigeon, P. Moreau, V. Masson, and P. Mestayer (2012). "Experimental characterization and

modelling of the nighttime directional anisotropy of thermal infrared measurements over an urban area: Case study of Toulouse (France)". In: *Remote Sens. Environ.* 117, pp. 19–33. DOI: 10.1016/j.rse.2011.06.022.

Lagouarde, J. P., P. Moreau, M. Irvine, J. M. Bonnefond, J. A. Voogt, and F. Solliec (2004). "Airborne experimental measurements of the angular variations in surface temperature over urban areas: Case study of Marseille (France)". In: *Remote Sens. Environ.* 93.4, pp. 443–462. DOI: 10.1016/j.rse.2003.12.011.

Lauwaet, D., H. Hooyberghs, B. Maiheu, W. Lefebvre, G. Driesen, S. Van Looy, and K. De Ridder (2015). "Detailed Urban Heat Island Projections for Cities Worldwide: Dynamical Downscaling CMIP5 Global Climate Models". In: *Climate* 3.2, pp. 391–415. DOI: 10.3390/cli3020391.

Lee, S. H. and J. J. Baik (2010). "Statistical and dynamical characteristics of the urban heat island intensity in Seoul". In: *Theor. Appl. Climatol.* 100.1, pp. 227–237. DOI: 10.1007/s00704-009-0247-1.

Lemonsu, A., R. Kounkou-Arnaud, J. Desplat, J.-L. L. Salagnac, and V. Masson (2013). "Evolution of the Parisian urban climate under a global changing climate". In: *Clim. Change* 116.3-4, pp. 679–692. DOI: 10.1007/s10584-012-0521-6.

Lettenmaier, D., V. Mishra, A. Ganguly, and B. Nijssen (2014). "Observed Climate Extremes in Global Urban Areas". In: *Environ. Res. Lett.* 16.2, p. 14787. DOI: 10.1088/1748-9326/10/2/024005.

Levin, N. and Q. Zhang (2017). "A global analysis of factors controlling VIIRS nighttime light levels from densely populated areas". In: *Remote Sens. Environ.* 190, pp. 366–382. DOI: 10.1016/j.rse.2017.01.006.

Li, D. and E. Bou-Zeid (2013). "Synergistic interactions between urban heat islands and heat waves: The impact in cities is larger than the sum of its parts". In: *J. Appl. Meteorol. Climatol.* 52.9, pp. 2051–2064. DOI: 10.1175/JAMC-D-13-02.1.

Li, D., E. Bou-Zeid, and M. Oppenheimer (2014). "The effectiveness of cool and green roofs as urban heat island mitigation strategies". In: *Environ. Res. Lett.* 9.5, p. 055002. DOI: 10.1088/1748-9326/9/5/055002.

Li, Z.-L., B.-H. Tang, H. Wu, H. Ren, G. Yan, Z. Wan, I. F. Trigo, and J. a. Sobrino (2013). "Satellite-derived land surface temperature: Current status and perspectives". In: *Remote Sens. Environ.* 131, pp. 14–37. DOI: 10.1016/j.rse.2012.12.008.

Liu, Z., C. He, Y. Zhou, and J. Wu (2014). "How much of the world's land has been urbanized, really? A hierarchical framework for avoiding

confusion". In: *Landsc. Ecol.* 29.5, pp. 763–771. DOI: 10.1007/s10980-014-0034-y.

Louf, R. and M. Barthelemy (2014). "How congestion shapes cities: From mobility patterns to scaling". In: *Sci. Rep.* 4.5561. DOI: 10.1038/srep05561.

Lovejoy, S. (1982). "Area-Perimeter Relation for Rain and Cloud Areas". In: *Science* 216.4542, pp. 185–187. DOI: 10.1126/science.216.4542.185.

Makse, H. A., J. S. Andrade, M. Batty, S. Havlin, and H. E. Stanley (1998). "Modeling urban growth patterns with correlated percolation". In: *Phys. Rev. E* 58 (6), pp. 7054–7062. DOI: 10.1103/PhysRevE.58.7054.

Martilli, A. (2014). "An idealized study of city structure, urban climate, energy consumption, and air quality". In: *Urban Clim.* 10, pp. 430–446. DOI: 10.1016/j.uclim.2014.03.003.

Masson, V. (2005). "Urban surface modeling and the meso-scale impact of cities". In: *Theor. Appl. Climatol.* 84.1-3, pp. 35–45. DOI: 10.1007/s00704-005-0142-3. URL: http://www.springerlink.com/index/10.1007/s00704-005-0142-3.

McCarthy, M. P., M. J. Best, and R. a. Betts (2010). "Climate change in cities due to global warming and urban effects". In: *Geophys. Res. L.* 37, p. L09705. DOI: 10.1029/2010GL042845.

McGarigal, K. and B. J. Marks (1994). *FRAGSTATS: spatial pattern analysis program for quantifying landscapes Structure*. Tech. rep. 503, p. 134.

Medalia, A. and G. Hornik (1972). "Pattern recognition problems in the study of carbon black". In: *Pattern Recognit.* 4.2, pp. 155–172. DOI: 10.1016/0031-3203(72)90026-X.

Meehl, G. a. and C. Tebaldi (2004). "More intense, more frequent, and longer lasting heat waves in the 21st century." In: *Science* 305.5686, pp. 994–7. DOI: 10.1126/science.1098704.

Menberg, K., P. Blum, A. Schaffitel, and P. Bayer (2013). "Long-term evolution of anthropogenic heat fluxes into a subsurface urban heat island." In: *Environ. Sci. Technol.* 47.17, pp. 9747–55. DOI: 10.1021/es401546u.

Mills, G. (2014). "Urban climatology: History, status and prospects". In: *Urban Clim.* 10.P3, pp. 479–489. DOI: 10.1016/j.uclim.2014.06.004.

Mohan, M. and A. Kandya (2015). "Impact of urbanization and land-use/land-cover change on diurnal temperature range: A case study of tropical urban airshed of India using remote sensing data". In: *Sci. Total Environ.* 506-507, pp. 453–465. DOI: 10.1016/j.scitotenv.2014.11.006.

Mostovoy, G., R. King, K. Reddy, V. Kakani, and M. Filippova (2006). "Statistical estimation of daily maximum and minimum air temper-

atures from MODIS LST data over the state of Mississippi". In: *GIScience Remote Sens.* 43.1, pp. 78–110.

Mueller, B. and S. I. Seneviratne (2012). "Hot days induced by precipitation deficits at the global scale." In: *Proc. Natl. Acad. Sci. U. S. A.* 109.31, pp. 12398–403. DOI: 10.1073/pnas.1204330109.

Norman, J. M. and F. Becker (1995). "Terminology in thermal infrared remote sensing of natural surfaces". In: *Remote Sens. Rev.* 12.3-4, pp. 159–173. DOI: 10.1080/02757259509532284.

Nunez, M., I. Eliasson, and J. Lindgren (2000). "Spatial variations of incoming longwave radiationin Göteborg, Sweden". In: *Theor. Appl. Climatol.* 67.3-4, pp. 181–192. DOI: 10.1007/s007040070007.

OECD (2014). *Cities and Climate Change: National governments enabling local action*. OECD Publishing, p. 19. DOI: 10.1787/9789264091375-en.

Ohashi, Y., Y. Genchi, H. Kondo, Y. Kikegawa, H. Yoshikado, and Y. Hirano (2007). "Influence of Air-Conditioning Waste Heat on Air Temperature in Tokyo during Summer: Numerical Experiments Using an Urban Canopy Model Coupled with a Building Energy Model". In: *J. Appl. Meteorol. Climatol.* 46.1, pp. 66–81. DOI: 10.1175/JAM2441.1.

Oke, T. R. (1973). "City size and the urban heat island". In: *Atmos. Environ.(1967)* 7, pp. 769–779. DOI: 10.1016/0004-6981(73)90140-6.

— (1982). "The energetic basis of the urban heat island". In: *Q. J. R. Meteorol. Soc.* 108.455, pp. 1–24. DOI: 10.1002/qj.49710845502.

— (1987). *Boundary Layer Climates*. 2nd. Methuen, London, 435 pp.

Oke, T. R., G. T. Johnson, D. G. Steyn, and I. D. Watson (1991). "Simulation of surface urban heat islands under 'ideal' conditions at night part 2: Diagnosis of causation". In: *Bound.-Layer Meteor.* 56.4, pp. 339–358. DOI: 10.1007/BF00119211.

Oke, T. (1988). "The urban energy balance". In: *Prog. Phys. Geogr.* 12.4, pp. 471–508. DOI: 10.1177/030913338801200401.

Oudin Åström, D., F. Bertil, and R. Joacim (2011). "Heat wave impact on morbidity and mortality in the elderly population: A review of recent studies". In: *Maturitas* 69.2, pp. 99–105. DOI: 10.1016/j.maturitas.2011.03.008.

Park, H.-S. (1986). "Features of the heat island in Seoul and its surrounding cities". In: *Atmos. Environ.* 20.10, pp. 1859–1866. DOI: 10.1016/0004-6981(86)90326-4.

Parker, D. E. (2010). "Urban heat island effects on estimates of observed climate change". In: *Wiley Interdiscip. Rev. Clim. Chang.* 1.1, pp. 123–133. DOI: 10.1002/wcc.21.

Peng, S., S. Piao, P Ciais, P. Friedlingstein, C. Ottle, F. M. Breon, H. J. Nan, L. M. Zhou, and R. B. Myneni (2012). "Surface Urban Heat

Island Across 419 Global Big Cities". In: *Environ. Sci. Technol.* 46.2, pp. 696–703. DOI: 10.1021/es2030438.

Pielke Sr., A. R. (2002). *Mesoscale Meteorological Modeling*. 2nd ed. San Diego: Academic Press, p. 676.

Piringer, M. et al. (2007). "The surface energy balance and the mixing height in urban areas - Activities and recommendations of COST-Action 715". In: *Boundary-Layer Meteorol.* 124.1, pp. 3–24. DOI: 10.1007/s10546-007-9170-0.

Pongrácz, R., J. Bartholy, and Z. Dezső (2010). "Application of remotely sensed thermal information to urban climatology of Central European cities". In: *Phys. Chem. Earth, Parts A/B/C* 35.1-2, pp. 95–99. DOI: 10.1016/j.pce.2010.03.004.

Prata, A. J., C V. Casellescoll, J. A. Sobrino, and C Ottle (1995). "Thermal remote sensing of land surface temperature from satellites: current status and future prospects". In: *Remote Sens. Rev.* 12.3-4, pp. 175–224. DOI: 10.1080/02757259509532285.

Prigent, C., A. Filipe, and B. R. William (2003). "Land surface skin temperatures from a combined analysis of microwave and infrared satellite observations for an all-weather evaluation of the differences between air and skin temperatures". In: *J. Geophys. Res.* 108.D10, p. 4310. DOI: 10.1029/2002JD002301.

Prihodko, L. and S. N. Goward (1997). "Estimation of air temperature from remotely sensed surface observations". In: *Remote Sensing of Environment* 60.3, pp. 335–346. DOI: 10.1016/S0034-4257(96)00216-7.

Rao, P. (1972). "Remote sensing of urban heat islands from an environmental satellite". In: *Bull. Am. Meteorol. Soc.* 53, pp. 647–648.

Roth, M., T. R. Oke, and W. J. Emery (1989). "Satellite-derived urban heat islands from three coastal cities and the utilization of such data in urban climatology". In: *Int. J. Remote Sens.* 10.11, pp. 1699–1720. DOI: 10.1080/01431168908904002.

Roth, M. (2007). "Review of urban climate research in (sub)tropical regions". In: *Int. J. Climatol.* 27.14, pp. 1859–1873. DOI: 10.1002/joc.1591.

Rouse, W. R., D. Noad, and J. McCutcheon (1973). "Radiation, Temperature and Atmospheric Emissivities in a Polluted Urban Atmosphere at Hamilton, Ontario". In: *J. Appl. Meteorol.* 12.5, pp. 798–807. DOI: 10.1175/1520-0450(1973)012<0798:RTAAEI>2.0.CO;2.

Rousseeuw, P. J. (1987). "Silhouettes: A graphical aid to the interpretation and validation of cluster analysis". In: *J. Comput. Math.* 20, pp. 53–65. DOI: 10.1016/0377-0427(87)90125-7.

Rozenfeld, H. D., D. Rybski, J. S. Andrade Jr., M. Batty, H. E. Stanley, and H. A. Makse (2008). "Laws of Population Growth". In: *Proc. Nat. Acad. Sci. U.S.A.* 105.48, pp. 18702–18707.

Rozenfeld, H. D., D. Rybski, X. Gabaix, and H. A. Makse (2011). "The Area and Population of Cities: New Insights from a Different Perspective on Cities". In: *Am. Econ. Rev.* 101.5, pp. 2205–2225. DOI: 10.1257/aer.101.5.2205.

Runnalls, K. and T. Oke (2000). "Dynamics and controls of the near-surface heat island of Vancouver, British Columbia". In: *Phys. Geogr.* 4.21, pp. 283–304. DOI: 10.1080/02723646.2000.10642711.

Rybski, D. (2013). "Auerbach's legacy". In: *Environ. Plan. A* 45.6, pp. 1266–1268. DOI: 10.1068/a4678.

Rybski, D., A. G. C. Ros, and J. P. Kropp (2013). "Distance weighted city growth". In: *Phys. Rev. E* 87.4, p. 042114. DOI: 10.1103/PhysRevE.87.042114.

Ryu, Y.-H. and J.-J. Baik (2012). "Quantitative Analysis of Factors Contributing to Urban Heat Island Intensity". In: *J. Appl. Meteorol. Climatol.* 51.5, pp. 842–854. DOI: 10.1175/JAMC-D-11-098.1.

Sailor, D. J. (2011). "A review of methods for estimating anthropogenic heat and moisture emissions in the urban environment". In: *Int. J. Climatol.* 31.2, pp. 189–199. DOI: 10.1002/joc.2106.

Sailor, D. J. and L. Lu (2004). "A top–down methodology for developing diurnal and seasonal anthropogenic heating profiles for urban areas". In: *Atmos. Environ.* 38.17, pp. 2737–2748. DOI: 10.1016/j.atmosenv.2004.01.034.

Sakabikara, Y. and E. Matsui (2005). "Relation between Heat Island Intensity and City Size Indices/Urban Canopy Characteristics in Settlements of Nagano Basin, Japan". In: *Geogr. Rev. Jpn.* 78.12, pp. 812–824. DOI: 10.4157/grj.78.812.

Sakai, S., I. Iizawa, M. Onishi, M. Nakamura, and K. Kobayashi (2009). "Fractal Geometry of the Ground Surface and Urban Heat Island". In: *Int. Conf. Urban Clim.* July, pp. 1–4.

Salamanca, F., A. Martilli, M. Tewari, and F. Chen (2011). "A Study of the Urban Boundary Layer Using Different Urban Parameterizations and High-Resolution Urban Canopy Parameters with WRF". In: *J. Appl. Meteorol. Climatol.* 50.5, pp. 1107–1128. DOI: 10.1175/2010JAMC2538.1.

Schatz, J. and C. J. Kucharik (2014). "Seasonality of the Urban Heat Island Effect in Madison, Wisconsin". In: *J. Appl. Meteorol. Climatol.* 53.10, pp. 2371–2386. DOI: 10.1175/JAMC-D-14-0107.1.

Schneider, A, M. A. Friedl, and D. Potere (2009). "A new map of global urban extent from MODIS satellite data". In: *Environ. Res. Lett.* 4.4, p. 044003. DOI: 10.1088/1748-9326/4/4/044003.

Schubert, S. and S. Grossman-Clarke (2013). "The Influence of green areas and roof albedos on air temperatures during Extreme Heat Events in Berlin, Germany". In: *Meteorol. Zeitschrift* 22.2, pp. 131–143. DOI: 10.1127/0941-2948/2013/0393.

Schwarz, N. (2010). "Urban form revisited – Selecting indicators for characterising European cities". In: *Landsc. Urban Plan.* 96.1, pp. 29–47. DOI: 10.1016/j.landurbplan.2010.01.007.

Schwarz, N. and A. M. Manceur (2015). "Analyzing the influence of urban forms on surface urban heat islands in Europe". In: *J. Urban Plan. Dev.* 141.3, A4014003. DOI: 10.1061/(ASCE)UP.1943-5444.0000263.

Schwarz, N., S. Lautenbach, and R. Seppelt (2011). "Exploring indicators for quantifying surface urban heat islands of European cities with MODIS land surface temperatures". In: *Remote Sens. Environ.* 115, pp. 3175–3186. DOI: 10.1016/j.rse.2011.07.003.

Shapiro, J. M. (2006). "Smart Cities: Quality of Life, Productivity, and the Growth Effects of Human Capital". In: *Rev. Econ. Stat.* 88.2, pp. 324–335. DOI: 10.1162/rest.88.2.324.

Shen, G. (2002). "Fractal dimension and fractal growth of urbanized areas". In: *Int. J. Geogr. Inf. Sci.* 16.5, pp. 419–437. DOI: 10.1080/13658810210137013.

Simon, A., J. Fons, R. Milego, and B. Georgi (2010). *Urban Morphological Zones version F2vo : Definition and procedural steps*. Tech. rep. Available at: http://www.eea.europa.eu/data-and-maps/data/urban-morphological-zones-2006-1. (Accessed: 11th May 2016). ETC/LUSI, EEA.

Snyder, W. C., Z. Wan, Y. Zhang, and Y.-Z. Feng (1998). "Classification-based emissivity for land surface temperature measurement from space". In: *Int. J. Remote Sens.* 19.14, pp. 2753–2774. DOI: 10.1080/014311698214497.

Stedman, J. R. (2004). "The predicted number of air pollution related deaths in the UK during the August 2003 heatwave". In: *Atmos. Environ.* 38.8, pp. 1087–1090. DOI: 10.1016/j.atmosenv.2003.11.011.

Steeneveld, G. J., S. Koopmans, B. G. Heusinkveld, L. W. a. Van Hove, and a. a. M. Holtslag (2011). "Quantifying urban heat island effects and human comfort for cities of variable size and urban morphology in the Netherlands". In: *J. Geophys. Res. Atmos.* 116.20, pp. 1–14. DOI: 10.1029/2011JD015988.

Stewart, I. D. (2011). "A systematic review and scientific critique of methodology in modern urban heat island literature". In: *Int. J. Climatol.* 31.2, pp. 200–217. DOI: 10.1002/joc.2141.

Stewart, I. D. and T. R. Oke (2012). "Local Climate Zones for Urban Temperature Studies". In: *Bull. Am. Meteorol. Soc.* 93.12, pp. 1879–1900. DOI: 10.1175/BAMS-D-11-00019.1.

Stone, B. (2008). "Urban sprawl and air quality in large US cities". In: *J. Environ. Manage.* 86.4, pp. 688–698. DOI: 10.1016/j.jenvman.2006.12.034.

Stone, B., J. J. Hess, and H. Frumkin (2010). "Urban form and extreme heat events: are sprawling cities more vulnerable to climate change than compact cities?" In: *Environ. Health Perspect.* 118.10, pp. 1425–8. DOI: 10.1289/ehp.0901879.

Streutker, D. R. (2002). "A remote sensing study of the urban heat island of Houston, Texas". In: *Int. J. Remote Sens.* 23.March 2015, pp. 2595–2608. DOI: 10.1080/01431160110115023.

— (2003). "Satellite-measured growth of the urban heat island of Houston, Texas". In: *Remote Sens. Environ.* 85.3, pp. 282–289. DOI: 10.1016/S0034-4257(03)00007-5.

Sugiura, N. (1978). "Further analysts of the data by Akaike' s information criterion and the finite corrections". In: *Communications in Statistics - Theory and Methods* 7, pp. 13–26. DOI: 10.1080/03610927808827599.

Sun, T., S. Grimmond, G.-H. Ni, C. S. B. Grimmond, and G.-H. Ni (2016). "How Do Green Roofs Mitigate Urban Thermal Stress under Heat Waves?" In: *J. Geophys. Res. Atmos.* 121.10, pp. 1–19. DOI: 10.1002/2016JD024873.

Taha, H. (1997). "Urban climates and heat islands: albedo, evapotranspiration, and anthropogenic heat". In: *Energ. Buildings* 25, pp. 99–103. DOI: 10.1016/S0378-7788(96)00999-1.

Taleghani, M., L. Kleerekoper, M. Tenpierik, and A. Van Den Dobbelsteen (2015). "Outdoor thermal comfort within five different urban forms in the Netherlands". In: *Build. Environ.* 83, pp. 65–78. DOI: 10.1016/j.buildenv.2014.03.014.

Tomlinson, C. J., L. Chapman, J. E. Thornes, and C. Baker (2011). "Remote sensing land surface temperature for meteorology and climatology: a review". In: *Meteorol. Appl.* 306, pp. 296–306. DOI: 10.1002/met.287.

Tran, H., D. Uchihama, S. Ochi, and Y. Yasuoka (2006). "Assessment with satellite data of the urban heat island effects in Asian mega cities". In: *Int. J. Appl. Earth Obs. Geoinf.* 8.1, pp. 34–48. DOI: 10.1016/j.jag.2005.05.003.

Trzaska, S. and E. Schnarr (2014). *A review of downscaling methods for climate change projections*. Tech. rep. September, pp. 1–42.

UN-Habitat (2011). *Cities and Climate Change: Global Report on Human Settlements 2011*. UN-Habitat, p. 300.

Unger, J., Z. Sümeghy, and J. Zoboki (2001). "Temperature cross-section features in an urban area". In: *Atmos. Res.* 58.2, pp. 117–127. DOI: 10.1016/S0169-8095(01)00087-4.

United Nations, Department of Economic and Social Affairs, Population Division (2015). *World Urbanization Prospects 2014: The 2014 Revision, (ST/ESA/SER.A/366)*. Tech. rep.

Voogt, J. A. (2008). "Assessment of an Urban Sensor View Model for thermal anisotropy". In: *Remote Sens. Environ.* 112.2, pp. 482–495. DOI: 10.1016/j.rse.2007.05.013.

Voogt, J. and T. Oke (2003). "Thermal remote sensing of urban climates". In: *Remote Sens. Environ.* 86.3, pp. 370–384. DOI: 10.1016/S0034-4257(03)00079-8.

Wan, Z. (2008). "New refinements and validation of the MODIS Land-Surface Temperature/Emissivity products". In: *Remote Sens. Environ.* 112, pp. 59–74. DOI: 10.1016/j.rse.2006.06.026.

— (2014). "New refinements and validation of the collection-6 MODIS land-surface temperature/emissivity product". In: *Remote Sens. Environ.* 140, pp. 36–45. DOI: 10.1016/j.rse.2013.08.027.

Wan, Z. and J. Dozier (1996). "A generalized split-window algorithm for retrieving land-surface temperature from space". In: *IEEE Trans. Geosci. Remote Sens.* 34.4, pp. 892–905. DOI: 10.1109/36.508406.

Weisstein, E. W. (2016). *Sigmoid Function*. MathWorld–A Wolfram Web Resource. URL: http://mathworld.wolfram.com/SigmoidFunction.html.

Weng, Q., D. Lu, and J. Schubring (2004). "Estimation of land surface temperature – vegetation abundance relationship for urban heat island studies". In: *Remote Sens. Environ.* 89.4, pp. 467–483. DOI: 10.1016/j.rse.2003.11.005.

Weng, Q. (2009). "Thermal infrared remote sensing for urban climate and environmental studies: Methods, applications, and trends". In: *ISPRS J. Photogramm. Remote Sens.* 64.4, pp. 335–344. DOI: 10.1016/j.isprsjprs.2009.03.007.

Weng, Q., U. Rajasekar, and X. Hu (2011). "Modeling urban heat islands and their relationship with impervious surface and vegetation abundance by using ASTER images". In: *IEEE Trans. Geosci. Remote Sens.* 49, pp. 4080–4089. DOI: 10.1109/TGRS.2011.2128874.

Wienert, U. and W. Kuttler (2005). "The dependence of the urban heat island intensity on latitude – A statistical approach". In: *Meteorol. Zeitschrift* 14.5, pp. 677–686. DOI: 10.1127/0941-2948/2005/0069.

Wilby, R. L. (2003). "Past and projected trends in London's urban heat island". In: *Weather* 58.7, pp. 251–260. DOI: 10.1256/wea.183.02.

Wouters, H., M. Demuzere, K. D. Ridder, and N. P. van Lipzig (2015). "The impact of impervious water-storage parametrization on urban climate modelling". In: *Urban Clim.* 11, pp. 24 –50. DOI: 10.1016/j.uclim.2014.11.005.

Yang, L., D. Niyogi, M. Tewari, D. Aliaga, F. Chen, F. Tian, and G. Ni (2016). "Contrasting impacts of urban forms on the future thermal environment: example of Beijing metropolitan area". In: *Environ. Res. Lett.* 11.3, p. 034018. DOI: 10.1088/1748-9326/11/3/034018.

Zhang, K., T.-h. Chen, and C. E. Begley (2015). "Impact of the 2011 heat wave on mortality and emergency department visits in Houston, Texas". In: *Environ. Heal.* 14.1, p. 11. DOI: 10.1186/1476-069X-14-11.

Zhao, L., X. Lee, R. B. Smith, and K. Oleson (2014). "Strong contributions of local background climate to urban heat islands". In: *Nature* 7508, pp. 216–219. DOI: 10.1038/nature13462.

Zhou, B., D. Rybski, and J. P. Kropp (2013). "On the statistics of urban heat island intensity". In: *Geophys. Res. Lett.* 40.20, pp. 5486–5491. DOI: 10.1002/2013GL057320.

Zhou, B., D. Lauwaet, H. Hooyberghs, K. De Ridder, J. P. Kropp, and D. Rybski (2016). "Assessing Seasonality in the Surface Urban Heat Island of London". In: *J. Appl. Meteorol. Clim.* 55.3, pp. 493–505. DOI: 10.1175/JAMC-D-15-0041.1.

Zhou, B., D. Rybski, and J. P. Kropp (2017). "The role of city size and urban form in the surface urban heat island". In: *Sci. Rep.* 7.1, p. 4791. DOI: 10.1038/s41598-017-04242-2.

Zhou, D., S. Zhao, L. Zhang, G. Sun, and Y. Liu (2015). "The footprint of urban heat island effect in China". In: *Sci. Rep.* 5.11160, srep11160. DOI: 10.1038/srep11160.

Zhou, D., S. Zhao, S. Liu, L. Zhang, and C. Zhu (2014). "Surface urban heat island in China's 32 major cities: Spatial patterns and drivers". In: *Remote Sens. Environ.* 152, pp. 51–61. DOI: 10.1016/j.rse.2014.05.017.

Zhou, Y. and J. M. Shepherd (2009). "Atlanta's urban heat island under extreme heat conditions and potential mitigation strategies". In: *Natural Hazards* 52.3, pp. 639–668. DOI: 10.1007/s11069-009-9406-z.

Zhu, K., P. Blum, G. Ferguson, K.-D. Balke, and P. Bayer (2010). "The geothermal potential of urban heat islands". In: *Environ. Res. Lett.* 5.4, p. 044002. DOI: 10.1088/1748-9326/5/4/044002.

Zipf, G. K. (2012). *Human Behavior and the Principle of Least Effort: An Introduction to Human Ecology (Reprint of 1949 Edition)*. Manfield Centre, CT: Martino Publishing.

Zupancic, T., C. Westmacott, and M. Bulthuis (2015). *The impact of green space on heat and air pollution in urban communities: A meta-narrative systematic review*. Tech. rep. March, pp. 1–68.

DECLARATION

I prepared this dissertation without illegal assistance. The work is original except where indicated by special reference in the text and no part of the dissertation has been submitted for any other degree. This dissertation has not been presented to any other University for examination, neither in Germany nor in another country.

Potsdam, December 5, 2017

Bin Zhou

COLOPHON

This document was typeset using the typographical look-and-feel `classicthesis` developed by André Miede. The style was inspired by Robert Bringhurst's seminal book on typography "*The Elements of Typographic Style*". `classicthesis` is available for both LaTeX and LyX:

https://bitbucket.org/amiede/classicthesis/

Happy users of `classicthesis` usually send a real postcard to the author, a collection of postcards received so far is featured here:

http://postcards.miede.de/